Volume 14, No. 4

February, 1964

SOVIET ATOMIC ENERGY

АТОМНАЯ ЭНЕРГИЯ
(ATOMNAYA ÉNERGIYA)

TRANSLATED FROM RUSSIAN

c/b CONSULTANTS BUREAU

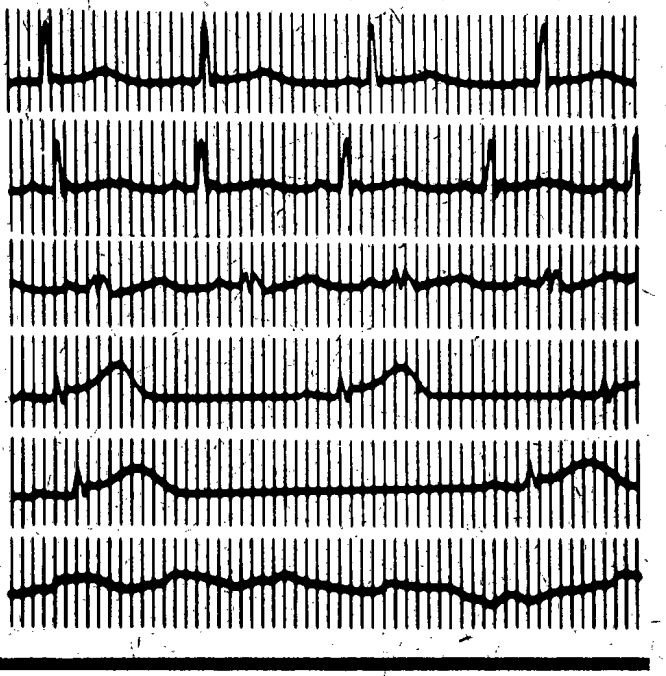

BIOMEDICAL SCIENCES INSTRUMENTATION

Volume 1

Edited by Dr. Fred Alt
National Institutes of Health

Proceedings of the First (1963) National Biomedical Sciences Instrumentation Symposium, sponsored by Instrument Society of America.

A publication of Instrument Society of America

The book examines some of the newest advances in biomedical sciences instrumentation, as well as discussing research projects now in the development stage. It covers such recent and even controversial areas as biomagnetism, fetal telemetry, clinical automation, and the use of simulators and computers in life science research. The rapidly expanding boundaries of space medicine and biotelemetry are pushed still further by papers on: Monitoring major and minor gases of manned space vehicles; telemetric quantitation of immunodiffusion reactions by means of a bio-telescanner; physiological monitoring of animals during space flight; etc. In already established areas of biomedical research, the newest advances in engineering methods and instrumentation are reviewed, e.g., in physiological monitoring, spectroscopy, cardiography, artificial organs, air pollution, and exobiology. In addition to specific information on biomedical engineering apparatus and techniques, several papers are devoted to questions of biomedical engineering education and the management problems of organizing engineering and instrumentation support for the life sciences in commercial firms, universities, and hospitals.

Medical and biological research has become increasingly dependent upon instrumentation for the study and comprehension of the processes of life, and the broad scope of this collection will provoke wide interest among those who are in any way concerned with the design, manufacture, and application of biomedical engineering methods and apparatus.

486 pages **$17.50**

PLENUM PRESS
227 West 17th Street, New York 11, N. Y.

Declassified and Approved For Release 2013/09/25 : CIA-RDP10-02196R000600100003-5

SOVIET ATOMIC ENERGY

A translation of **ATOMNAYA ÉNERGIYA**
A publication of the Academy of Sciences of the USSR

Vol. 14, No. 4 February, 1964

CONTENTS

(continued)

Annual Subscription: $95 **Single Issue: $30** **Single Article: $15**

CONTENTS (continued)

NOTE: The Table of Contents lists all materials that appear in Atomnaya Énergiya. Those items that originated in the English language are not included in the translation and are shown enclosed in brackets. Whenever possible, the English-language source containing the omitted reports will be given.

Consultants Bureau Enterprises, Inc.

INVESTIGATION OF ELECTROMAGNETIC RADIATION FROM A STRAIGHT HIGH-CURRENT DISCHARGE

V. A. Suprunenko, Ya. B. Fainberg, V. T. Tolok, E. A. Sukhomlin, N. I. Reva, P. Ya. Burchenko, N. I. Rudnev, and E. D. Volkov

Translated from Atomnaya Énergiya, Vol. 14, No. 4,
pp. 349-352, April, 1963
Original article submitted June 9, 1962

In this work we investigate the formation of runaway electrons in the electric field of a gas discharge. It is shown that the interaction of the runaway beam with the plasma results in the production of intense coherent electromagnetic radiation at frequencies in the region of the plasma frequency. The power of this radiation is much greater than the thermal noise power.

Among the processes that occur in gas discharges an important role is played by the interaction of charged particle beams with the plasma. This interaction is very efficient; it evidently causes instabilities in a plasma, results in the establishment of a Maxwellian distribution in the absence of collisions, and can have an effect on transport processes (conductivity, diffusion across the magnetic field).

In the present work we have carried out an experimental investigation of the electromagnetic radiation produced by a high-current discharge under conditions for which there was an appreciable current of runaway electrons [1], yielding the possibility of beam-type instabilities [2, 3]. The radiation in this case should be considerably different from the radiation of an equilibrium plasma, both in intensity and spectral composition.

At the present time there are available several papers on the theory of fluctuations in a non-equilibrium plasma [4-8], in particular, in a plasma in which there is a current of runaway electrons. As shown by calculations in [4], at some critical runaway current the beam becomes unstable and the intensity of the fluctuations rises sharply and increases with time. The critical current is given by

$$I_{\text{beam}} \geqslant nV_e^2 \frac{V_{TI}^2}{V_{TO}^3} e^{-\frac{V_e^2}{2V_{TO}^2}}, \quad (1)$$

where n is the plasma density, V_e is the velocity of the runaway electrons, V_{TO} and V_{TI} are the thermal velocities of the plasma and beam respectively. In order to describe fluctuations under these conditions one must develop a theory for an unstable plasma that is not in equilibrium. This topic has been treated in [9] for the case in which the density of the electron beam is much smaller than the plasma density; the initial stages in the development of the instability were treated in this work. The nonlinear theory of the interaction of a beam and plasma [10] indicates that $1/3$ of the beam energy can be dissipated in the excitation of longitudinal waves. Thus, the question of fluctuations caused by longitudinal waves in a non-equilibrium unstable plasma with no collisions has been studied to a sufficient degree to afford a reasonable comparison with experiment.

However, a direct measurement of the spectrum of longitudinal waves excited in a plasma is difficult, especially in high-current discharges. For this reason, in the present work we have investigated the radiation from the plasma. This radiation can be produced as a result of the transformation of longitudinal waves into transverse waves at plasma inhomogeneities. However, as shown in [11, 12] it is also possible to have direct excitation of transverse waves in a plasma that is not in a magnetic field or one that is in a very strong magnetic field. The spectrum and intensity of the fluctuations caused by the transverse waves for a non-equilibrium but stable plasma can be determined from general relations given in [8]. However, the determination of the spectrum of these waves for an unstable plasma requires special investigation.

The excitation of plasma oscillations caused by electron beams has also been studied experimentally in [13-16]. In these papers the longitudinal plasma oscillations at the following frequency were investigated:

$$\omega_0^2 = \frac{4\pi ne^2}{m}. \quad (2)$$

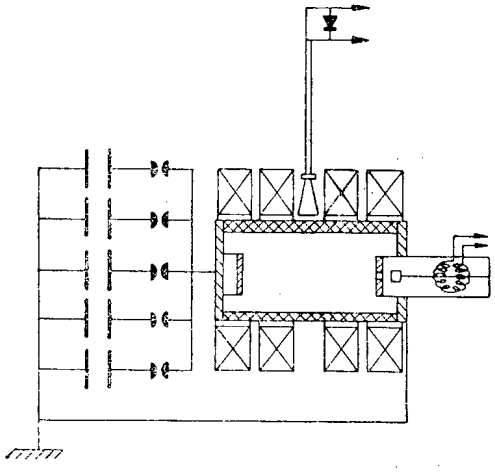

Fig. 1. Diagram of the apparatus.

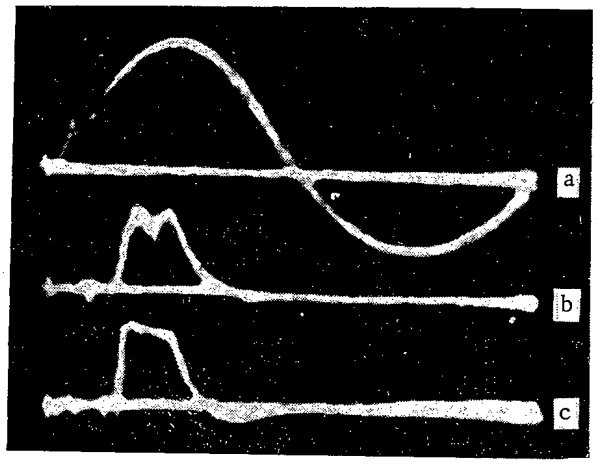

Fig. 2. Oscillogram showing the total discharge current in the gas (a), the current of runaway electrons (b) and the microwave radiation signal (c).

It is the purpose of the present work to report an experimental investigation of the production of intense radiation, the establishment of a correlation between the runaway current and the radiation intensity, and a determination of the spectral composition of the radiation. In addition, we have investigated the coherence of the radiation, a characteristic which is important for an understanding of the radiation process.

In order to determine the mechanism responsible for the radiation it will be necessary to carry out further investigations of the spectrum in the region of the Langmuir frequency (under the present conditions this means wave lengths of the order of 0.3-1.0 mm) as well as the spectrum and intensity of the longitudinal waves.

The experiments were carried out with an apparatus (Fig. 1) consisting of a straight tube of aluminum 10 cm in diameter and 25 cm long usually filled with hydrogen to a pressure of 10^{-2} mm Hg. At the two ends of the tube there are plane aluminum electrodes between which a condenser bank with a capacity of 15 μF is discharged. The condenser bank is charged to 30-40 kV.

The discharge current is 100 kA. The discharge chamber is located in a magnetic field which can be raised to 10 kG. In order to obtain reliable breakdown the gas is subject to preliminary ionization by means of a Penning discharge. In order to improve the reproduceability of the results we took measures to obtain good vacuum conditions (the joints and gaskets were made with metal seals and evacuation was carried out by means of a titanium pump). Before operation was started the chamber was heated to 300 deg C and cleaned by discharge cleaning.

Preliminary experiments have shown [17] that in the first 3-5 μsec of a high-current discharge there is a highly ionized hot plasma pinch which is isolated from the walls and in which magnetohydrodynamic instabilities have not yet developed. The diameter of the pinch is approximately 4 cm. The charge density at the axis of the discharge is 10^{15}-10^{16} cm^{-3} and the electron temperature is several tens of electron volts.

In the present experiment the current of runaway electrons was detected by means of a Faraday cylinder located behind an aperture (ϕ 8 mm) at the center of the electrode at a distance appreciably greater than the mean free path of thermal electrons in the gas, thus insuring that only fast electrons were detected.

The circuit between the current collector and the main electrode should have as little resistance as possible in order that the voltage drop across it will not appear in the gas. The current to the current collector was recorded by means of a Rogowski loop.

The maximum beam energy can be estimated roughly by means of photographic films covered with aluminum foil located behind the aperture in the electrode; this energy was found to vary from 3 to 5 kW. The electric field measured in all experiments varied from 100 to 500 V/cm and was of the order of magnitude of the critical field [1] at which all the electrons become runaway electrons:

$$E_{\mathrm{C}} = 1{,}58 \cdot 10^{-8} \frac{n}{T_e\ (\mathrm{deg})} \simeq 10^3\ \mathrm{V/cm}. \qquad (3)$$

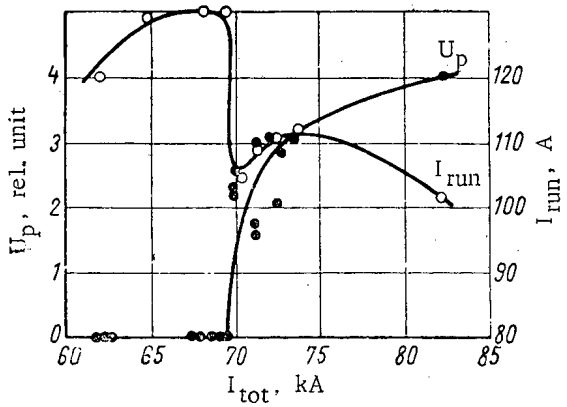

Fig. 3. The intensity of the radiation from the plasma and the runaway electron current as functions of the total discharge current at hydrogen pressures of $2 \cdot 10^{-2}$ mm Hg and a magnetic field of 6 kG.

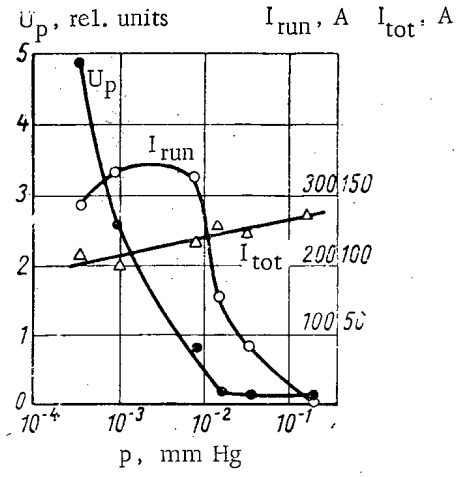

Fig. 4. The discharge current, the runaway electron current and the radiation intensity as functions of the initial gas pressure in the chamber.

The electromagnetic radiation from the plasma was recorded by means of a microwave horn (located in line with the porcelain wall of the discharge chamber) and a crystal detector. The signal from the crystal detector was applied to the amplifier of an OK-17M oscilloscope. The signal at the input of the oscilloscope was proportional to the intensity of the total radiation in the region from 8 to 14.4 mm. The lower limit of the measured radiation was determined by the detector sensitivity and the upper limit by the cutoff wavelength of the waveguide between the horn and the detector.

The radiation spectrum was investigated by using the limiting waveguide technique [10]. It was found that the radiation peak lies in the region of the plasma frequency. However, all characteristics of the radiation were investigated at frequencies below the plasma frequency as well.

The radiation from the plasma is polarized in such a way that the electric field is perpendicular to the runaway electron beam while the magnetic field is parallel to the beam. The radiation intensity is approximately 10^7 times greater than the intensity of the thermal radiation [10] from a plasma at an electron temperature of 10 eV. The investigations were carried out with a receiver tuned to a frequency appreciably below the plasma frequency in which case the noise power, as shown in [18], is much less than 10^{-10} W/ cm^2.

We have also investigated the coherence of the radiation. Two horns, each of which was sensitive to radiation at a wave length of 2 cm, were located at the axis of the discharge and separated by a distance of 11 cm. The phases of the radiation picked up by the horns were compared by means of an 8-millimeter interferometer.

The experiments have shown that the radiation is coherent over the entire range of initial gas pressures and that the intensity of the radiation is constant along the length of the discharge.

In Fig. 2 we show oscillograms of the runaway electron current, the signal from the detector, and the total discharge current. The microwave radiation appears at a peak of the discharge current and shows good correlation with the runaway electron current. The investigations were carried out at a magnetic field of 6 kG, which provides plasma containment for 3-4 μsec.

Changing the magnetic field from 0 to 8 kG had no effect on the amplitude or other properties of the radiation.

It is of interest to investigate the dependence of the intensity of the radiation and current of runaway electrons on the electric field in the plasma. A direct measurement of electric field in a plasma is extremely difficult since placement of probes in the discharge disturbs the radiation. Hence, a Rogowski loop was used to measure the total plasma current which is assumed to be a monotonic function of the electric field.

It is evident from Fig. 3 that there is a critical current in the plasma and, consequently, a critical electric field, below which there is essentially no electromagnetic radiation from the plasma. Above the critical current value the radiation rises sharply and then increases weakly with current. The current of runaway electrons increases

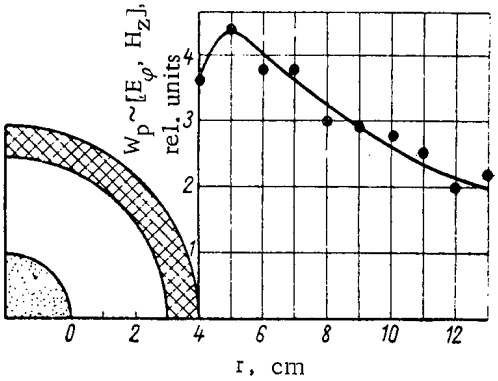

Fig. 5. The radiation intensity as a function of distance from the plasma boundary.

monotonically with electric field; at a critical value of the total current the current of runaway electrons is reduced suddenly by 20-30% and then changes slightly. This dependence indicates that the excitation of electromagnetic waves in a plasma occurs by virtue of the energy of the runaway electrons.

In Fig. 4 we show the intensity of the radiation as a function of initial gas density in relative units. The total current through the gas does not change appreciably during the entire experiment. At pressures below 10^{-2} mm Hg the radiation intensity increases sharply (by a factor of approximately 25); at high pressures it is essentially independent of the pressure.

It is characteristic that as long as the radiation intensity remains small the current of runaway electrons rises sharply as the pressure is reduced, in accordance with the theory given by Harrison [1]. However, as soon as the radiation intensity starts to increase the current of runaway electrons no longer increases and is indeed reduced at high radiation intensities. This experiment indicates once again that electromagnetic radiation from a plasma occurs by virtue of the energy in the current of runaway electrons.

In Fig. 5 we show the intensity of the radiation as a function of distance from the boundary of the pinch. Under the assumption that the pinch radius is 2 cm the power flux of the radiation shows good agreement with inverse distance to the edge of the discharge, except for the points at the edge of the porcelain chamber, which may be explained by the effect of the chamber walls on the antenna impedance.

Thus, it may be stated that the coherent electromagnetic radiation from a plasma observed and investigated here at frequencies close to the Langmuir frequency is excited by the runaway electron beams.

The experimental observation of transverse electromagnetic oscillations excited by electron beams is of obvious importance.

In conclusion the authors wish to thank Acad. K. D. Sinel'nikov for discussion and for his interest in this work, and P. I. Blinov, Cand. Tech. Sci., L. A. Dushin and K. A. Leontovich for help in carrying out the microwave measurements.

LITERATURE CITED

1. E. Harrison, Phil. Mag., 3, 1318 (1958).
2. A. I. Akhiezer and Ya. B. Fainberg, DAN SSSR, 69, 555 (1949).
3. D. Bohm and E. Gross, Phys. Rev., 75, 1851 (1949).
4. N. Rostoker, Nuclear Fusion, 1, 101 (1961).
5. E. Salpeter, Phys. Rev., 122, 1663 (1961).
6. A. I. Akhiezer, I. A. Akhiezer, and A. G. Sitenko, ZhETF, 41, 644 (1961).
7. V. P. Silin, ibid, 42, 969 (1961).
8. A. A. Rukhadze and V. P. Silin, Usp. Fiz. Nauk, 76, 79 (1962).
9. I. A. Akhiezer, ZhETF, 42, 584 (1962).
10. V. D. Shapiro and V. I. Shevchenko, ibid, 42, 1515 (1962).
11. B. Fried, Phys. Fluids, 2 337 (1959).
12. J. Neufeld et al., Phys. Rev., 121, 654 (1961).
13. I. F. Kharchenko et al., ZhTF, 31, 761 (1961).
14. R. A. Demirkhanov, A. G. Govorkov, and A. F. Popov, ibid, 30, 315 (1960).
15. L. Boyd et al., Phys. Rev., 109, 1399 (1958).
16. E. V. Bogdanov, E. Ya. Kislov, and Z. S. Chernov, Radiotekh. i élecktronika, 5, 228 (1960).
17. V. A. Suprunenko et al., ZhTF, 31, 1057 (1961).
18. M. M. Larionov, Conference on Plasma Physics and Nuclear Fusion, Salzburg, 1961, Report 10/241.

MIKHAIL ALEKSANDROVICH LEONTOVICH

Translated from Atomnaya Énergiya, Vol. 14, No. 4,
p. 353, April, 1963

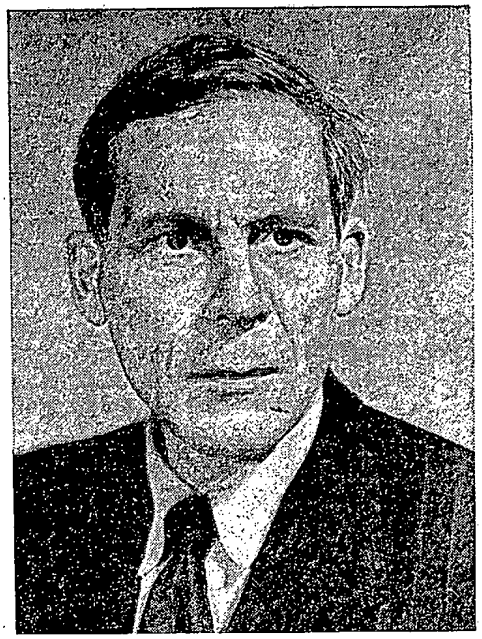

The seventh of March, 1963, marked the passage of sixty years since the birth of one of the greatest of theoretical physicists, Academician Mikhail Aleksandrovich Leontovich.

M. A. Leontovich is known for his work in the most diverse branches of physics: electrodynamics, optics, statistical physics and thermodynamics, quantum mechanics, the theory of oscillations, acoustics, radio physics, and plasma physics.

The start of Mikhail Aleksandrovich's scientific activity is associated with the name of the prominent soviet physicist, L. I. Mandel'shtam, with whom Mikhail Aleksandrovich studied, and with whom he worked in his early years. In one of their first papers, they observed the phenomenon of subbarrier transition in quantum mechanics. In 1929, Mikhail Aleksandrovich took part in developing the complete classical theory of Raman scattering in crystals.

In 1937, Mandel'shtam and Leontovich proposed a general method for treating dissociation phenomena in systems with finite relaxation time. This method is widely used in solid state physics and in gas dynamics.

Associated with the name of Mikhail Aleksandrovich are the so-called "Leontovich boundary conditions" for the electromagnetic field at the surface of solids with large complex dielectric constant. These boundary conditions turned out to be extremely useful in the study of a wide range of problems in electrodynamics.

During the war years, M. A. Leontovich turned his attention to the solution of radio engineering problems of importance to defense, and his influence on the development and practical applications of radio physics dates from

this time. In 1946, M. A. Leontovich (together with V. A. Fok) published his well known paper on the propagation of radio waves along the surface of the earth. M. A. Leontovich has done much to lay the foundations of the theory of thin wire antennas.

His profound understanding of electro- and thermodynamics has enabled M. A. Leontovich (together with S. M. Rytov) to establish the mutual relation between the correlation of current fluctuations and the conductivity in a medium.

In 1951 Mikhail Aleksandrovich became head of the theoretical work on plasma physics and the problem of controlled thermonuclear synthesis. He has educated a school of theoreticians working in the field of plasma physics, and this school is the leading one in our country. M. A. Leontovich is an initiator and an active participant in the majority of the researches in the new and surging development of this branch of physics.

Mikhail Aleksandrovich's ideas are always of great influence, not on the development of theory alone, but at the same time on the experimental work in the branch of science which he has taken up.

M. A. Leontovich's services to science are generally recognized. In 1939, he was elected a corresponding member, and in 1946 a full member of the Academy of Sciences, USSR. For his work on radio physics, he was awarded the A. S. Popov gold medal in 1952. For his work in the field of plasma physics, M. A. Leontovich won the Lenin Prize in 1958. Mikhail Aleksandrovich has been honored by many orders and medals of the USSR. On the occasion of his sixtieth birthday, he was honored with the third order of Lenin.

Mikhail Aleksandrovich Leontovich is a man with a great soul. Among physicists, his honesty, his uncompromising devotion to principle, his cordial relation to people, and his extreme modesty have become truly proverbial.

PASSAGE OF A PLASMA BURST THROUGH A MAGNETIC MIRROR MACHINE

N. N. Brevnov and A. I. Matulis

Translated from Atomnaya Énergiya, Vol. 14, No. 4,
pp. 354-358, April, 1963
Original article submitted July 27, 1962

A study has been made of the behavior of plasma bursts as they move along the axis of an "Ogrenok" magnetic mirror machine. The bursts were accelerated by a coaxial plasma injector. For the parameters chosen, the main plasma current was injected in the form of two bursts with velocities of 10^7 and $2 \cdot 10^6$ cm/sec. In passing through the first magnetic mirror, both bursts were broken up into streams. This occurred to a larger extent in the burst with the lower velocity. The first burst passed through 350 cm of machine in a time of the order of 90 μsec. The luminescence from the streams in the machine lasted 700 μsec.

Introduction

The study of plasma containment in magnetic mirror machines is closely bound up with the problem of injection and filling the machine with plasma of sufficiently high density, temperature, and degree of ionization. There is some interest in producing a plasma of this sort by capturing bursts accelerated in "plasma injectors". This method of filling is used in a number of physical experiments [1, 2]. In the present paper, a study was made of the passage of plasma bursts through magnetic mirrors and of the motion of bursts in a large size mirror machine.

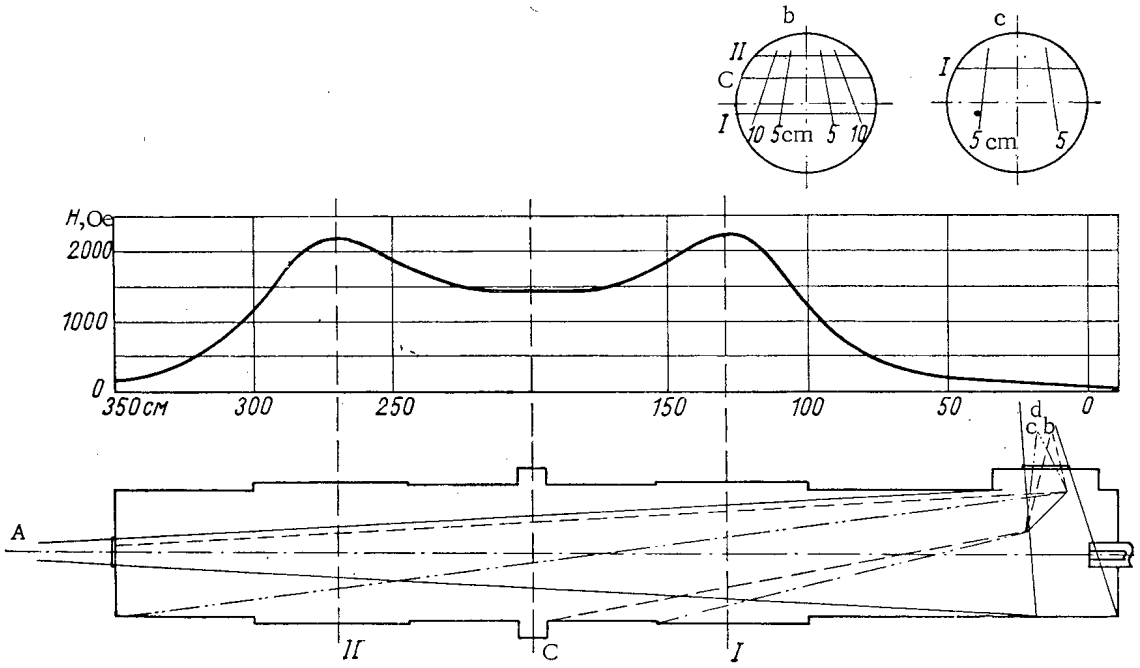

Fig. 1. Geometry of the setup.

Setup

The experiments were made in an "Ogrenok" machine [3]. The magnetic field configuration is given in Fig. 1. The mirror ratio was 1.5. The constant magnetic field was varied from 0 to 6600 Oe*.

*The magnetic field configuration was not changed; the field values given are for the magnetic field in the mirrors.

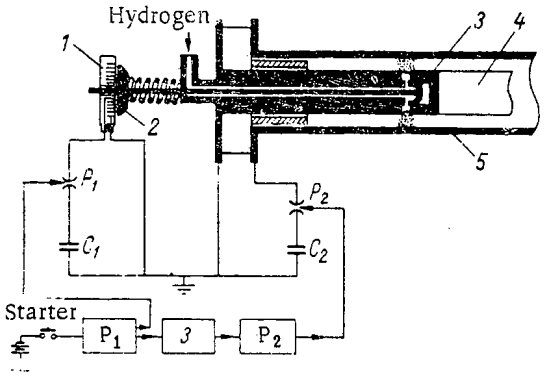

Fig. 2. Diagram of plasma injector: 1) Electrodynamic hammer; 2) anvil; 3) valve; 4, 5) electrodes.

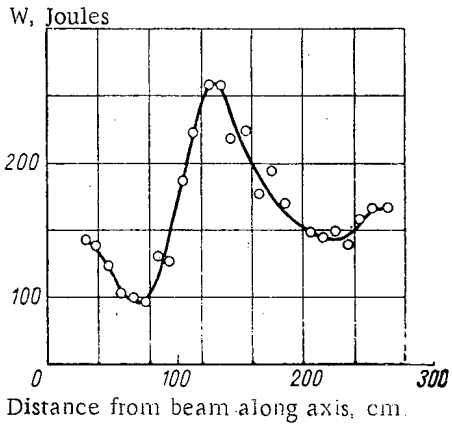

Fig. 3. Energy W, given to the calorimeter by the bursts, as a function of distance to injector (H = 2000 Oe).

The plasma bursts were produced by a coaxial plasma injector, similar to the one described in [4-6]. The electrical circuit is shown in Fig. 2. The current change period in the injector circuit was 10 μsec. The delay time between applying the voltage to the injector electrodes and opening the valve was 400 μsec. When the valve was open, 45 μg of hydrogen was introduced into the injector. The injector gave two successive pulses with velocities 10^7 and $2 \cdot 10^6$ cm/sec. The initial residual gas pressure in the chamber of the machine was 10^{-6} mm Hg.

In the experiments under discussion, a study was made of the changes in geometric dimensions of the bursts (by photographing them with an ultra high speed camera), of the velocity of the bursts while moving in the magnetic field (by means of magnetic probes), and of the energy density in the bursts (with calorimeters provided with sensitive thermocouples).

Results

The plasma bursts were injected along the axis of the machine. If there is no magnetic field, after the bursts leave the injector, they quickly go to pieces and hit the walls of the chamber. Figure 3 shows a characteristic curve

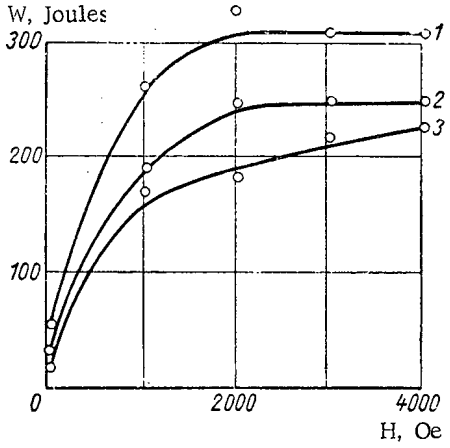

Fig. 4. Energy at calorimeter as a function of magnetic field intensity: 1) first magnetic mirror; 2) center of the machine; 3) second magnetic mirror.

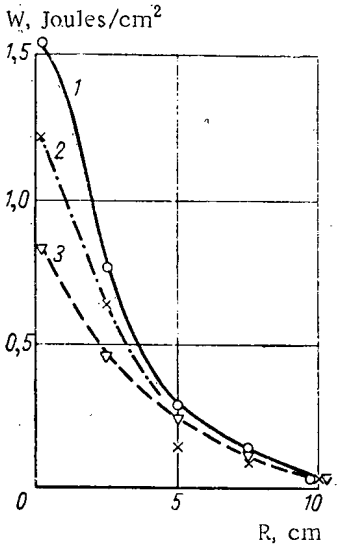

Fig. 5. Radial distribution of energy density w in first magnetic mirror: 1) H = 4400 Oe; 2) H = 2200 Oe; 3) H = 1100 Oe.

of the change in energy given to the calorimeter as a function of the distance to the injector with a magnetic field in the machine. The calorimeter was a copper cylinder (8 cm in diameter, 30 cm long) with a conical input. The input diameter was 18 cm. The calorimeter was moved along the axis of the machine. It follows from Fig. 3 that at distances greater than 80 cm from the injector, the bursts begin to be compressed by the magnetic field. However, the rapid decrease in energy in the calorimeter in the region behind the magnetic mirror shows that the radial divergence of the bursts is greater than the divergence of the lines of force. This is supported by Fig. 4, which shows the energy given to the calorimeter as a function of magnetic field intensity. In the first magnetic mirror, a field of 2000 Oe is sufficient to compress the bursts to the size of the calorimeter. The energy given to the calorimeter does not change with increase in field. There is no saturation in the second magnetic mirror, which shows that the bursts are of considerable size along the diameter of the chamber.

Figure 5 shows the radial distribution of the energy density of the bursts at a distance of 130 cm from the injector as measured with small sized calorimeters. The energy density is a maximum at the axis for all values of magnetic field intensity. The bursts have a dense core of the order of 5 cm in diameter. After the first magnetic mirror, fluctuations start in the transverse dimensions of the bursts, especially at strong magnetic fields, so that the measurements made with small sized calorimeters become inaccurate. The data obtained with the calorimeters show that the plasma bursts are compressed on entering the magnetic field, forming a dense core. The beams spread out in the radial direction as they move on in the magnetic field, so that their transverse dimensions have increased considerably by the time they get to the second magnetic mirror.

Measured values of the velocity of the first burst at different distances from the injector for a magnetic field of 2200 Oe are given below.

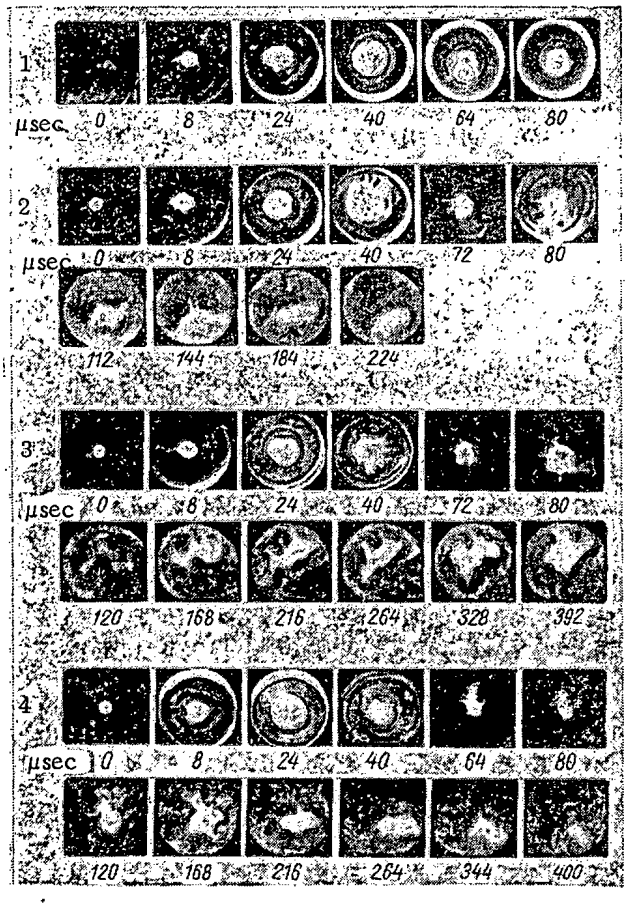

Fig. 6. Burst shapes (type a pictures); 1) H = 0; 2) H = 2200 Oe; 3) H = 4400 Oe; 4) H = 6600 Oe. The time after the start of injection is shown under each frame.

Fig. 7. Passage of plasma bursts through a magnetic mirror (type c pictures); 1) H = 2200 Oe; 2) H = = 4400 Oe; 3) H = 6600 Oe.

Distance from injector to first winding, cm	0	80	130	200
Velocity, cm/sec	$12 \cdot 10^6$	$7 \cdot 10^6$	$3.6 \cdot 10^6$	$4.4 \cdot 10^6$

The velocity was measured from the displacement between the pulses from two windings ~ 200 mm in diameter, located 40 cm apart on the axis. The data show that the velocity of the plasma burst decreases several times when it goes into the magnetic mirror, and increases several times when it comes out.

The change in velocity of the second beam was thus difficult to find because of the smallness of the signal.

The change in shape of the bursts was investigated by using the ultra high speed camera as a time magnifier. The field of vision of the objective is shown in Fig. 1 for four types of pictures. The upper part of the figure shows the image of the lines in the focal plane; I, C, and II are horizontal lines perpendicular to the axis of the machine and intersecting it at the first magnetic mirror, in the center, and at the second magnetic mirror respectively. The oblique lines are horizontal lines parallel to and 5 or 10 cm from the axis of the machine.

Using pictures of type d made it possible to photograph bursts coming directly out of the injector. Analysis of a large number of films has shown that the main plasma current from the injector lasts up to 30 μsec, and changing the magnetic field in the machine has no appreciable effect on the way the injector works.

Figure 6 shows pictures of bursts taken from the end of the chamber (type a picture). In all cases where the magnetic field is different from zero, tongues grow out in the plasma, and are clearer the higher the magnetic field intensity. Control pictures, taken at a small angle between the axis of the machine and the optical axis of the camera, show that, after 90 μsec, the first burst has already reached the end window, causing it to be uniformly luminescent. If the time is read from the start of discharge, the luminescence of the plasma will be a minimum for t = 70 μsec, which corresponds with the arrival of the first beam in the second mirror, and of the second beam in the first mirror. Appreciable luminescence in the chamber persists for a time of the order of 700 μsec.

Figure 7 shows bursts passing through a magnetic mirror (type c picture). The first burst approaches the first magnetic mirror in the form of a broad luminous wall, which is then transformed into a conical channel. The plasma passes through the magnetic mirror in a thin stream along the axis of the machine. This evidently indicates that the magnetic field is still not able to diffuse into the first burst, and the plasma stream probably penetrates through the magnetic mirror by the mechanism described by Tuck [7]. It should be noted that the first burst shows inhomogeneities consisting of screw type exfoliation of the plasma stream.

The passage of the second burst through the magnetic mirror is different. This is clearly visible in the pictures 3 of Fig. 7, which show the shape of the second burst alone. At a distance of the order of 80 cm from the injector, the second burst breaks up into separate streams which behave like a poorly conducting plasma. They are weakly compressed in the magnetic mirror, and pass through the machine with a large total luminescence.

Thus, calorimetric measurements and photographing the bursts show that there is a dense plasma stream moving along the axis of the machine (first burst), and that there are plasma streams that become displaced and diverge radially as they get farther from the injector (second beam). The fluctuations in the data from the calorimetric measurements are obvious, and are caused by the inhomogeneity produced by the streams.

Discussion of Results

The grooving of the surface of the plasma bursts as they move in a nonuniform field was observed by Dickinson [8], and was explained by him as a manifestation of inertial instability which shows up from the radial acceleration of the plasma occurring when the burst is compressed by an increasing magnetic field. In our case, the formation of the streams is of a similar nature to inertial instability, although the rate of increase of the magnetic field is small (10^8 Oe/sec), while the radial compression rates of the burst are of the order of the thermal velocities of the ions.

The formation of the streams may also be explained in terms of the instabilities inherent in the plasma when it is bounded by curved lines of magnetic force.

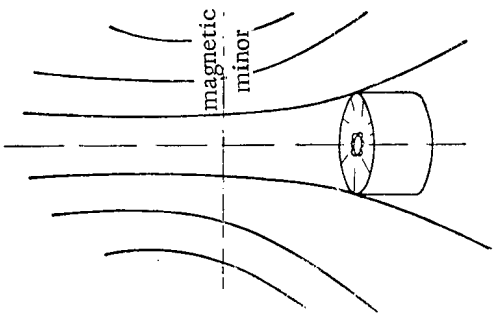

Fig. 8. Configuration of lines of magnetic force.

The configuration of the lines of magnetic force ahead of the mirror is that of a beam converging toward the axis (Fig. 8).

The density of the plasma burst is a minimum at the axis when it leaves the coaxial injector. It may be assumed roughly that they are similar in shape to a hollow cylinder. At the entrance to the magnetic mirror, the external surface of the plasma is bounded by convex lines of magnetic force, and the boundary will be stable. However the internal surface of the plasma cylinder is bounded by concave lines of force and trough type instabilities can develop on the inside surface of the plasma, and these are capable of dividing the plasma cylinder into separate streams. After passing through the magnetic mirror, the external surface of the plasma may become unstable to trough formation. The grooving of the surface of plasma bursts shows up more clearly in the second burst, which is moving at a lower velocity.

The data obtained permit us to assume that bursts with a velocity of 10^7 cm/sec can pass through a distance of the order of several meters in a magnetic field of several thousand oersted, and still have a compact shape. Bursts with smaller velocities break up into separate streams as a result of instabilities and behave like a plasma with poor conductivity in the magnetic field.

It is possible that formation of streams will favor capturing the plasma in a magnetic mirror machine.

LITERATURE CITED

1. S. Yu. Luk'yanov et al., ZhÉTF, 37, (17), 27 (1959).
2. F. Goensgen et al., Phys. Fluids, 2, 230 (1959).
3. N. N. Brevnov et al., Atomnaya Énergiya, 13, No. 5, 421 (1962).
4. L. A. Artsimovich, Controlled Thermonuclear Reactions [in Russian], Gosatomizdat, Moscow (1961).
5. J. Marshall, Phys. Fluids, 3, 13 (1960).
6. John Marshall, Transactions of the Second International Conference on the Peaceful Uses of Atomic Energy (Geneva, 1958). Selected papers by foreign scientists, Vol. 1 [in Russian], Atomizdat, Moscow (1959), page 290.
7. I. Tuck, Phys. Rev. Lett., 3, 313 (1959).
8. H. Dickinson et al., Phys. Fluids, 3, 480 (1960).

All abbreviations of periodicals in the above bibliography are letter-by-letter transliterations of the abbreviations as given in the original Russian journal. *Some or all of this periodical literature may well be available in English translation.* A complete list of the cover-to-cover English translations appears at the back of this issue.

6.5 MeV MICROTRON FOR ELECTRON INJECTION IN A SYNCHROTRON

K. A. Belovintsev, A. Ya. Belyak, A. M. Gromov, E. M. Moroz, and P. A. Cherenkov

Translated from Atomnaya Énergiya, Vol. 14, No. 4,
pp. 359-363, April, 1963
Original article submitted June 27, 1962

A discussion is given of the possibility of using a microtron as an external electron injector in a synchrotron. The construction of the equipment is described, and startup results are given for a 6.5 MeV microtron.

Introduction

In the majority of synchrotrons for energies up to 500 MeV, the electron source ordinarily used is an internal injector, located in the acceleration chamber close to the external boundary of the working region of the accelerator. As a rule, the energy of the electrons injected in this case is 50-100 keV, which makes it necessary to give the electrons a preliminary acceleration to energies of the order of 3-4 MeV ($\beta = v/c \simeq 1$), and only after this does the actual synchrotron acceleration begin. The preliminary electron acceleration is accomplished by classical betatron acceleration, i.e., by means of eddy current e.m.f.'s.

In synchrotrons operating above 500 MeV, use is ordinarily made of high voltage injection of electrons (with an energy of several megaelectron volts), obtained from an external source. Here, the input magnetic fields are sufficient to give the required field with the necessary accuracy. It is no longer necessary in this case to give the electrons a preliminary acceleration in the betatron cycle, or to vary the frequency of the accelerating voltage in the synchrotron. High voltage injection of course has its problems, due to the necessity of getting the injected beam through the input channel. However, as we know, these problems are not fatal, and have been successfully solved in all large accelerators.

With high voltage injection, the choice of the method of giving the electrons the preliminary acceleration (Van de Graaf generator, pulse generator, linear accelerator, etc.) is determined by the effort to get the greatest possible electron beam intensity at the output of the injector accelerator, with due regard for the other parameters of the beam, such as the energy spread, the angular divergence, etc., which are of great importance from the point of view of capture efficiency.

We have made a detailed treatment of the possibility of using an accelerator of microtron type as an electron injector, the idea of which had already been put forth in 1944 [1]. (The first successful attempt at using a microtron as an injector was made by Wernholm [2]. However, no details of the attempt have yet been published.)

An analysis of the data showed that the relatively high electron beam intensity obtainable in already existing microtrons [2, 3] ($\sim$ 20 mA in the pulse), the simplicity of construction, and the ease of getting a large portion of the electrons out of the accelerator, the large faction of monoenergetic electrons, and the small angular divergence of the beam, as well as some other properties of the microtron make this accelerator a very promising one to use as a synchrotron injector.

In order to gain experimental verification of some of the conclusions drawn, we developed and started up a microtron designed to accelerate electrons to 6.5 MeV (in the first stage).

It is proposed to test the microtron as an injector on the 280 MeV synchrotron of the P. N. Lebetev Physics Institute of the Academy of Sciences, USSR (PIAS).

Calculation of the Efficiency of the Microtron as an Electron Injector in a 280 MeV Synchrotron

With high voltage injection, there is a considerable reduction in the Coulomb repulsion effect of the electrons in the synchrotron beams. This produces a substantial increase in the maximum number, N_{max}, of electrons which can be held in a synchrotron orbit by focusing forces.

It may be shown that N_{max} is expressed in the following way:

$$N_{\max} \simeq 10^{13} \frac{\varrho^2}{R} (1-n)\,\gamma\,(\gamma^2-1), \tag{1}$$

where ρ is the half width of the working range, R is the radius of the equilibrium orbit, n is the magnetic field drop-off index, and $\gamma = 1 + W/E_0$ is the relative energy of the electrons. For the accelerator under discussion, ρ = 6 cm, R = 82 cm, n = $^2/_3$, and the injection energy is W_i = 70 keV.

It follows in particular from this formula that going from an injection energy of 70 keV to an injection energy of ~ 6 MeV (an energy easily obtained when using the microtron as an injector) increases N_{max} by a factor more than 6000.

The energy spread of the electrons injected into the synchrotron will be

$$\frac{\Delta E}{E_0} \ll \frac{\varrho}{R} (1-n) \left(\gamma - \frac{1}{\gamma}\right) \simeq 0{,}3. \tag{2}$$

The beam of electrons obtained in a microtron with $\Delta E/E_0 \simeq 5 \cdot 10^{-2}$, satisfies this requirement completely, which is a factor favoring high electron capture efficiency in the synchrotron acceleration cycle.

The angular characteristics of the electron beam accelerated in the microtron are also very favorable to efficient capture of the electrons. The maximum permissible values of angular divergence of the injected electrons may be found from the formulas for the angle of spread in the vertical direction

$$\alpha_z < \frac{h\sqrt{n}}{2R};$$

and for the angle of spread in the radial direction

$$\alpha_R < \frac{\sqrt{2k(1-n)\,\varrho\Delta R}}{3R}.$$

As applied to the case under discussion (assuming that the number of effective rotations during injection is k = 5, and the spacing of the orbit directors is ΔR = 0.2 cm) these formulas give

$$(\alpha_z)_{inj} < 6 \cdot 10^{-2} \text{ and } (\alpha_R)_{inj} < 10^{-2}.$$

A calculation of the same parameters for the microtron beam gives the following values:

$$(\alpha_z)_{\min} \simeq \frac{d}{\lambda\gamma^2} \simeq 10^{-3},$$

where d is the diameter of the opening in the resonator, and λ is the wave length, and

$$(\alpha_R)_{\min} \leqslant 10^{-2},$$

which also favors a high capture efficiency η in the synchrotron acceleration cycle. Calculation gives a value of $\eta \gtrsim 0.1$.

Using the data of typical presentday microtrons [2, 3] (beam current I ≃ 0.02 A in a pulse of $\tau \simeq 2$ μsec duration), it is not difficult to find the number N of electrons which can be captured in a synchrotron acceleration cycle when using the microtron as injector. This calculation gives $N \simeq 6.25 \cdot 10^{12} \eta I_{(A)} \tau_{\mu sec} > 2.5 \cdot 10^{10}$ electrons.

This analysis has shown that even at the presentday level of development of this type of accelerator, the microtron is a very efficient injector for a synchrotron. There is no doubt that further improvements in the microtron (principally in increasing the intensity) will make it even more promising for injection purposes.

We now give a short description of the 6.5 MeV PIAS microtron, which was started in 1961.

Magnet and Vacuum System

A general view of the microtron with the upper magnet pole removed is shown in Fig. 1. The magnet pole (600 mm in diameter) and the plates were made of Steel 3, while the yoke was made of Armco iron. In order to increase the working range of the magnetic field, ringshaped steel shims of cyclotron type were mounted on the poles,

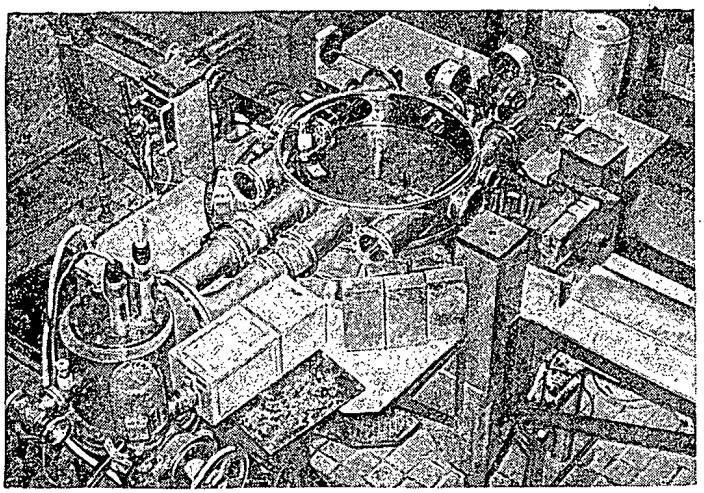

Fig. 1. General view (plan) of the microtron with the upper magnet pole removed.

giving a diameter of the working range of about 500 mm. The relative irregularities in the working region of the magnetic field, as measured by nuclear resonance, do not exceed 0.3%, and are a maximum in the regions closest to the yokes of the magnetic circuit.

The exciting winding of the magnet has natural air cooling, and consists of copper wire (5 mm diameter) insulated with fiberglass. The magnetic circuit and the exciting winding are designed with a safety factor of four times the nominal rating.

The magnet power supply has an operating rating ($H \simeq 1000$ Oe) of about 450 W. The total weight of the microtron magnet in winding is 2 tons. The magnet power supply is stabilized to $\sim 0.03\%$.

The vacuum system of the accelerator consists of a VN-1 forevacuum pump, a 500 liter M-5 oil vapor pump, a Venetian blind type nitrogen trap with a reflector, a DU-160 vacuum cutoff, and finally the vacuum tubing and the accelerator chamber. The trap uses up 5 liters of liquid nitrogen per 10 h of continuous operation without addition).

The vacuum chamber of the microtron is made of shut brass, and consists of a ring with nine pipe connections sealed in (see Fig. 1). The poles of the magnets serve to close the ends of the chamber. Wilson packing is used where movable elements enter the chamber. The electrical connections pass through feed-through insulators made of epoxide resin.

There is a by-pass vacuum system for preliminary evacuation of the accelerator chamber when the oil vapor pump is hot. Here the output of the oil vapor pump is connected to the compensating volume. This evacuation system makes it possible to get a working vacuum. ($\sim 2 \cdot 10^{-6}$ mm Hg) in the accelerator chamber 1.3 hours after starting while with the oil vapor pump hot it takes 25 minutes.

In case of sudden loss of vacuum in the chamber to pressure above 10^{-4} mm Hg, an emergency switch is provided which automatically disconnects the chamber from the oil vapor pump.

High Frequency System

In the first experiments, the high frequency system of the microtron was made up according to the circuit generally used [3] consisting of the following elements: magnetron oscillator, phase rotator, three-way in the E plane, accelerating resonator, and stabilizing water load.

The 10 centimeter band magnetron oscillator gives pulses of 3 μsec duration with a repetition frequency of 50 c.p.s. The rectangular wave guide has a cross section of 72×44 mm^2 and operates on the fundamental H_{01} mode. The construction of the plain cylindrical resonator is similar to that described in [3]. The resonator and the T-junction are insulated from the atmosphere by diaphragms (made of teflon, 2 mm thick), mounted in standard choke connectors ahead of the T-junction on the same side as the water load and the phase rotator. With this form of high frequency system, it was possible to start the microtron. The fluoroplast diaphragms did almost no harm to the standing wave ratio in the wave guide circuit, but required some treatment at low power levels in the high frequency oscillator to prevent breakdowns on the surface.

It should be noted that it is important with this form of high frequency circuit for the length of wave guide from the resonator to the characteristic cross section of the T-junction not to be equal to a whole number of half wave length. If this condition is not fulfilled, when the resonator is detuned, the energy does not get to the stabilizing water load, and the standing wave ratio in the guide from the magnetron to the T-junction exceeds the permissible limit for the operation of the magnetron oscillator.

Later on, when tuning the wave guide circuit of the microtron, it turned out to be possible to do away with the water load, and use a ferrite valve [4] as the decoupling element, which made it considerably easier to tune the

high frequency system. In addition to giving good matching of the oscillator to the circuit, the ferrite valve permits smooth control of the power flow by simply changing the direct current in its magnet windings. The losses in the ferrite valve corresponding with maximum damping in the reverse direction are about 25% of the power supplied. This change in the high frequency circuit permits a reduction by a factor of about 2 in the power requirements on the magnetron oscillator for a given accelerator electron level.

Preliminary experiments show that the new high frequency system in the microtron is distinguished by simplicity and convenience. However, it will take further study to make a complete analysis of the system.

The power indicating systems in the load and the resonator, as well as the system giving the envelope of the high frequency voltage pulse on the resonator are similar to those described in [3].

Injecting and Taking Out Electrons

A special type of cathode construction was developed for injecting electrons into the microtrons (Fig. 2). The cathode material used was lanthanum boride, LaB_6, pressed into a tantalum tube. The heater is a conical spiral of tungsten wire (0.3 mm in diameter). In order to reduce the energy loss from thermal radiation, the spiral is surrounded by two tantalum reflectors.

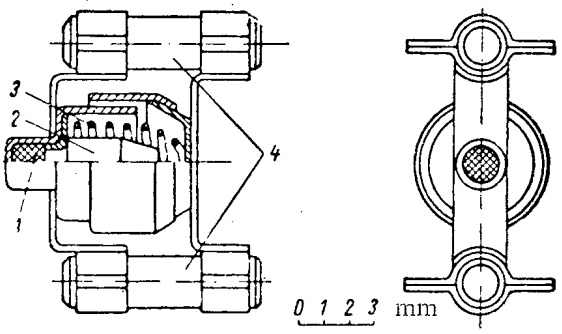

Fig. 2. Cathode construction: 1) lanthanum boride; 2) molybdenum rod; 3) spiral of 0.3 mm diameter tungsten wire (spacing of spiral, 0.6 mm); 4) porcelain rods.

The cathode provides a steady emission current of 400 mA with the emitting surface at a temperature of 1450 deg C. The heating current under these conditions is about 6 A, and the power consumed by the heater is 35 W.

The cathode is insulated from the resonator case with fluoroplast packing. The cathode is fastened to the resonator in such a way that it may be quickly replaced without taking the resonator apart or changing its position in the microtron chamber.

The cathode construction used, which provides normal operation at comparatively small heater current, prevents the magnetic field of the heater current from having any effect on the electron acceleration cycle in the microtron, such as was observed in [3].

An indication of the current in the orbits is obtained by oscillographic observation of the signal from a brass probe, movable over the diameter of the chamber, as well as by means of a television system showing the brightness and shape of the luminous spot on a luminescent coating on the probe. A simple system of two mirrors, one of which is fastened directly to the probe, makes it possible to project the image of the beam from any orbit onto the television pickup tube with practically no distortion.

In taking the electrons out of the microtron, use is made of a magnetic channel consisting of a conical tube of soft steel with an input opening 7 mm in diameter. In order to get the optimum angular and energy parameters of the beam taken out, provisions are made for taking the electrons out of any of the last three orbits.

The magnetic channel is moved about in the vacuum chamber by remote control from the control panel. A special device was provided so that the channel could be set in the optimum position relative to the orbit. An indication of the position could be obtained in two ways: from the minimum in luminescence at the input into the channel (covered with luminophor), as shown by the television circuit, or from a minimum in amplitude of the pulse of current from the beam electrons incident on the walls of the channel.

The magnitude of the electron current taken out was measured with a graphitized brass Faraday cylinder.

The system used permitted taking out 90% of the electrons from the last orbit of the microtron. The extraction losses, amounting to 10%, are due to the fact that the extraction equipment distorts the uniformity of the magnetic field of the accelerator, which produces some displacements in the centers of curvature of the previous orbits and causes the equilibrium phase to slip down.

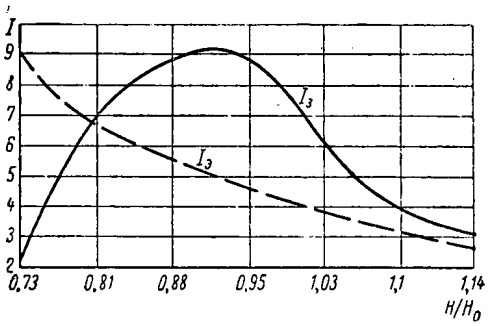

Fig. 3. Microtron beam intensity as a function of magnetic field with other parameters constant. The dotted curve gives the cathode emission current.

Accelerator Operation

All control of the operation of the accelerator is concentrated at a control panel and is done remotely. The control panel of the microtron is separated from the microtron room by a demountable wall 1 meter thick, put together with concrete blocks.

The microtron is adjusted for optimum operation by regulating the cathode heater current and tuning the resonator frequency. Here the magnetic field of the microtron, the current through the magnet winding of the ferrite valve, and the high frequency oscillator power are set on the basis of calculations and the data from preliminary experiments.

Measurements have shown that the maximum current in the last, eleventh orbit of the microtron reaches 22 mA for a pulse length of about 2 μsec, and, after the first two orbits, is practically constant.

Figure 3 gives an experimental curve of the probe current at the eighth orbit of the microtron as a function of the magnetic field. In these measurements, for each value of microtron field, the cathode emission current was adjusted to give maximum beam intensity at the probe. The remaining parameters remain constant. The curve has a definite maximum. The maximum comes at a value of magnetic field where the microtron is operating on auto-electron emission (the accelerated auto-emission electron current was, in our case, 0.5 mA per pulse).

The beam diameter in the last orbit is 4 mm on the average; however, by changing the equilibrium phase, the beam may be deformed considerably in both the radial and the vertical direction.

In conclusion, the authors use this occasion to express their gratitude to the following workers in the Institute of Physical Problems, Academy of Sciences, USSR: S. P. Kapitsa, V. P. Bykov, and V. N. Melekhin, for their valuable advice in developing the design of the microtron, as well as to V. I. Gridasov, V. S. Malofeev, and A. G. Borisov for their help in developing various parts of the accelerator, and to N. G. Kotel'nikov for aligning the vacuum system.

LITERATURE CITED

1. V. I. Veksler, Dokl. AN SSSR, 43, 435 (1944); J. Phys. USSR, 9, 153 (1945).
2. Sci. and Industry, 8, No. 5, 9 (1961).
3. S. P. Kapitsa, V. P. Bykov, and V. N. Melekhin, ZhÉTF, 41, 368 (1961).
4. H. Reich, Nucl. Instrum. Metals, 3, 97 (1958).

EFFECT OF SINGLE CHANNELS AND SLITS ON REACTIVITY

Ya. V. Shevelev

Translated from Atomnaya Énergiya, Vol. 14, No. 4,
pp. 364-370, April, 1963
Original article submitted May 31, 1962

The change in reactivity due to the change in transport cross section in an inclusion in the form of a cylinder or a plain layer is expressed as a perturbation of the neutron flux at some distance from the inclusion, where the diffusion approximation holds. By using the results of flux calculations in the layer medium, and in the cylinder, a relation may be found between the change in reactivity and the characteristics of the inclusion (such as transport cross section, volume, shape, where it is located, etc.). The effect of shape shows up in the coefficients $B_{\parallel}$ and $B_{\perp}$ being different from unity. These same coefficients are what determine the average diffusion coefficients $D_{\perp}$ and $D_{\parallel}$. An interpolation formula is constructed for $B_{\perp}$ based on the various limiting expressions.

Introduction

A large amount of work has been devoted to the question of the effect of channels and slits on reactivity. A study has been made of a lattice of channels in [1, 2], as well as of a lattice of cylinders consisting of a material different from that surrounding them [3-7]. A discussion has been given of a single channel [8, 9] and of a slit [10], but the formulas obtained hold only for the case where there is no resultant neutron flux in the transverse direction. We shall throw off this limitation and at the same time discuss the effect of cylindrical and plane inclusions where the transport cross section Σ'_{tr} differs from the transport cross section of the surrounding medium (Σ_{tr}) by any arbitrary amount (in a void, $\Sigma'_{tr} = 0$).

We shall assume that the change in reactivity, ρ, from the change in Σ_{tr} is small in comparison with $k_{\infty}-1$, so that we can limit ourselves to the first approximation of perturbation theory, and shall further assume that the cross-sectional dimensions of the region where Σ_{tr} is changed are small in comparison with the longitudinal dimensions. If a is the half width of the slit (layer) or the radius of the channel (cylinder), and H is the length of the channel or the characteristic dimension in the plane of the slit, quantities of the order of (a/H) ln (H/a) in the case of the channel and 1/ln (H/a) in the case of a slit will be neglected (in comparison with unity).

Taking part of the material out of the active zone so as to form a void produces the following effects (the same effects are produced by introducing another kind of material):

1) There is a change in the number of neutron transitions from one energy group to another (moderation), as well as in the number of new neutrons born (if there was fissionable material in place of the void), and in the number of neutron captures (if there was an absorber in the material removed);

2) there is a change in neutron flux at the void, since the material is removed which formerly produced neutron scattering, i.e., there is a change in the number of neutron transitions from places with one neutron value to places with a different neutron value.

All this leads to a change in worth of the neutrons and correspondingly to a change in reactivity. However, we shall concentrate our attention solely on effects of the second kind, since for them, in contrast with effects of the first kind, it is impossible to write the simple formula of perturbation theory in the diffusion approximation directly. As a matter of fact a formula of the type

$$\varrho = \int dE \int dV \,(\nabla\Phi^{+})\,(\nabla\Phi)\,D\,\frac{\delta\Sigma_{tr}}{\Sigma_{tr}} \,/\, \mathrm{VFN} \qquad (1)$$

($D = 1/3\Sigma_{tr}$ is the diffusion coefficient, Φ is the flux, Φ^{+} is the conjugated flux value and VFN is the total value of the fission neutrons formed in the reactor per unit of time) assumes $|\Sigma'_{tr}-\Sigma_{tr}| = |\delta\Sigma_{tr}| \ll \Sigma_{tr}$. But formation of a void, is a large local perturbation ($\delta\Sigma_{tr} = -\Sigma_{tr}$). Further, the diffusion approximation does not hold in the vicinity of the void.

Nevertheless, in order to get simple and visualizable formulas of type (1), we go out a distance of the order of $\lambda_{tr} = 1/\Sigma_{tr}$ from the surface of the void, and there draw an effective boundary separating the region containing the void (internal region) from the rest of the reactor (external region). The results of a calculation made on the nondiffusion approximation [11, 12] may be used for the internal region. The diffusion equations hold for the external region. The desired change in reactivity comes from the change in flux (and in the flux gradient) at the effective boundary.

Perturbation Theory Formulas

The external region is the reactor, where, at a part of the boundary (the effective boundary) the flux Φ (and the gradient $\nabla\Phi$) are given by homogeneous conditions of special type. The presence of the void changes the properties of the internal region and thus changes the boundary conditions. The reactivity changes accordingly.

By using the ordinary procedure of perturbation theory, we obtain

$$\varrho = \int dE \int dV \,(\Phi^+\nabla D\nabla\Phi' - \Phi'\nabla D\nabla\Phi^+)/\,\mathrm{VFN}, \tag{2}$$

where

$$\Phi' = \Phi + \delta\Phi \tag{3}$$

is the "perturbed" flux. It is normalized in such a way that the VFN is the same in either a "perturbed" or an "unperturbed" reactor.

On the external surface, Φ^+ and Φ' are equal to zero, since the Gauss formula converts (2) into an integral over the effective surface (dS is the element of surface with its normal turned toward the void):

$$\varrho = \int dE \oint dS\, D\,(\Phi^+\nabla\Phi' - \Phi'\nabla\Phi^+)/\,\mathrm{VFN}. \tag{4}$$

In the unperturbed reactor, where $\Phi' = \Phi$, the reactivity is equal to zero. Accordingly Φ, with any constant multiplier, may be subtracted from Φ', and formula (4) will remain correct. In particular,

$$\varrho = \int dE \oint dS\, D\,(\Phi^+\nabla\delta\Phi - \delta\Phi\nabla\Phi^+)/\,\mathrm{VFN}. \tag{5}$$

The effective surface may be chosen arbitrarily, as long as it doesn't get too close to the void. The VFN is determined for a reactor with no internal region. But if the internal region is not too large, the VFN may, without appreciable error, be thought of as an integral extending over the whole unperturbed reactor, including the internal region, where the void is then formed.

The value Φ^+ may be determined for the whole unperturbed reactor. In the vicinity of the void, Φ^+ is a smooth function of the coordinates, and the change in $\nabla\Phi^+$ may be neglected at distances comparable with the transverse dimensions of the void, writing in (5)

$$\Phi^+(\mathbf{r}) \simeq \Phi^+(\mathbf{r}_v) + (\mathbf{r} - \mathbf{r}_v)\,\nabla\Phi^+(\mathbf{r}_v), \tag{6}$$

where r_v is a point in the void, which only moves when $\underline{r}$ is displaced in the direction of the axis $\underline{z}$ of the channel, or in the plane $\underline{z}$, $\underline{y}$ of the slit. Let

$$dS = dF_v ds, \tag{7}$$

where

$$dF_v = \begin{cases} dz & \text{for a channel;} \\ dz\,dy & \text{for a slit.} \end{cases} \tag{8}$$

Then

$$\varrho = \int dE\,(T_{\parallel} + T_{\perp} + T_0)/\,\mathrm{VFN} \tag{9}$$

where

$$\left.\begin{aligned} T_{\parallel} &= \int dF_v\, D\Phi^+(\mathbf{r}_v) \oint \nabla\delta\Phi\, ds; \\ T_{\perp} &= -\int dF_v\, D\nabla\Phi^+(\mathbf{r}_v) \oint \delta\Phi\, ds; \\ T_0 &= \int dF_v\, D\nabla\Phi^+(\mathbf{r}_v) \oint (\mathbf{r} - \mathbf{r}_v)(\nabla\delta\Phi\, ds). \end{aligned}\right\} \tag{10}$$

Choice of the Effective Surface

The only source of flux perturbation will be taken to be the change in scattering power of the medium, while the rest of the effects (particularly the change in neutron moderation) is neglected. Here, the component of $\delta\Phi$ which owes its origin to the flux renormalization may be neglected (see derivation of formula 5). Then the part of $\delta\Phi$ that we are interested in will be determined solely by the gradient of the unperturbed flux at the point where the void is formed, and its symmetry will not be lower than the symmetry of the system (the void plus the vector $\nabla\Phi$). Note that if $\nabla\Phi = 0$, a change in Σ_{tr} cannot affect the flux.

Divide $\nabla\Phi$ into two components perpendicular and parallel to the axes of the channel or the plane of the slit, i.e.,

$$\nabla\Phi = \nabla_{\perp}\Phi + \nabla_{||}\Phi. \tag{11}$$

The $\underline{x}$ coordinate goes from the center of the channel (slit) in the direction $\nabla_{\perp}\Phi$.

Obviously, the flux perturbation produced by $\nabla_{||}\Phi$ will be a symmetric function of $\underline{x}$ (if we neglect the component coming from the renormalization). In exactly the same way, $\nabla_{\perp}\Phi$ produces an antisymmetric component of $\delta\Phi$.

As the effective surface we take the assembly of the two planes

$$x = x_0; \quad x = -x_0.$$

It may be shown that this choice of the effective surface is incompatible with formula (6) for the case of the channel, but as a matter of fact $\delta\Phi$ is small at large distances from the channel where formula (6) is inaccurate. With the choice made for the effective surface, the symmetric component of $\delta\Phi$ cannot make a contribution to the integrals $T_{\perp}$ and T_0, while the antisymmetric component makes a contribution to $T_{||}$. Therefore

$$\left.\begin{aligned} T_{||} &= \int dF_v\, D\Phi^+(\mathbf{r}_v) \oint \nabla\delta\Phi_{||}\, ds; \\ T_{\perp} &= -\int dF_v\, D\nabla\Phi^+(\mathbf{r}_v) \oint \delta\Phi_{\perp}\, ds; \\ T_0 &= \int dF_v\, D\nabla\Phi^+(\mathbf{r}_v) \oint (\mathbf{r}-\mathbf{r}_v)(\nabla\delta\Phi_{\perp}\, ds), \end{aligned}\right\} \tag{12}$$

where $\delta\Phi_{||}$ is the perturbation produced by $\nabla_{||}\Phi$, while $\delta\Phi_{\perp}$ is produced by $\nabla_{\perp}\Phi$.

In the integral for T_0, symmetry conditions permit us to drop the component of the vector $\mathbf{r}-\mathbf{r}_v$ perpendicular to the $\underline{x}$ axis. After this

$$\left.\begin{aligned} T_0 &= \int dF_v\, D\frac{\partial\Phi^+}{\partial x} \oint x\nabla\delta\Phi_{\perp}\, ds, \\ T_0 &= \int dF_v\, D\frac{\partial\Phi^+}{\partial x} 2x_0 \frac{\partial}{\partial x_0} \int\limits_{x=x_0} \delta\Phi_{\perp}\, ds. \end{aligned}\right\} \tag{13}$$

We shall see later on that $\int\delta\Phi_{\perp}ds$ is independent of the absolute value of x_0, so that $T_0 = 0$.

The Transverse Flux Gradient

In a layer medium with weak absorption, for the transverse flux gradient we must use the diffusion approximation, since the problem of the flux in a nonabsorbing medium may be reduced to the problem of the flux in a medium with constant scattering cross section[13], if instead of the $\underline{x}$ coordinate we introduce the "optical thickness" $\int\Sigma dx$. In particular, the diffusion approximation is applicable to a slit. The flux in the slit does not vary in the $\underline{x}$ direction, since $D' = \infty$ and forming the slit produces the following flux perturbation (see figure):

$$\delta\Phi_{\perp} = -a\frac{\partial\Phi}{\partial x}\frac{x}{|x|}. \tag{14}$$

Correspondingly

$$\left.\begin{aligned} &\nabla\delta\Phi_{\perp} = 0; \quad T_0 = 0; \\ &T_{\perp} = -\int dF_v\, D(\nabla\Phi^+)(\nabla_{\perp}\Phi)\, 2a. \end{aligned}\right.$$

If we imagine $2a\,dF_v$ to be the element of void volume dV_v, (9) may be written as:

$$\varrho = -\int dE \int dV_v\, (\nabla\Phi^+)(\nabla_{\perp}\Phi)\, D/\ \text{VFN}. \tag{15}$$

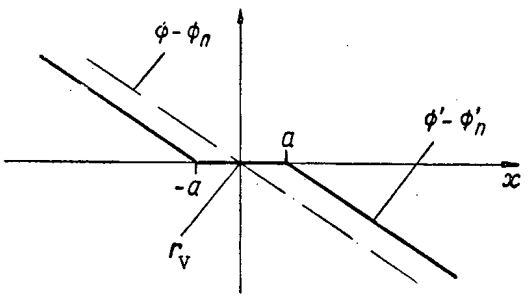

Flux perturbation by a slit.

Note that in this case formula (1) gives the same results, since

$$\frac{\delta\Sigma_{tr}}{\Sigma_{tr}} = -1. \tag{16}$$

Similar calculations for an arbitrary change in Σ_{tr} leads to a formula identical with (1).

The expression for $\delta\Phi_\perp$ in the case of the channel of circular cross section is derived in [12]. Far from the channel

$$\delta\Phi_\perp = -\frac{a^2}{2} B_\perp \frac{x}{x^2+y^2} \cdot \frac{\partial\Phi}{\partial x}, \tag{17}$$

where $B_\perp$ is a function of the ratio of the channel radius to the transport length. A simple interpolation formula is given for it:

$$B_\perp = 1 + \frac{a}{a+\lambda_{tr}} = 2 - \frac{\lambda_{tr}}{a+\lambda_{tr}}. \tag{18}$$

Integrating (17) along the length x = const, z = const, we obtain

$$\int \delta\Phi_\perp \, dy = -\frac{a^2}{2} B_\perp \frac{\partial\Phi}{\partial x} \int_{-\infty}^{\infty} \frac{x\,dy}{x^2+y^2} = -\frac{\pi a^2}{2} B_\perp \frac{\partial\Phi}{\partial x} \cdot \frac{x}{|x|}. \tag{19}$$

Hence

$$T_\perp = -\int dF_v D (\nabla\Phi^+)(\nabla_\perp\Phi) \pi a^2 B_\perp. \tag{20}$$

Since (19) depends only on the sign, but not on the magnitude of x, $T_0 = 0$, as in the case of the slit.

The element of volume will now be $\pi a^2 dF_v$, so that

$$\varrho = -\int dE \int d\vec{V}_v (\nabla\Phi^+)(\nabla_\perp\Phi) D B_\perp / \text{VFN}. \tag{21}$$

Formula (1) no longer gives the correct result except for the case where $B_\perp = 1$ (extremely small channels, where $a/\lambda_{tr} \ll 1$). For large channels ($a/\lambda_{tr} \gg 1$) formula (1) gives values for the effect which are too small by a factor of two. Since the diffusion approximation holds in this limiting case, an explanation of the effect may be given in the language of the diffusion approximation: a cylindrical void draws the neutron flow lines together, while formula (1) is based on the assumption that the flow lines are not distorted.

It is not difficult to derive a formula on the diffusion approximation for the more general case: $\Sigma'_{tr} \neq 0$. Instead of (17) we obtain

$$\delta\Phi_\perp = \frac{\delta\Sigma_{tr}}{\Sigma_{tr}} \cdot \frac{a^2}{2} \cdot \frac{2D'}{D'+D} \cdot \frac{x}{x^2+y^2} \cdot \frac{\partial\Phi}{\partial x}, \tag{22}$$

from which, setting for this case

$$B_\perp = 1 + \frac{D'-D}{D'+D} = \frac{2D'}{D'+D}, \tag{23}$$

we arrive at the formula

$$\varrho = \int dE \int dV_v (\nabla\Phi^+)(\nabla_\perp\Phi) B_\perp \frac{\delta\Sigma_{tr}}{\Sigma_{tr}} D / \text{VFN}, \tag{24}$$

which may be regarded as a generalization of formula (1).

There is one more special case, easily amenable to calculation, where the following inequalities hold simultaneously:

$$\lambda'_{tr} \ll a \ll \lambda_{tr}.$$

Here the total scattering cross section of the cylinder is equal to $\frac{1}{4}$ of its external surface, so that the effective mac-

roscopic scattering cross section is equal to 1/2a, and the relative increase in Σ_{tr} is equal to

$$\frac{\frac{1}{2a}-\Sigma_{tr}}{\Sigma_{tr}}=\frac{\lambda_{tr}}{2a}-1=B_{\perp}\frac{\delta\Sigma_{tr}}{\Sigma_{tr}}.$$

Hence

$$B_{\perp}\simeq\frac{\lambda'_{tr}}{2a}. \tag{25}$$

By using (18), (23), and (25), an interpolation formula may be derived which is good in the limiting cases. For example,

$$B_{\perp}=\left(\frac{\lambda_{tr}}{\lambda'_{tr}+2a}+2\right):\left(\frac{\lambda_{tr}}{\lambda_{tr}+2a}+1+\frac{\lambda_{tr}}{\lambda'_{tr}}\right). \tag{26}$$

For a plane layer, $B_{\perp}$ = 1 always.

The Longitudinal Flux Gradient

The symmetric component of $\delta\Phi$ owes its origin to the neutron leakage into the channel or slit. From the balance equation on the diffusion approximation, which holds at the effective surface, we obtain

$$-dF_v D\oint\nabla\delta\Phi_{||}\,ds=dF_v\,\mathrm{div}\,\delta\mathbf{J}, \tag{27}$$

where δJ is the additional flux vector along the void (the flux due to the formation of the void). Thus

$$T_{||}=\int dF_v\Phi^+(\mathbf{r}_v)\nabla\delta\mathbf{J}=\int\nabla(\Phi^+\delta\mathbf{J})\,dF_v-\int\delta\mathbf{J}\nabla\Phi^+\,dF_v.$$

At the edges of the void, either Φ^+ = 0 (reactor boundary), or δJ = 0 ("dead end"), so that the first integral, after Gaussian transformation, vanishes, and

$$T_{||}=-\int dF_v\delta\mathbf{J}\nabla\Phi^+. \tag{28}$$

The additional flux in a plane layer with $\Sigma'_{tr}\neq\Sigma_{tr}$, and, in particular, in a slit (Σ'_{tr} = 0) may be found by using the results of [11]. In a layer system, the neutron flux in the plane of the layers may be calculated on the diffusion approximation, as long as the boundaries of the layers are displaced in a definite way, by thickening the layers with small transport lengths. The required displacement is equal to:

$$\delta a=\frac{9}{16}(D-D')(1-\bar{f}). \tag{29}$$

The function $\bar{f}$ tabulated in [11] approaches zero exponentially with increase in "optical" thickness of the layers. In the case under discussion, the layers surrounding the "perturbed" layer are thick, and $\bar{f}$ reduces to the function

$$\bar{f}=\varphi_{v1}\left(\frac{2a}{\lambda'_{tr}}\right),\ \text{where}\ \varphi_{v1}(\mu)=4\int_0^1(1-u^2)ue^{-\mu/u}au. \tag{30}$$

If $\lambda'_{tr}\gg 2a$, it is necessary to use the expansion

$$\varphi_{v1}(\mu)=1-\frac{8}{3}\mu+2\mu^2\ln\frac{1}{\mu}+\ldots. \tag{31}$$

In a layer of effective thickness 2(a + δa), there is the additional neutron flux

$$\delta\mathbf{J}=-\nabla_{||}\Phi(D'-D)\,2(a+\delta a)=\nabla_{||}\Phi D\frac{\delta\Sigma_{tr}}{\Sigma_{tr}}B_{||}2a, \tag{32}$$

where, from (29), (30), and (32),

$$B_{||}=\frac{D'}{D}\left(1+\frac{\delta a}{a}\right)=\frac{D'}{D}\left[1-\frac{9}{16}\frac{D'}{a}\left(1-\frac{D}{D'}\right)\right](1-\varphi_{v1}). \tag{33}$$

From (32), (28), and (9) we obtain the formula

$$\varrho = \int dE \int dV_v \, (\nabla\Phi^+)\,(\nabla_{||}\Phi)\, B_{||} \frac{\delta\Sigma_{tr}}{\Sigma_{tr}} D/\mathrm{VFN}, \tag{34}$$

which is entirely similar to (24). We give values of function φ_{v1} [11]:

$2a/\lambda'_{tr}$	0,0	0,1	0,2	0,3	0,4	0,6	0,8	1,0	1,5	2,0	3,0	4,0	∞
φ_{v1}	1,000	0,790	0,640	0,525	0,434	0,305	0,217	0,157	0,074	0,035	0,009	0,002	0,000

In order to go to a slit, we substitute the expansion (31) and (33). This gives

$$B_{||} = 1 + \left(1 - \frac{D}{D'}\right) \frac{a}{2D} \ln \frac{\lambda'_{tr}}{2a}. \tag{35}$$

This expression converges logarithmically as λ'_{tr} approaches infinity. But it is clear from physical considerations that increasing λ'_{tr} beyond the longitudinal dimensions of the layer will not affect the neutron flux. Accordingly, for a slit ($\lambda'_{tr} = \infty$) we obtain, with logarithmic accuracy (with an accuracy up to the term of order $\frac{B_{||}-1}{\ln \frac{H}{a}}$)

$$B_{||} = 1 + \frac{a}{2D} \ln \frac{H}{2a}. \tag{36}$$

In the other limiting case ($\lambda'_{tr} \ll a$)

$$B_{||} = \frac{D'}{D}\left(1 - \frac{9}{16}\frac{D'-D}{a}\right). \tag{37}$$

For a cylinder, the effective displacement of the boundary is given by the formula

$$\left(1 + \frac{\delta a}{a}\right)^2 = 1 + \frac{9}{8}\frac{D-D'}{a}\left[1 - \varphi_v\left(\frac{2a}{\lambda'_{tr}}\right)\right], \tag{38}$$

where

$$\varphi_v(\mu) = \frac{16}{\pi}\int_1^\infty dp \int_0^1 du \, \frac{\sqrt{p^2-1}}{p^5} e^{-\mu p\sqrt{1-u^2}}. \tag{39}$$

This function has been tabulated by N. I. Laletin. For small arguments

$$\varphi_v(\mu) = 1 - \frac{4}{3}\mu + \frac{4}{3}\mu^2 - \frac{\mu^3}{2}\ln\frac{1}{\mu} + \ldots, \tag{40}$$

while for large arguments, in contrast with φ_{v1}, φ_c does not decrease exponentially but as $1/2\mu^2$. The additional neutron flux due to the formation of the cylinder with the effective radius $a+\delta a$, is equal to

$$\delta \mathbf{J} = -\nabla_{||}\Phi(D'-D)\,\pi(a+\delta a)^2 = \nabla_{||}\Phi B_{||}\frac{\delta\Sigma_{tr}}{\Sigma_{tr}} D\pi a^2, \tag{41}$$

where, from (38) to (41),

$$B_{||} = \frac{D'}{D}\left(1 + \frac{\delta a}{a}\right)^2 = \frac{D'}{D}\left[1 - \frac{9}{8}\frac{D'}{a}\left(1 - \frac{D}{D'}\right)(1 - \varphi_v)\right]. \tag{42}$$

Equation (34) follows from (41). The function φ_c given below is from N. I. Laletin's data.

$2a/\lambda'_{tr}$	0,0	0,1	0,2	0,3	0,5	0,7	1,0	1,5	2,0	3,0	5,0	∞
φ_c	1,000	0,880	0,787	0,698	0,552	0,443	0,322	0,200	0,130	0,062	0,021	0,000

In going to a channel, we substitute the expansion (40) and (42). This gives

$$B_{||} = 1 + \left(1 - \frac{D}{D'}\right) \frac{2a}{3D} \left(1 - \frac{a}{4D'} \ln \frac{\lambda'_{tr}}{2a}\right), \tag{43}$$

where the logarithmic term is a small correction. For an empty channel (D' = ∞)

$$B_{||} = 1 + \frac{2a}{3D} \tag{44}$$

with an accuracy up to terms obtained by substituting H for D' in (43), i.e., with an accuracy up the term of order

$$\frac{a}{H} \ln \frac{H}{a} (B_{||} - 1).$$

In the second limiting case ($\lambda'_{tr} \ll a$), we have

$$B_{||} = \frac{D'}{D} \left[1 - \frac{9}{8} \frac{D' - D}{a} \left(1 - \frac{9D'^2}{8a^2}\right)\right]. \tag{45}$$

Conclusion

The effect on reactivity of cylindrical and plane inclusions with a transport cross section different from the surrounding medium, is given by the formula

$$\varrho = \int dE \int dV_v \, (\nabla\Phi^+)(B_\perp \nabla_\perp \Phi + B_{||} \nabla_{||} \Phi) \times \frac{\delta\Sigma_{tr}}{\Sigma_{tr}} D/\,\text{VFN}. \tag{46}$$

The coefficients $B_\perp$ and $B_{||}$ may be calculated from Eqs. (26), (33), and (42) and the tables of the functions φ_{v1} and φ_c given above [see also Eqs. (36), (37), (44), and (45)]. The reactivity changes due to change in neutron worth without being moved spatially, are not taken account of by Eq. (46) and must be calculated separately.

If the material of the inclusion is located in a region large in comparison with the transverse dimension of the inclusion, but small in comparison with the reactor, Eqs. (1) and (11) give

$$\varrho = \int dE \int dV_v \, (\nabla\Phi^+)(\nabla_\perp \Phi + \nabla_{||} \Phi) \frac{\delta\Sigma_{tr}}{\Sigma_{tr}} D/\,\text{VFN}.$$

Accordingly, a departure of $B_\perp$ or $B_{||}$ from unity means that the shape of the inclusion is not without importance. A pure effect of shape

$$\delta_{shape} = \int dE \int dV_v \, (\nabla\Phi^+)[(B_\perp - 1)\nabla_\perp \Phi + (B_{||} - 1)\nabla_{||}\Phi] \frac{\delta\Sigma_{tr}}{\Sigma_{tr}} D/\,\text{VFN} \tag{47}$$

can show up, if thermal expansion causes the slits to close up without producing any substantial mean displacements of material with respect to the center of the reactor.

If, in some region of the reactor, there is a group of cylindrical or plane inclusions, arranged more or less regularly, and sufficiently sparsely (the volume fraction ε is small), the smoothed out flux in the region may be calculated from the anisotropic diffusion equation. Applying the perturbation theory method to these equations, we obtain by analogy with (1)

$$\varrho = \int dE \int dV \, (\nabla\Phi^+) \times \left(D \frac{\delta\Sigma_\perp}{\Sigma_{tr}} \nabla_\perp \Phi + D \frac{\delta\Sigma_{||}}{\Sigma_{tr}} \nabla_{||} \Phi\right)/\text{VFN}.$$

For this equation to give a correct result in agreement with (46), we must set

$$\frac{1}{3D'_\perp} = \Sigma'_\perp = \Sigma_{tr} + \varepsilon B_\perp \delta\Sigma_{tr};$$
$$\frac{1}{3D'_{||}} = \Sigma'_{||} = \Sigma_{tr} + \varepsilon B_{||} \delta\Sigma_{tr}. \tag{48}$$

For the special case of transverse diffusion in a medium with large cylindrical inclusions ($a \gg \lambda_{tr} + \lambda'_{tr}$), where $B_\perp$ is given by Eq. (23), this result has already been obtained by other methods in [6], and then again in [5]. However, the derivation in the present paper makes clear the parallelism inherent in the effect of an inclusion on the average

diffusion coefficient and on the reactivity: both quantities may be expressed as a perturbation of the neutron flux. For the case of cylinders, the relation between the quantity $\varepsilon B_\perp^2 \delta\Sigma_{tr}$ and the effective change in transport cross section, i.e., with the diffusional resistance to the neutron flux, is most easily seen by comparing Eqs. (14) and (19). A row of cylinders set along the y axis produces the same jump in the neutron flux as a plane layer of the same material, if the volume of the cylinders, multiplied by the coefficient $B_\perp^2$, is equal to the volume of the layer. If there is a series of layers and of rows of cylinders equivalent to them, the mean diffusion coefficients in these cases will be the same, since it is determined by the ratio of the neutron flux to the average gradient, i.e., the ratio of the gradient in the space between the layers to the sum of the flux jumps and the flux changes between layers.

LITERATURE CITED

1. D. Behrens, Proc. Phys. Soc., A 62, 607 (1949).
2. C. Carter, J. Nucl. Energy, parts A/B, 15, No. 2/3, 76 (1961).
3. N. I. Laletin, Transactions of the Second International Conference on the Peaceful Uses of Atomic Energy (Geneva, 1958). Papers by Soviet scientists, Vol. 2 [in Russian] Atomizdat, Moscow (1959) page 634.
4. P. Benoist, Rapport S. P. M. No. 522 (1958).
5. A. D. Galanin, Atomnaya Énergiya, 9, No. 2, 89 (1960).
6. Ya. V. Shevelev and V. S. Osmachkin, Transactions of the Second International Conference on the Peaceful Uses of Atomic Energy (Geneva, 1958). Papers by Soviet scientists, Vol. 2 [in Russian] Atomizdat, Moscow (1959) chapter 3, page 464.
7. D. Leslie, J. Nucl. Energy, parts A/B, 16, 1 (1962).
8. Peshkhagen, Materials from the International Conference on the Peaceful Uses of Atomic Energy (Geneva, 1959). Vol. 5, Part IV, A. M. [in Russian] Academy of Sciences Press, USSR (1958) page 306.
9. E. Gritoph and R. Pearce, J. Nucl. Energy, 4, 445 (1957).
10. J. Chernick and J. Kaplan, J. Nucl. Energy, 2, 41 (1955).
11. Ya. V. Shevelev, Atomnaya Énergiya, II, No. 3, 224 (1957).
12. C. Carter and R. Jarvis, J. Nucl. Energy, parts A/B, 15, No. 2/3, 113 (1961).
13. L. Trlifai, Atomnaya Énergiya, II, No. 3, 231 (1957).

All abbreviations of periodicals in the above bibliography are letter-by-letter transliterations of the abbreviations as given in the original Russian journal. *Some or all of this periodical literature may well be available in English translation.* A complete list of the cover-to-cover English translations appears at the back of this issue.

BOUNDARY CONDITIONS FOR THE SOLUTION OF BOLTZMANN'S EQUATION IN PERIODIC LATTICES

G. Ya. Rumyantsev

Translated from Atomnaya Énergiya, Vol. 14, No. 4,
pp. 371-374, April, 1963.
Original article submitted May 31, 1962.

A generalization is made of the methodological approach to the solution of the transport equations in heterogeneous periodic lattices, which was presented in the diffusion approximation in [1]. The boundary conditions at the outside surface of the cell are derived for making an accurate solution of the one velocity Boltzmann kinetic equations, which permits considering a single cell of the heterogeneous medium. A short discussion is given of methods of solving the problem with these boundary conditions and of the question of eigenvalues.

A general solution for the whole heterogeneous medium in accurate and macroscopic (averaged) form is made up of the special solutions found for a single cell, using the same principle as in [1].

The boundary conditions formulated for a plane one dimensional lattice may be extended to a two dimensional lattice.

Introduction

The approach described in [1] to a solution of the diffusion equation in periodic lattices and the rules for homogenizing lattices derived from it are quite general. However, the diffusion approximation there used for simplicity does not always lead to satisfactory results, which is especially true in calculating the effective macroscopic diffusion coefficients for different directions. In these problems, diffusion theory does not give a correct representation of the transition to a homogeneous medium, with the result that taking account of the heterogeneity, as is done in the diffusion approximation, may lead to an even greater error than simple homogenization without taking any account of the detailed neutron distribution, if the lattice spacing is small in comparison with the mean free path.

In the present paper, the methodological idea of [1] has been developed to apply to the accurate (one velocity) Boltzmann kinetic equation, and as a result accurate boundary conditions have been found which make it possible (as in the diffusion approximation) to limit the problem to the solution of the equation within a single cell.

Because of the generality of the boundary conditions, the methods of solving the kinetic equation may be chosen at will, depending on the accuracy required and practical convenience. The special solutions found for a single cell are used to obtain a general solution in the whole medium, and to calculate the characteristics of the homogenized medium in exactly the same way as was done in [1].

Derivation of Boundary Conditions

Consider a plain one dimensional lattice with spacing 2a. Let x be a coordinate read from the center of some cell in a direction perpendicular to the layers in the lattice, and let Ω be a unit vector in the direction of the neutron velocity. We shall look for the boundary conditions for the one velocity kinetic equation

$$\Omega_x \frac{\partial}{\partial x} F(x, \Omega_x) + \Sigma(x) F(x, \Omega_x) - \Sigma_s(x) \int_{4\pi} F(x, \Omega'_x) W(\mu_0)\, d\Omega' = 0, \tag{1}$$

which will permit limiting the discussion to a single cell of the medium.

It is not difficult to see that if $F(x, \Omega_x)$ is a solution of the equation, $F(-x, -\Omega_x)$ and $F(x+2na, \Omega_x)$, where n is a whole number, are also solutions (we will recall that $\mu_0 = \Omega_x\Omega'_x + \Omega_y\Omega'_y + \Omega_z\Omega'_z$). On the basis of this we can look for a solution in each cell of number k in the piece representation*:

$$F(x, \Omega_x) \equiv F(x_k + \xi, \Omega_x) = A_k F_s(\xi, \Omega_x) + B_k F_{as}(\xi, \Omega_x). \tag{2}$$

* The notation and terminology are the same as in [1].

The functions F_s and F_{as} are partial solutions with the following symmetry properties:

$$F_s(-\xi, -\Omega_x) = F_s(\xi, \Omega_x),$$
$$F_{as}(-\xi, -\Omega_x) = -F_{as}(\xi, \Omega_x). \tag{3}$$

It is now necessary to write the conditions for the continuity of the neutron flux at the boundary of two neighboring cells with the numbers $\underline{k}$ and $k+1$. It is more convenient to write the continuity conditions for the function $F(x, \Omega_x) + F(x, -\Omega_x)$ and $F(x, \Omega_x) - F(x, -\Omega_x)$ in the range $0 \leq \Omega_x \leq 1$, which is equivalent to the continuity condition of the function $F(x, \Omega_x)$ in the range $-1 \leq \Omega_x \leq 1$.

Using Eq. (2) and the properties (3), we write these conditions for the point $\xi = a$:

$$A_k[F_s(\Omega_x) + F_s(-\Omega_x)] + B_k[F_{as}(\Omega_x) + F_{as}(-\Omega_x)] = A_{k+1}[F_s(-\Omega_x) +$$
$$+ F_s(\Omega_x)] - B_{k+1}[F_{as}(-\Omega_x) + F_{as}(\Omega_x)], \; A_k[F_s(\Omega_x) - F_s(-\Omega_x)] + B_k[F_{as}(\Omega_x) -$$
$$- F_{as}(-\Omega_x)] = A_{k+1}[F_s(-\Omega_x) -$$
$$- F_s(\Omega_x)] - B_{k+1}[F_{as}(-\Omega_x) - F_{as}(\Omega_x)]. \tag{4}$$

By comparing the conditions (4) with the conditions written in [1] in the diffusion approximation, it is a simple matter to see the analogy between them, if the functions $F_s(\Omega_x) + F_s(-\Omega_x)$, $F_{as}(\Omega_x) + F_{as}(-\Omega_x)$, $F_s(\Omega_x) - F_s(-\Omega_x)$, and $F_{as}(\Omega_x) - F_{as}(-\Omega_x)$ are compared respectively with the functions Φ_s, Φ_{as}, Φ'_s, and Φ'_{as}. Thus, the results of [1] hold in the present problem. They consist of the following.

The equations of continuity are satisfied for any $\underline{k}$, if we set $A_k = C(x_k)$ and $B_k = aC'(x_k)$, where $C(x)$ is the solution of the equation

$$\frac{d^2}{dx^2} C(x) + \varkappa^2 C(x) = 0, \tag{5}$$

and the following boundary conditions are satisfied simultaneously at $\xi = a$:

$$F_{as}(\Omega_x) + F_{as}(-\Omega_x) = \frac{\operatorname{tg} \varkappa a}{\varkappa a}[F_s(\Omega_x) + F_s(-\Omega_x)],$$
$$F_s(\Omega_x) - F_s(-\Omega_x) =$$
$$= -\varkappa a \operatorname{tg} \varkappa a [F_{as}(\Omega_x) - F_{as}(-\Omega_x)]. \tag{6}$$

The equation (6) can only be satisfied for definite values of $\varkappa$, i.e., this parameter is an eigenvalue of the homogeneous problem. Replacing the solution F_{as} by F^*_{as}, which differs from the former in the normalization

$$F^*_{as}(\xi, \Omega_x) = \frac{\varkappa a}{\operatorname{tg} \varkappa a} F_{as}(\xi, \Omega_x), \tag{7}$$

we write the boundary conditions (6) in the form

$$F^*_{as}(\Omega_x) + F^*_{as}(-\Omega_x) = F_s(\Omega_x) + F_s(-\Omega_x),$$
$$F_s(\Omega_x) - F_s(-\Omega_x) = \lambda [F^*_{as}(\Omega_x) - F^*_{as}(-\Omega_x)] \tag{8}$$

where $\lambda = -\tan^2 \varkappa a$.

It is obvious that in solving the system of equations (8) the eigenvalues may be found as values of λ, which then give the values of $\varkappa$.

Eigenvalues and the Form of the General Solution

For practical purposes, the kinetic equation is always solved by some approximate method. Here, the conditions (8) must be satisfied to the same approximation in which the functions F_s and F^*_{as} are found. We shall consider the most useful methods of solving the kinetic equation.

Spherical Harmonic Method. In the P_N approximation of the spherical harmonic method [2-4], equations (8) must first be multiplied by Ω_x, and then solved approximately by means of spherical moments of order up to N inclusive in the segment $-1 \leq \Omega_x \leq 1$ (the need for multiplying by Ω_x is shown in [5]).

It is obvious that for the first conditon of (8) multiplied by Ω_x, only odd moments are nontrivial, while for the second condition, conversely, only even moments are nontrivial. As a result, each pair of moments of the functions

$\Omega_x F_s$ and $\Omega_x F_{as}$ will satisfy only one condition, depending on the parity. It may be shown in exactly the same way as was done in [5] that the system of conditions (8) in the P_N approximation will consist of N equations for N even, and of N+1 equations for N odd. Half of these will contain the parameter λ. Accordingly, the determinant of the system is a polynomial in λ of degree N/2 or (N+1)/2, depending on the parity of N, i.e., the number of eigenvalues will be the same as for a homogeneous medium.

The set of eigenvalues, $\varkappa_j$ (the sign is of no importance) is determined by the set of special solutions $F_s^{(j)}(\xi, \Omega_x)$, $F_{as}^{(j)}(\xi, \Omega_x)$ and the functions $C_j(x)$ corresponding to them. It is understood that each of the special solutions in the P_N approximation is the sum of spherical harmonics of order 0 to N inclusive, with the zero harmonic – the scalar neutron flux – being even in the $F_s^{(j)}$ solutions, but odd with respect to ξ in the $F_{as}^{(j)}$ solutions.

Discrete direction methods. In some numerical methods, such as for example Karlson's S_n method [2, 3], the Wick-Chandrasekhar method [3, 4] et al., the distribution function is only calculated for several discrete values of Ω_x. In this case, the conditions (8) need only be written for these values of Ω_x. It is obviously necessary for the segment $-1 \leq \Omega_x \leq 1$ to be divided symmetrically, i.e., each point Ω_{xl} must correspond with a point $-\Omega_{xl}$. If l takes on N values, the conditions (8) become a system of 2N equations.

In solving the kinetic equation, only the distribution of the neutrons incident on the medium can be fixed, in the present case, the set of values $F_s(a, -\Omega_{xl}) = m_l$, and $F_{as}(a, -\Omega_{xl}) = n_l$. The following reflection conditions hold in the central plane of the cell:

$$F_s(0, \Omega_x) = F_s(0, -\Omega_x),$$
$$F_{as}(0, \Omega_x) = -F_{as}(0, -\Omega_x). \tag{9}$$

The distribution of neutrons leaving the cell, i.e., the set of values $F_s(a, \Omega_{xl})$ and $F_{as}(a, \Omega_{xl})$ is expressed linearly in terms of the assembly of values of m_l and n_l. Thus, the conditions (8) will contain 2N unknowns, as many as there are equations. The determinant of the system of equations in λ will be a polynomial of degree N, and thus the number of eigenvalues of λ is also equal to N. Each value, λ_j, has its own set of values of m_{lj} and n_{lj}, its own value of $\varkappa_j$, and its own form for the function $C_j(x)$.

Of all the eigenvalues $\varkappa_j$, an especially important one is $\varkappa_1$, having the smallest modulus and corresponding to the asymptotic solution. There is some reason to assume that this is the only value for which all the values of m_{l_1} and n_{l_1} are positive.

It is probable that $\varkappa_1$ may be found by an iteration method, based on the fact that in practice we almost always have $|\varkappa_1| a \ll 1$. Naturally, the schemes discussed do not exhaust the possible methods of solving the kinetic equation in the present problem.

On the basis of the analogy between an homogenized medium and a truly homogeneous medium, it is to be expected that except for the asymptotic value $\varkappa_1$, which may be either real or imaginary, all the other values $\varkappa_j$ will be imaginary and will have moduli much greater than $\varkappa_1$. The conditions in the form (8) are not entirely convenient for finding these values, since the corresponding values of λ_j will be only slightly different from unity. This difficulty may be eliminated in the following way.

Let $\varkappa = i\varepsilon$, and

$$f(\xi, \Omega_x) = F_s(\xi, \Omega_x) + \varepsilon a F_{as}(\xi, \Omega_x).$$

Then conditions (6) may be written in the form

$$f(-a, \Omega_x) = e^{-2\varepsilon a} f(a, \Omega_x),$$
$$-1 \leqslant \Omega_x \leqslant 1. \tag{10}$$

In this form, the boundary conditions are a generalization of the conditions used in [6, 7].

The even and odd solutions are constructed from the solution $f(\xi, \Omega_x)$ in the following way:

$$F_s(\xi, \Omega_x) = \frac{1}{2}[f(\xi, \Omega_x) + f(-\xi, -\Omega_x)],$$
$$F_{as}(\xi, \Omega_x) = \frac{1}{2\varepsilon a}[f(\xi, \Omega_x) - f(-\xi, -\Omega_x)]. \tag{11}$$

After having found the complete set of eigenvalues and solutions, the general solution for the entire heterogeneous medium may be written in the form:

$$F(x, \Omega_x) = \sum_j [C_j(x_k) F_s^{(j)}(\xi, \Omega_x) + aC_j'(x_k) F_{as}^{(j)}(\xi, \Omega_x)], \tag{12}$$

where $F_s^{(j)}$ and $F_{as}^{(j)}$ are, depending on the method, represented as a sum of spherical harmonics, a set of discrete values, or in some other way. Each of the functions $C_j(x)$ contains two arbitrary coefficients, the values of which are determined by the conditions on the external boundaries of the medium, the requirements of boundedness, symmetry, etc., in other words, by the macroscopic properties of the solution.

The integral of the expression (12) over the total solid angle gives the global neutron flux as a function of the x coordinate:

$$\Phi(x) = \sum_j [C_j(x_k) \Phi_s^{(j)}(\xi) + aC_j'(x_k) \Phi_{as}^{(j)}(\xi)]. \tag{13}$$

The macroscopic dependence of the flux on the x coordinate is of the following form:

$$\bar{\Phi}(x) = \sum_j \langle \Phi_s^{(j)} \rangle \frac{\varkappa_j a}{\sin \varkappa_j a} C_j(x), \tag{14}$$

where $\langle \Phi_s^{(j)} \rangle$ is the mean value of the function $\Phi_s^{(j)}(\xi)$ on the segment $-a \leq \xi \leq a$.

In a similar way, exact and macroscopic expressions may be obtained for the other spherical moments of the distribution function, from a comparison of which it is possible in principle to find the various homogenized characteristics of the medium, including those which do not occur in elementary diffusion theory.

Generalization of the Results

So far, the homogeneous problem has been under discussion, but the basic relationships obtained also hold for the problem with a source, under the condition that the distribution function for the sources in the medium is represented in a form analogous to (12). The transition to the inhomogeneous problem is described in [1]. Using the exact kinetic equation does not introduce any essential difficulties in this respect. It may be pointed out once again that in the special solutions of the inhomgeneous equation, the parameter $\varkappa$ is fixed. The system of equations to which the conditions (8) or (10) reduce will be inhomogeneous, so that the question of finding the eigenvalues does not arise here. The results are readily applied to two dimensional lattices, if the cells are rectangular.

Let the lattice spacing in the x and y directions be 2a and 2b respectively. A solution may be looked for with macroscopically separating variables, i.e., in the form

$$F(x, y, \Omega_x, \Omega_y) = X(x_n) Y(y_m) F_{00} + aX'(x_n) Y(y_m) F_{10} + bX(x_n) Y'(y_m) F_{01} + abX'(x_n) Y'(y_m) F_{11}, \tag{15}$$

where x_n and y_m are the coordinates of the center of the cell of number nm, while F_{00}, F_{10}, F_{01}, and F_{11} are special solutions having the following symmetry properties:

$$\begin{aligned}
F_{00}(\xi, \eta, \Omega_x, \Omega_y) &= F_{00}(-\xi, \eta, -\Omega_x, \Omega_y) = F_{00}(\xi, -\eta, \Omega_x, -\Omega_y),\\
F_{10}(\xi, \eta, \Omega_x, \Omega_y) &= -F_{10}(-\xi, \eta, -\Omega_x, \Omega_y) = F_{10}(\xi, -\eta, \Omega_x, -\Omega_y),\\
F_{01}(\xi, \eta, \Omega_x, \Omega_y) &= F_{01}(-\xi, \eta, -\Omega_x, \Omega_y) = -F_{01}(\xi, -\eta, \Omega_x, -\Omega_y),\\
F_{11}(\xi, \eta, \Omega_x, \Omega_y) &= -F_{11}(-\xi, \eta, -\Omega_x, \Omega_y) = -F_{11}(\xi, -\eta, \Omega_x, -\Omega_y).
\end{aligned} \tag{16}$$

Here ξ and η are the running coordinates read from the center of the cell in question. The functions X(x) and Y(y) are solutions of the equations

$$\begin{aligned}
\frac{d^2}{dx^2} X(x) + \alpha^2 X(x) &= 0,\\
\frac{d^2}{dy^2} Y(y) + \beta^2 Y(y) &= 0.
\end{aligned} \tag{17}$$

The solution in the form (15) makes it possible to formulate the conditions on the cell boundaries according to the same principle as was used in the present paper for the one dimensional problem.

In solving the two dimensional problem, there are, in the majority of cases, some simplifying conditions:

1. Rectangular cells are usually square, i.e., a = b.

2. The most interesting solution is most often the asymptotic inhomogeneous solution, for which the values of αa and βb are nearly zero.

3. It is sufficient for many practical purposes to find only the effective macroscopic parameters of the homogenized medium, so as to proceed to a macroscopic discussion of the problem. It is sufficient for this to have simply the averaged values of the functions F_{00}, F_{10}, F_{01}, and F_{11} at the sides of the cell. If a P_N approximation of not very high order is used here, it is comparatively easy to solve the two dimensional problem. An example of a calculation for nonabsorbing cells in the P_2 approximation is given in [8].

Something, in particular, that can be reduced to finding the solution in the form (15) is the problem of the effective macrscopic parameters when neutrons are diffusing at different angles to the axes of the lattice.

LITERATURE CITED

1. G. Ya. Rumyantsev, Atomnaya Énergiya, 13, No. 6, 556 (1962).
2. G. I. Marchuk, Methods of calculating nuclear reactors [in Russian] Gosatomizdat, Moscow (1961).
3. A. Weinberg and E. Wigner, Physical theory of nuclear reactors [Russian translation] IL, Moscow (1961).
4. B. Davison, Neutron transport theory, Atomizdat, Moscow (1960).
5. G. Ya. Rumyantsev, Atomnaya Énergiya, 10, No. 1, 26 (1961).
6. B. I. Spinrad, J. Appl. Phys., 26, 548 (1955).
7. Ya. V. Shevelev, Atomnaya Énergiya, 2, No. 3, 224 (1957).
8. G. Ya. Rumyantsev, The spherical harmonic method and neutron transport theory in the P_2 approximation, Dissertation, MIFI, (1961).

All abbreviations of periodicals in the above bibliography are letter-by-letter transliterations of the abbreviations as given in the original Russian journal. *Some or all of this periodical literature may well be available in English translation.* A complete list of the cover-to-cover English translations appears at the back of this issue.

CORROSION RESISTANCE OF STAINLESS CHROME – NICKEL STEELS IN SODIUM AS A FUNCTION OF ITS OXYGEN CONTENT

Georgi Ilincev

G. V. Akimov State Scientific Research Institute for the Preservation of Materials, Prague, Czechoslovak Soviet Socialist Republic

Translated from Atomnaya Énergiya, Vol. 14, No. 4, pp. 375-382, April, 1963
Original article submitted May 9, 1962

The article describes an experimental apparatus for studying the corrosion resistance of construction materials in circulating liquid sodium, as well as methods for the continuous removal of oxides from the sodium by means of porous metal filters and for the determination of its oxygen content. It describes the results of corrosion experiments and measurements of mechanical properties performed on six brands of stainless steel, specimens of which were placed in sodium containing $3 \cdot 10^{-3}$% and $(4-5) \cdot 10^{-2}$% oxygen at a temperature of 550° C. The flow rate was 1.5 m/sec. The results of the corrosion experiments indicate that the corrosion rate of Type 18Cr8Ni stainless steels in sodium containing as much as $(4-5) \cdot 10^{-2}$% oxygen does not exceed 21.3 mg/dm^2 per month; these steels are not subject to intergranular corrosion, and their mechanical properties remain virtually unchanged.

One of the basic problems in the use of liquid metals, particularly sodium and potassium, as coolants is the prevention of corrosion in the structural materials. The effect of alkali metals on structural materials at high temperatures and the factors which influence the corrosion of these materials have not yet been completely explained. Metals in liquid sodium are adversely affected by certain impurities present in the sodium, particularly oxygen and carbon. Oxygen, even in very small quantities, increases the solubility of the structural materials and accelerates the mass transfer [1, 2]. Thus, for example, the solubility of iron is considerably increased as the oxygen content increases [3]. Practically no data exist concerning the solubility of other elements found in steel (chromium, nickel, etc.). Carbon may cause carburization of the surfaces of these materials, which results in poorer mechanical properties [4, 5].

Most of the corrosion studies on structural steels in sodium containing various amounts of oxygen which are described in the literature were performed under static conditions [1,6], and the corrosion resistance of the materials was determined only on the basis of weight changes and metallographic analysis of the specimens. Reference [5] describes a study of the changes in the mechanical properties and structure of specimens of two brands of stainless steel (1Cr18Ni9Ti and Cr18Ni12Mo2Ti) after corrosion tests under dynamic conditions in sodium containing $(7-8) \cdot 10^{-3}$% and $2 \cdot 10^{-2}$% oxygen. The authors of that study found that the mechanical properties of the steels after the corrosion tests were considerably worse, especially after tests in sodium with a high oxygen content, while the elongation per unit length of the specimens in tension was practically zero.

The purpose of the present study is to obtain experimental data on the corrosion resistance of stainless chrome-nickel steels in liquid sodium as a function of its oxygen content. For this purpose we performed dynamic corrosion tests under conditions approaching those found in the operation of power stations.

Experimental Apparatus for Conducting the Dynamic Corrosion Tests

The corrosion tests on the stainless steels investigated were made in the high-temperature loop of a pilot installation (Figs. 1 and 2) with forced circulation of sodium [7]. The loops and all parts in contact with the sodium were made of brand 17246 stainless steel (1Cr18Ni9Ti). The working volume of the loop is approximately 10 liters. The apparatus includes a low-temperature loop (4) and a high-temperature loop (12); the heat transfer between these is effected by means of a countercurrent heat exchanger (11). The low-temperature loop is connected to an overflow tank and a tank for filling the loop (1), a main expansion tank (6), a filtration loop (8), and an analyzer (15) to measure the Na_2O content. This loop also includes an electromagnetic pump (9). The high-temperature

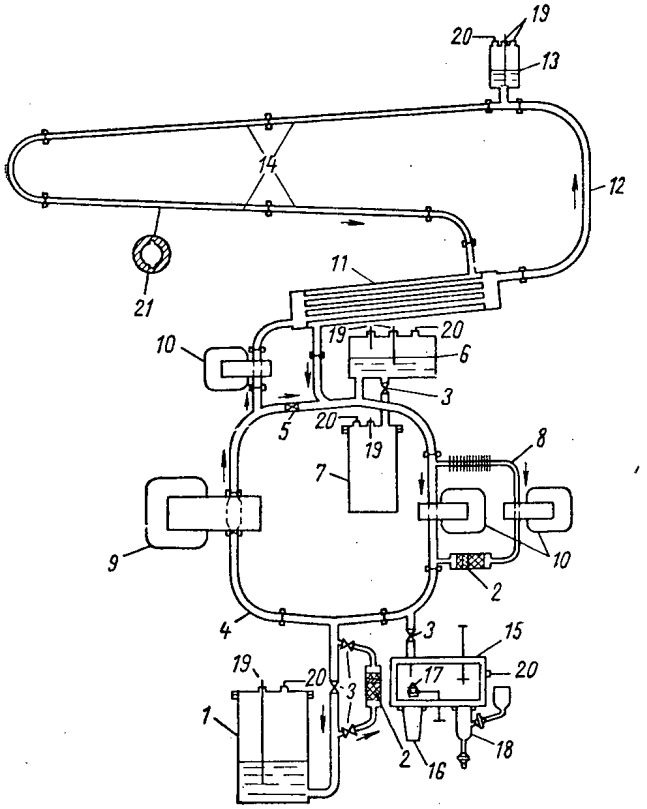

Fig. 1. Diagram of the experimental sodium loop for studying the corrosion resistance of structural materials: 1) Overflow tank and tank for filling the loop; 2) filters; 3) and 5) valves; 4) low-temperature loop; 6) expansion tank; 7) overflow tank; 8) filtration loop; 9) electromagnetic pump; 10) electromagnetic flow meters; 11) regenerative metal-metal heat exchanger; 12) and 13) heater and small expansion tank of high-temperature loop; 14) segment containing the specimens; 15) Na_2O analyzer; 16) cup for overflow of sodium; 17) cup for taking sodium specimens; 18) mercury extractor; 19) level indicators; 20) argon-vacuum lines; 21) slots for placing experimental specimens.

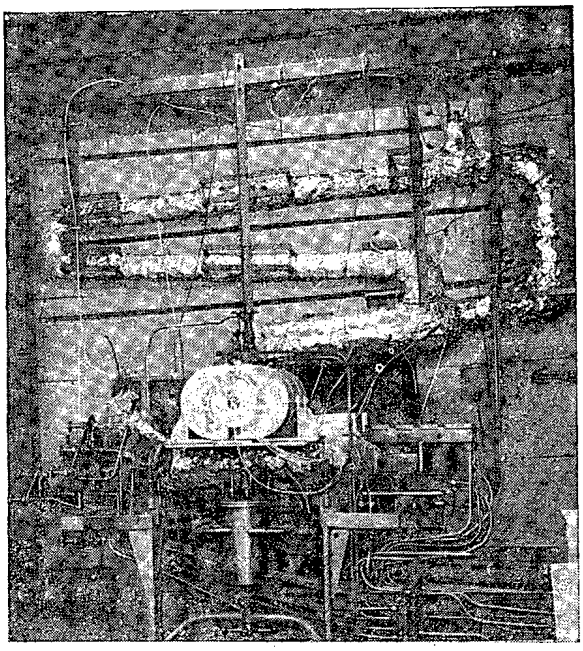

Fig. 2. Experimental sodium loop.

loop consists of a heater (12), a small auxiliary expansion tank (13), and a segment (14), in which the test specimens are placed.

The apparatus was operated for a long time at a temperature of 550 ± 5°C in the high-temperature loop and 400-420°C in the low-temperature loop. The rate of circulating sodium in the loop containing the test specimens was kept at 430 liters/hour (a velocity of 1.5 m/sec), and the rate in the low-temperature loop was kept at about 1000 liters/hour. The oxygen content of the sodium was $3 \cdot 10^{-3}$%. The sodium flow in the two loops was regulated by a valve (5).

The corrosion tests using high oxygen content $(4-5) \cdot 10^{-2}$% were made on a similar apparatus but without a high-temperature loop; moreover, the basic low-temperature loop was connected to an expansion tank through which all of the circulating sodium passed [8]. The loop was also connected to a small loop containing the test specimens. The circulation rate and temperature of the sodium were 1.5 m/sec and 550 ± 5°C, respectively, as in the previous case.

For added safety, the two experimental installations were operated from control panels in adjacent rooms.

Removal of Oxides from the Sodium

After the internal surfaces of the loops were degreased and cleaned, both test setups were charged with sodium. Before charging, the sodium was kept at 400-450°C for several days and was passed through porous filters made of stainless steel, with pore dimensions of 5-10 μ at a temperature of 130-150°C to remove the oxides and carbon.

During the corrosion tests the required concentration of oxygen was maintained by continuously-operating filtration loops. In the unit with a $3 \cdot 10^{-3}$% oxygen concentration in the sodium the filtration took place at a temperature of 150-200°C. In the second unit, with the higher oxygen concentration, $(4-5) \cdot 10^{-2}$%, the filtration of the sodium took place at 390-430°C, and sodium peroxide was added periodically, so that the cold trap always contained a sufficient amount of oxides.

The tests showed that the flow rate should not exceed 3-4 mm/sec, and a considerable amount of oxides will also be removed from the trap [9].

During the corrosion tests, especially in the case using high oxygen content, a small amount of carbon was also deposited on the filters; this had been formed by the interaction of the sodium with the surface of the steel.

Determining the Oxygen Content of the Sodium

The task of obtaining exact results in the study of the corrosive effect of sodium on structural materials is made more difficult by the necessity of precisely determining even small amounts of oxygen present in the sodium. The oxygen content in both units was checked by the amalgamation method [10]. The sodium samples were taken and extracted by means of a special analyzer, which is schematically illustrated in Fig. 1. Maximum accuracy in the determination of very low percentages of oxygen in the sodium requires the establishment of an absolutely pure inert medium when the sodium samples are taken and amalgamated. For that reason the small amount of oxygen (about 0.01%) was removed from the industrial argon by means of a refining apparatus in which the reaction medium was sodium heated to 400-420° C. A reaction column 1500 mm high was filled with sodium, using a metal wire rammer, to two-thirds of its height. The upper, unheated, part of the column contained a sodium vapor separator, consisting of a perforated sheet iron cylinder about 150 mm high, also filled by means of a metal rammer and hung from the cover of the column. The argon was purified at a pressure of 0.2-0.4 atmospheres; when the analyzer was charged, the argon flow rate varied between 0.4 and 0.6 liters/minute. Before we took the samples, the unit was evacuated four or five times and washed with purified argon. The samples were taken at a low argon pressure after a certain amount of sodium (50-100 cm^3) had overflowed into a metal cup (16). The purity of the inert medium was considered satisfactory if, after the overflow, the metallic luster of the surface of the drop was retained for several minutes. A 1 gram sample of sodium was taken in a small glass cup (17); after solidifying, the sample was transported by a special mechanism to the glass extractor (18). The amalgamation of the sodium was carried out at a very slow rate. We then added 40-50 cm^3 of mercury; the extractor containing the amalgam was heated to about 60° C, and a rod with a perforated stainless steel plate attached to the end was used to stir the amalgam until it was completely dissolved. In most cases, after five or six such extractions all the oxides were removed from the sodium. The amounts of sodium and oxygen were determined thereafter by the usual analytical methods [1, 10]. The results of our measurements of the solubility of oxygen in sodium at various temperatures are in good agreement with data published earlier [1, 2]:

Temperature of filtration loop, °C	Oxygen content of the sodium, % by weight
160	$2.8 \cdot 10^{-3}$
170	$2.9 \cdot 10^{-3}$
180	$3.4 \cdot 10^{-3}$
400	$4.9 \cdot 10^{-2}$
420	$5.3 \cdot 10^{-2}$
440	$6.0 \cdot 10^{-2}$

The accuracy in determining small percentages of oxygen is about $\pm 5 \cdot 10^{-4}$%.

Corrosion Resistance of Stainless Steels

We investigated the effect of chromium, nickel, and other elements (carbon, molybdenum, titanium, niobium, and manganese) on the corrosion resistance of chrome-nickel stainless steels; the chemical compositions are shown in Table 1. The stainless steel of type 1Cr18Ni9 investigated included two brands with differing carbon content (0.08 and 0.12%).

TABLE 1. Chemical Composition of Chrome-Nickel Stainless Steels Tested

Number of specimen	Brand of steel	Elements, %								
		C	Mn	Si	Cr	Ni	Mo	Nb	Ti	N_2
1	1Cr18Ni9(17241)	0,08	0,28	0,33	18,15	8,50	—	—	—	—
2	1Cr18Ni9Ti (17246)	0,09	0,56	0,45	18,40	8,55	—	—	0,17	—
3	1Cr18Ni9(17241)	0,12	0,45	0,42	17,67	9,70	—	—	—	—
4	Cr18Ni12Mo2Ti(17347)	0,07	0,44	0,36	16,93	9,45	2,60	—	0,71	—
5	Cr18Ni9Nb(N7247)	0,08	0,95	0,43	17,40	10,00	—	0,88	—	—
6	Cr18Ni10Mo2Nb(N7348)	0,08	0,50	0,75	18,17	10,10	2,65	1,06	—	—
7	1Cr18Ni5Mn7(AKM)	0,07	8,20	1,00	17,48	5,00	—	—	—	0,15

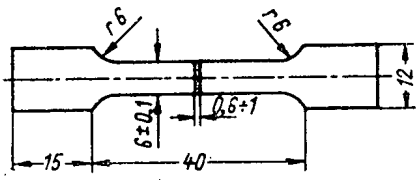

Fig. 3. Specimens for determining mechanical properties.

Specimens of all the test materials, in the form of well-polished strips 0.6-0.8 mm thick, were placed in the slots (21)(see Fig. 1) of the test loops. By using these specimens, we were able to perform a complex determination of the corrosion resistance of the materials both by the method of weighing and metallographic study of the structure and by determining the mechanical properties. Welded seams were tested on thin sheet metal specimens welded by electric arc using a special electrode or in an inert medium with an electrode of the same material. On one side of the sheet the welded seams were polished until a smooth surface was obtained, while on the other side they were only cleaned superficially.

The original structure and mechanical properties of the materials and seams were determined after heat treatment at 550° C for 750 hours in an inert medium. The mechanical properties of the steels tested, before and after the corrosion tests, were determined for flat rupture-test specimens (Fig. 3).

Corrosive Effect

The weighing and metallographic estimates of the corrosive deterioration of the chrome-nickel steels tested in sodium containing $3 \cdot 10^{-3}$% oxygen indicated (Table 2) that the corrosion of these materials at 550° C is very slight (maximum 4 mg/dm^2·month). All the specimens retained their original luster, except for a specimen of 1Cr18Ni5Mo7 steel, the surface of which became somewhat dull and in which a relatively high corrosion rate (11.2 mg/dm^2·month) was observed.

TABLE 2. Corrosion of Steels in Sodium Containing $3 \cdot 10^{-3}$% Oxygen at 550° C after 1280 Hours

Number of specimen	Brand of steel	Corrosion rate, mg/dm^2·month	Results of tests
1	1Cr18Ni9(0.08% C)	3.2	No corrosion observed. Surface of specimen retained its original luster
2	1Cr18Ni9Ti	4.0	Same
3	1Cr18Ni9(0.12% C)	3.8	Maximum depth of corrosion: to 5 μ. Surface of specimen retained its original luster
4	Cr18Ni12Mo2Ti	2.9	No corrosion observed. Surface of specimen retained luster
5	Cr18Ni9Nb	3.2	Same.
6	Cr18Ni10Mo2Nb	3.0	Same
7	1Cr18Ni5Mn7	11.2•	Depth of corrosion: to 10 μ. Surface of specimen became somewhat dull.

• Corrosion tests lasted 2030 hours.

A change in rate was found in the steel specimens after corrosion tests in sodium containing $(4-5) \cdot 10^{-2}$% oxygen (Table 3). The weight was found to have increased in specimens of steels containing a relatively large amount of chromium or manganese. The high chemical affinity of these materials for carbon produced a very small degree of carburization of the surfaces.

In steels alloyed with molybdenum or containing a smaller amount of chromium (specimens 3-6), we found a decrease in rate approximately five to ten times as great as after the corrosion tests in sodium with a low oxygen content. No carburized layer was formed on the surface of these specimens.

The corrosion of the steels tested at the indicated oxygen concentrations in the sodium was quite small (maximum 5-10 μ), and none of these steels exhibited intercrystalline corrosion (Fig. 4). It can be seen from Fig. 5 that corrosion accompanied by a decrease in weight follows an almost linear law.

The effect of individual alloy elements (molybdenum, titanium, niobium) on the corrosion resistance of the materials tested in sodium at 550° C is not sufficiently clear, and the corrosion was approximately the same for most of the steels.

The estimate of weight changes and the metallographic analyses indicated no substantial difference between the corrosion rate of welded seams and that of the basic materials tested in sodium containing oxygen at concentrations up to $(4-5) \cdot 10^{-2}$%. However, seams welded in an inert medium with an electrode of the same material were corroded less than seams obtained by using a special electrode.

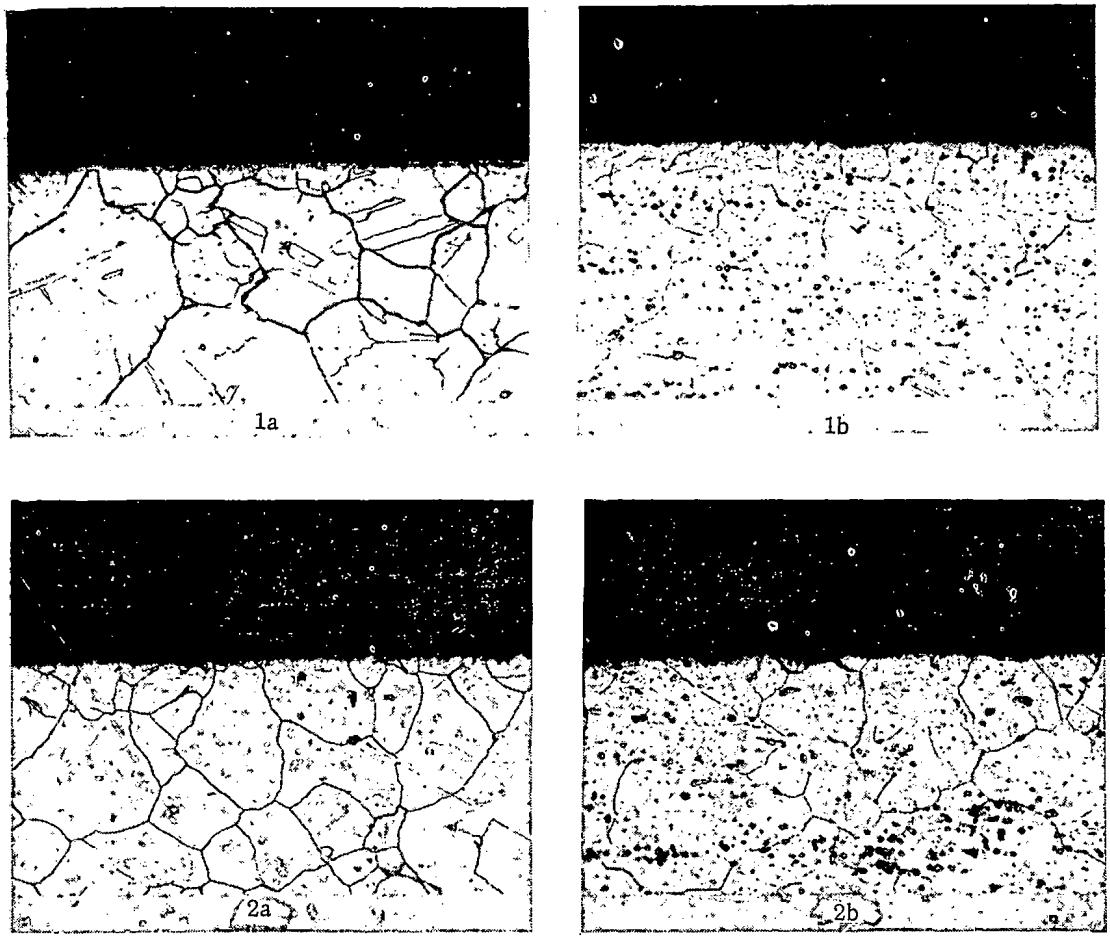

Fig. 4. Microphotographs of steels after corrosion tests in sodium containing $3 \cdot 10^{-3}$% oxygen for 2030 hours (1) and in sodium containing $(4-5) \cdot 10^{-2}$% oxygen for 1880 hours (2) at 550° C (electrolytically etched with 10% $H_2C_2O_4$ (×250): a) 1Cr18Ni9Ti; b) Cr18Ni12Mo2Ti.

Change in Mechanical Properties

The mechanical properties of the steels were tested on flat rupture-test specimens. The resulting values of σ_b, the ultimate strength, and δ, the elongation per unit length, for the materials tested after heat treatment and corrosion in sodium having different values of oxygen content are shown in Tables 4 and 5, from which it can be seen that the effect of sodium containing either $3 \cdot 10^{-3}$% or $(4-5) \cdot 10^{-2}$% oxygen has practically no effect on the

TABLE 3. Corrosion of Steels in Sodium Containing $(4-5) \cdot 10^{-2}$% Oxygen at 550° C after 1150 and 1880 Hours

Number of specimen	Brand of steel	Corrosion rate, mg/dm²·month		Results of tests
		After 1150 hrs.	After 1880 hrs.	
1	1Cr18Ni9(0.08% C)	+10.8	+7.1	No corrosion observed. A lustrous brownish-black coating was found on the surface of the specimen
2	1Cr18Ni9Ti	+12.5	+10.0	Same
3	1Cr18Ni9(0.12% C)	-0.6	-1.0	No corrosion observed. Surface of specimen gray, slightly dull
4	Cr18Ni12Mo2Ti	-21.3	-19.4	Depth of corrosion: to 5-10 μ. Surface of specimen was pale gray, slightly dull
5	Cr18Ni9Nb	-14.7	-17.0	Same
6	Cr18Ni10Mo2Nb	—	-11.8	Same
7	1Cr18Ni5Mn7	—	+5.9	No corrosion observed. Surface of specimen was brownish-black and lustrous

TABLE 4. Mechanical Properties of Steels after Corrosion Tests in Liquid Sodium Containing $3 \cdot 10^{-3}$% Oxygen

Number of specimen	Brand of steel	Thickness of specimen (mm)	After heat treatment in inert medium at 550° C for 750 hours		After tests in circulating sodium at 550° C					
					750 hours		1280 hours		2030 hours	
			σ_b, kg/mm^2	δ, %	σ_b, kg/mm^2	δ, %	σ_b, kg/mm^2	δ, %	σ_b, kg/mm^2	δ, %
1	1Cr18Ni9 (0,08% C)	0,63	63,1	61,7	63,7	61,0	64,0	58,6	64,7	57,8
2	1Cr18Ni9Ti	0,72	65,6	60,6	67,6	57,3	68,2	56,6	68.4	54,2
3	1Cr18Ni9 (0,12% C)	0,70	65,5	54,6	69,3	50,0	69,9	45,5	71,7	44,5
4	Cr18Ni12Mo2Ti	0,86	65,7	46,3	66,2	45,0	65,5	45,5	65,8	44,4
5	Cr18Ni9Nb	0,73	60,8	51,9	60,9	49,6	60,8	48,0	60,9	50,3
6	Cr18Ni10Mo2Nb	0,73	69,0	47,2	—	—	—	—	69.4	42,0
7	1Cr18Ni5Mn7	0,78	80,4	44,0	—	—	—	—	78,5	40,3

mechanical properties of stainless steels. The most noticeable changes in the mechanical properties are observed in 1Cr18Ni9 steel with a high percentage of carbon (0,12%) and in 1Cr18Ni5Mn7 steel. It may be that even these relatively small changes in mechanical properties are caused not only by the effect of the sodium but also by changes in the structure (chiefly separation of $Me_{23}C_6$ carbides at the grain boundaries) resulting from the fact that the tested materials were subjected to longer heat treatment than the calibration specimens.

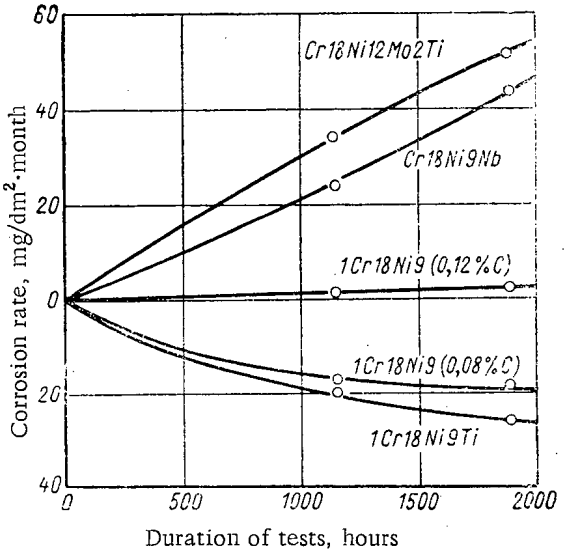

Fig. 5. Corrosion of steel in sodium containing (4-5)·$\cdot 10^{-2}$% oxygen at 550° C, as a function of time.

Conclusions

The results of a general survey of the above mentioned corrosion tests on chrome-nickel steels at 550° C indicate that:

1) If the oxygen content of the sodium does not exceed the solubility limit, there is no intergranular corrosion.

2) The corrosion rate in the steels calculated from the loss of weight in sodium containing $3 \cdot 10^{-3}$% and (4-5)·$\cdot 10^{-2}$% oxygen is relatively slow and does not exceed 1 and 4 μ/year, respectively.

3) The considerable deterioration observed earlier [5] in the mechanical properties of stainless chrome-nickel steels under the effects of sodium, especially with high oxygen content ($2 \cdot 10^{-2}$%), was not corroborated. The tests indicated that the deterioration in mechanical properties of 18Cr8Ni type stainless steels after corrosion in

TABLE 5. Mechanical Properties of Steels after Corrosion Tests in Liquid Sodium Containing (4-5)·10^{-2}% Oxygen

Number of specimen	Brand of steel	Thickness of specimen (mm)	After heat treatment in inert medium at 550° C for 750 hours		After testing in circulating sodium at 550° C					
					730 hours		1150 hours		1880 hours	
			σ_b, kg/mm^2	δ, %	σ_b, kg/mm^2	δ, %	σ_b, kg/mm^2	δ, %	σ_b, kg/mm^2	δ, %
1	1Cr18Ni9 (0,08% C)	0,63	63,1	61.7	64,0	61,2	62,6	61,5	63,3	60,0
2	1Cr18Ni9Ti	0,72	65,6	60,6	65,8	57,8	64,3	58,8	65,6	56,3
3	1Cr18Ni9(0,12% C)	0,70	65,5	54,6	—	—	66,1	51,9	67,6	50,1
4	Cr18Ni12Mo2Ti	0,86	65,7	46,3	—	—	65,4	45,0	67,3	43,3
5	Cr18Ni9Nb	0,73	60,8	51,9	51,3	51.4	60,8	52,0	61,7	50,7
6	Cr18Ni10Mo2Nb	0,73	69,0	47,2	—	—	—	—	69,9	46,3
7	1Cr18Ni5Mn7	0,78	80,4	44,0	—	—	—	—	81,3	35,7

sodium containing up to $(4-5)\cdot10^{-2}$% oxygen is relatively small and cannot cause damage in stainless steel units in which sodium is used as the coolant.

LITERATURE CITED

1. Liquid Metal Coolants [in Russian], Collection of articles collected by A. E. Sheindlina, Izd-vo inostr. lit., Moscow (1958).
2. Nuclear Reactors, Vol. II (Nuclear Reactor Engineering) [Russian translation]. Materials of the United States Atomic Energy Commision, Izd-vo inostr. lit., Moscow (1957), page 227.
3. R. Baus et al., Proceedings of the International Conference on the Peaceful Uses of Atomic Energy (Geneva, 1955) [Russian translation], Vol 9, Goskhimizdat, Leningrad (1958), page 438.
4. E. Hoffman and W. Manly, Problems in Nuclear Engineering, V.I.N.Y., Pergamon Press (1957), page 128.
5. V. S. Lyashenko et al., Proceedings of the Second International Conference on the Peaceful Uses of Atomic Energy (Geneva, 1958) [in Russian], Reports of Soviet Scientists, Vol. 3, Atomizdat, Moscow (1959), page 642.
6. E. Brush, Construction Materials for Liquid Sodium System, Corrosion II, June 1955, page 229 t.
7. G. Ilincev, J. Chalupa, and Z. Kubista, Obehove zarizeni pro korozni zkousky materialu v proudicich roztavenych kovech, SVUOM 22/1959.
8. J. Chalupa, Vyvoj zarizeni pro zkouseni koroze materialu roztavenymi kovy, SVUOM 22/58.
9. P. L. Kirillov et al., Atomnaya Énergiya, Vol. 8, No. 1, p. 30 (1960)
10. L. Pepkowitz and W. Judd, Analyt. Chem., 22, 1283 (1950).

All abbreviations of periodicals in the above bibliography are letter-by-letter transliterations of the abbreviations as given in the original Russian journal. *Some or all of this periodical literature may well be available in English translation.* A complete list of the cover-to-cover English translations appears at the back of this issue.

COMPLEXING REACTIONS IN URANIUM CHEMICAL TECHNOLOGY

I. I. Chernyaev and G. V. Ellert

Translated from Atomnaya Énergiya, Vol. 14, No. 4,
pp. 383-394, April, 1963
Original article submitted May 19, 1962

On the basis of current data on the chemistry of uranium coordination compounds, the present article discusses complexing reactions employed in the principal chemical processing operations on uranium-bearing materials. It is shown that the overwhelming majority of dissolution, precipitation, and extraction reactions involving uranium compounds are reactions involving the formation of uranium complexes. New ideas are expressed on the mechanism involved in some dissolution, precipitation, and extraction reactions involving uranyl compounds.

The scope of this article is restricted to a discussion of the complexing reactions employed in the principal chemical processing operations.

As is widely known, the overwhelming majority of major chemical operations in the processing of uranium-bearing products takes place between aqueous solutions of salts or between aqueous and organic phases, with the participation of water molecules. In uranium production technology, a group of pyrochemical techniques (fused-metal and fused-salt extraction, oxidative slagging, etc.) are also employed. Although the decisive factors in many stages of pyrochemical processes are complexing reactions, e.g. in the interaction between uranium salts and fused salts of alkali metals and alkali earths, they will not be under discussion in the remainder of the article.

The chemical reactions in uranium technology (predominantly in the technology of hexavalent uranium) belonging to the class of "wet processes" may be subdivided into two principal subclasses: reactions involving precipitation of uranium compounds and dissolution reactions; despite the already known analogy of the processes, e.g. of dissolution and extraction, the chemical processes inherent in extraction and sorption will be discussed apart from dissolution and precipitation reactions in the further discussion.

Complexing Reactions in the Dissolution of Uranium Compounds

An analysis of uranium dissolution reactions reveals the high propensity of uranium to form complexes and bonds, preponderantly with oxygen-bearing molecules. The first consequence of this complexing proclivity is the fact that uranium metal, uranium oxides, and other uranium compounds difficultly soluble in water become subject with relative ease to the effects of not only oxygen-containing inorganic acids, but also such solvents as neutral and even basic oxygen-containing reagents. A second factor, not always given its due, is the exceedingly prominent role of water as a neutral ligand in the formation of uranyl complexes. With the foregoing discussion taken into account, we now consider several examples of uranium compounds going into solution.

The first stage of primary and secondary chemical processing is, as a rule, the dissolution of the uranium-bearing products (ores, uranium and thorium rods from plutonium reactors, various types of power-reactor fuel elements, solid by-products of the production of uranium and other materials) in sulfuric, nitric, hydrochloric, and hydrofluoric acids, sometimes with F^-, PO_4^{3-}, $Hg(NO_3)$, etc. as admixtures. As an example, consider in detail two reactions: the dissolution of uranium trioxide in sulfuric acid and the dissolution of uranium metal in nitric acid. The most common form, encountered in almost all monographs on uranium technology, for writing down these reactions is the following:

$$UO_3 + H_2SO_4 = UO_2SO_4 + H_2O, \quad (1)$$

$$2U + 3O_2 + 4HNO_3 = 2H_2O + 2UO_2(NO_3)_2, \quad (2)$$

i.e. as a result of the interaction between uranium trioxide and uranium metal with aqueous salts of sulfuric and nitric acids, uranyl sulfate anhydrate and uranyl nitrate anhydrate are formed. This formulation of the reactions does

not conform to the reality even in the case where Eqs. (1) and (2) are assumed to total. The trouble is that uranyl sulfate anhydrate may be obtained, e.g. by drying out the trihydrate at an elevated temperature, or else by evaporating the sulfate solution with concentrated sulfuric acid. In all the remaining cases, crystals which contain 3 gram-moles of water are formed, as a rule.

The job of isolating uranyl nitrate anhydrate is even more difficult. There are no entirely reliable indications or information (in fact, proof of the individuality of the product is even lacking) on the possibility of isolating $UO_2(NO_3)_2$ anhydrate by forming the intermediate compound $UO_2(NO_3)_2 \cdot 2NO_2$. Under ordinary conditions, the hexahydrate salt crystallizes out. At the present time, a fairly large body of experimental evidence has accumulated to justify the irrefutable statement that the so-called simple uranyl salts $UO_2SO_4 \cdot 3H_2O$, $UO_2(NO_3)_2 \cdot 6H_2O$ (and several others: $UO_2Cl_2 \cdot 3H_2O$, $UO_2Br_2 \cdot 3H_2O$, $UO_2C_2O_4 \cdot 3H_2O$, $UO_2(CH_3COO)_2 \cdot 2H_2O$, etc.) are typical complex compounds (e.g. [1]). For the hydrates of uranyl sulfate and uranyl nitrate, we may assume the existence of several genetically related complexes:

A	B
1. $[UO_2(H_2O)_6]^{++}SO_4$	1. $[UO_2(H_2O)_6]^{++}(NO_3)_2$
2. $[UO_2(H_2O)_4(SO_4)]^0$	2. $[UO_2(H_2O)_5(NO_3)]^+(NO_3)$
3. $[UO_2(SO_4)(H_2O)_3]^0_n$	3. $[UO_2(H_2O)_4(NO_3)_2]^0$
4. $[UO_2(SO_4)(H_2O)_2]^0$	4. $[UO_2(H_2O)_2(NO_3)_2]^0_n$.
5. $[UO_2(SO_4)(H_2O)]^0_n$	

Among these compounds, there are the cationic complexes A-1, B-1 and B-2, the neutral complex A-2, A-3, A-4, A-5, B-3 and B-4. For some of them, the analytic coordination number of which is not six, we assume not a chain configuration rather than a backbone configuration. The preferential formation of one complex or the other is decided by the concentrations of uranium and of the corresponding acid, and by the temperature. In dilute solutions of uranyl sulfate ($^1/_{500}$), the uranium is found preferentially in the form of the cation complex hexaaqueuranyl sulfate $[UO_2(H_2O)_6]SO_4$, which, for instance, is evidenced by the fact that the molar electrical conductivity of its aqueous solutions and, under conditions where the trihydrate crystallizes out, in the form of a neutral chain-configuration triaquo sulfato uranyl salt $[UO_2(SO_4)(H_2O)_3]_n$. Under intermediary conditions prevailing in aqueous solutions, the formation of both cationic and neutral mononuclear and polynuclear aquocomplexes is possible. For nitrate (and other "simple" uranium compounds), these points are fully applicable. The number of water molecules included in the inner coordination sphere, in the case of complexes having inorganic acid residues of complex structure, as for example

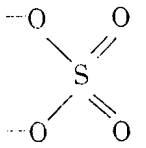
and
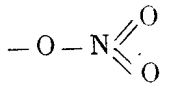

is related, aside from anything else, to the possibility of their attaching in different ways to the central atom, the acceptor; in other words, the possibility of their having different coordinating powers.

Taking the foregoing into account, the dissolution reaction of metallic uranium in nitric acid of medium concentration may be recorded as:

$$2U + 3O_2 + 4HNO_3 + 10H_2O = \\ = 2[UO_2(H_2O)_6](NO_3)_2. \quad (3)$$

The reaction of the dissolution of uranium trioxide in sulfuric acid is probably more complicated, but its equation

$$UO_3 + H_2SO_4 + 3H_2O = [UO_2SO_4(H_2O)_4] \quad (4)$$

will be more accurate a representation than (1). Eqs. (3) and (4) describe the formation of aquocomplex nitrate and sulfate compounds of the uranyl ion, and emphasize the complete equivalence of the aquo groups on the one hand and the nitrato and sulfato groups on the other. These divergences in the expression of the equations for reactions (1), (2), and (3), (4) are of a fundamental character, and must be given due attention not only by research workers, but likewise by chemistry instructors in the classroom. The importance of this point comes out with particular sharpness, for example, in the discussion of extraction, sorption, back-extraction, eluting, salting-out mechanisms, or in the study of various processes for the dehydration of uranium compounds. As mentioned above, various additives are employed when dissolving uranium-bearing materials in acids on occasion, principally in order to speed up

the reactions. For example, the addition of fluoride compounds when uranium-zirconium alloys are being dissolved accelerates the reaction and averts any mild explosive effects. Several other uranium alloys are also rather stable to attack by nitric acid. In these cases, they are brought into solution more rapidly by the addition of small amounts of phosphate, sulfate, or fluoride ions. The effect of the ions mentioned is determined by the formation of more soluble homogeneous or mixed complexes, with the uranyl ion and the accompanying elements, than those pure aquo-nitrate complex compounds which form when the alloys are dissolved with no additives.

The role of complexing in the dissolution of uranium-bearing materials stands out with unusual sharpness in the discussion of reactions with salts (preponderantly salts of the alkali metals) of inorganic acids, such as carbonic acid, hydrofluoric acid, sulfuric acid; with salts of various organic acids, such as oxalic acid, acetic acid, citric acid and various other acids, and with peroxides of the alkali metals. The most characteristic trait of these dissolution reactions, important in the removal of impurities from uranium, is the high degree of selectivity. Of the non-acid solvents enumerated, the carbonates of the alkali metals and ammonium carbonate have acquired unusually widespread application [3, 4]. The dissolution reaction of uranium trioxide by sodium carbonate in an aqueous solution is usually recorded as follows:

$$UO_3 + 3Na_2CO_3 \xrightarrow{H_2O} Na_4[UO_2(CO_3)_3] + 2NaOH. \quad (5)$$

After treating the uranium trioxide with a solution of sodium carbonate, the uranium is found to enter a comparatively readily water-soluble complex known as sodium tricarbonato uranylate. The complex nature of this compound is proved most convincingly, and the coordination representation of its formula $Na_4[UO_2(CO_3)_3]$ has won general acceptance. However, Eq. (5) is a total formula, and does not reflect the involved nature of the processes occurring in the dissolution of uranium trioxide in carbonate solutions. It would be of interest to make a complete rundown of the reactions taking place in carbonate media which have been studied to a reasonable extent at the present time, and which present compelling illustrations of the importance of the study of the reaction of ligands within the coordination sphere in the chemistry of uranyl complexes:

$$2UO_3 + 4H_2O = 2[UO_2(OH)_2(H_2O)], \quad 2[UO_2(OH)_2(H_2O)] + 2Na_2CO_3 + 4H_2O \quad (6)$$

$$= 2Na[UO_2(OH)(CO_3)(H_2O)_3] + 2NaOH, 2Na[UO_2(OH)(CO_3)(H_2O)_3] + Na_2CO_3 \quad (7)$$

$$= Na_3[(UO_2)_2(OH)(CO_3)_3(H_2O)_5] + NaOH + H_2O, \quad (8)$$

$$Na_3[(UO_2)_2(OH)(CO_3)_3(H_2O)_5] + Na_2CO_3 = 2Na_2[UO_2(CO_3)_2(H_2O)_2] + NaOH + H_2O, \quad (9)$$

$$2Na_2[UO_2(CO_3)_2(H_2O)_2] + Na_2CO_3 = Na_6[(UO_2)_2(CO_3)_5(H_2O)_2] + 2H_2O, \quad (10)$$

$$\underline{Na_6[(UO_2)_2(CO_3)_5(H_2O)_2] + Na_2CO_3 = 2Na_4[UO_2(CO_3)_3] + 2H_2O,} \quad (11)$$

$$2UO_3 + 8H_2O + 6Na_2CO_3 = 4NaOH + 6H_2O + 2Na_4[UO_2(CO_3)_3]$$

$$UO_3 + 3Na_2CO_3 + H_2O = Na_4[UO_2(CO_3)_3] + 2NaOH. \quad (12)$$

Reaction (6) of the interaction of uranium trioxide with water, leading to the formation of the monoaquo dihydroxo uranyl complex (a neutral hydroxo complex) is the first stage of the process. The gist of the subsequent reactions (7 to 11) is the transition from a neutral uranyl complex containing aquo and hydroxo groups in its coordination sphere to an anionic complex containing carbonate ions in its coordination sphere, by means of successive substitutions of OH^- and H_2O by $CO_3^{=}$ groups. The formation by this process of several compounds: triaquo hydroxocarbonato uranylate, pentaquo hydroxocarbonato uranylate, pentaquo tricarbonato hydroxo diuranylate, diaquo pentacarbonato diuranylate, and tricarbonato uranylate, all of sodium, has been proved by various methods.

The total equation (12) of the reactions is entirely satisfactory for performing calculations and for describing the processes at work in dilute solutions (e.g. in ore leach solutions). However, when pure uranium trioxide or various other uranium-rich materials are being dissolved, the stepwise nature of the process asserts itself with particular clarity (thickening of the solution, liquefying, color changes, etc.), and an understanding of these steps cannot be attained by a simple knowledge of Eq. (12). Changes in the physical properties of the precipitates and of the solution are satisfactorily explained by the difference in the composition of the intermediary compounds. Soda leaching, as Eq. (12) will demonstrate, will result in the formation of NaOH, which may have the effect of greatly slowing up the dissolution process, or even causing a process of partial precipitation of the uranium either in the form of sparingly soluble aquohydroxo carbonates, or aquohydroxo complexes. Sodium bicarbonate should therefore be added to the leach liquor, to neutralize the alkali:

$$NaOH + NaHCO_3 = Na_2CO_3 + H_2O. \quad (13)$$

The dissolution of uranium trioxide in ammonium carbonate, potash, or other carbonates of the alkali metals will be characterized by the same equations as those applying to Na_2CO_3, so that there is no need to run through them all in this survey. In some technological operations, the need arises to introduce the tricarbonate complexes, e.g. $Na_4[UO_2(CO_3)_3]$, $K_4[UO_2(CO_3)_3]$ or $(NH_4)_4[UO_2(CO_3)_3]$ into other compounds, in accord with subsequent processing steps in the flowchart; these are most commonly aquonitrate complexes. This is accomplished by decomposing a dry nitrate (or its aqueous solution). The decarbonization reaction proceeds in stages, as does the reaction of the formation of sodium tricarbonato uranylate. In solution or in precipitate form (depending on the uranium concentration), several compounds, similar to those described above, are formed in succession:

$$2Na_4[UO_2(CO_3)_3] + 2HNO_3 + H_2O = Na_6[(UO_2)_2(CO_3)_5(H_2O)_2] + 2NaNO_3 + CO_2, \quad (14)$$

$$Na_6[(UO_2)_2(CO_3)_5(H_2O)_2] + 2HNO_3 + H_2O = 2Na_2[UO_2(CO_3)_2(H_2O)_2] + CO_2 + 2NaNO_3, \quad (15)$$

$$2Na_2[UO_2(CO_3)_2(H_2O)_2] + HNO_3 + H_2O = Na_3[(UO_2)_2(CO_3)_3(OH)(H_2O)_5] + NaNO_3 + CO_2, \quad (16)$$

$$Na_3[(UO_2)_2(CO_3)_3(OH)(H_2O)_5] + HNO_3 + H_2O = 2Na[UO_2(CO_3)(OH)(H_2O)_3] + NaNO_3 + CO_2 \quad (17)$$

$$2Na[UO_2(CO_3)(OH)(H_2O)_3 + 6HNO_3 + 2H_2O = 2[UO_2(H_2O)_6](NO_3)_2 + 2NaNO_3 + 2CO_2, \quad (18)$$

$$Na_4[UO_2(CO_3)_3] + 6HNO_3 + 3H_2O = [UO_2(H_2O)_6](NO_3)_2 + 4NaNO_3 + 3CO_2. \quad (19)$$

Equations (14) to (18) reflect, probably inadequately, the actual process occurring, but it may be stated with confidence that we are dealing in this case with the successive transition from an anionic uranyl complex to its cationic counterpart, by gradual substitution reactions within the coordination sphere of the carbonato groups on hydroxo and aquo groups.

Uranyl peroxide complexes are very similar in their properties to the uranyl carbonate complexes. From the point of view of industrial production, both carbonates and peroxides exhibit some prized properties: they react with comparative ease with sparingly soluble uranium compounds, to form stable solutions (in alkaline media containing an excess of peroxide); they have the ability to transfer uranium to precipitate form quantitatively under certain conditions, and may be transformed, without any particular trouble, into any desired uranyl compound which would simplify the flow diagram [4, 5]. All of this accounts for the high selectivity of the operations involved in the use of hydrogen peroxide. The specificity of the formation of uranyl carbonate and peroxide compounds may be compared, in this respect, to the gold cyanide complexes.

The reaction between uranyl salts and alkaline peroxides has not been studied as extensively as the reaction involving uranyl carbonates, but there is every reason for interpreting the peroxide reactions to be complexing reactions. In articles and monographs on uranium technology, the coordination approach in the discussion of such reactions is unfortunately distinguished by its conspicuous absence, and even the information available on the dissolution mechanism is highly contradictory. One typical example of the usual manner in which the dissolution reaction is depicted may be seen in the following equation:

$$UO_2 + 2H_2O_2 + 2NaOH \longrightarrow Na_2UO_5 + 3H_2O, \quad (20)$$

from which we see that uranium dioxide, on interacting with hydrogen peroxide and caustic soda, forms a soluble compound of composition Na_2UO_5 containing, in all likelihood, one peroxo group. Now this is only partly true. Stable uranyl peroxide solutions are obtained in the presence of an excess of hydrogen peroxide and alkali. But then the uranyl ion must attach to itself the maximum possible number of peroxo groups ($OO^=$). Investigations have revealed [6, 7] that the uranyl ion is capable of coordinating no more than three peroxo groups (compare the carbonates) and of forming compounds of such composition as: $Na_4[UO_2(OO)_3]$. The reaction of uranium dioxide going into solution is stated more correctly, therefore, as:

$$UO_2 + H_2O_2 = UO_3 + H_2O, \quad (21)$$

$$UO_3 + 2H_2O = [UO_2(OH)_2(H_2O)], \quad (22)$$

$$H_2O_2 + 2NaOH = Na_2O_2 + 2H_2O, \quad (23)$$

$$[UO_2(OH)_2(H_2O)] + 3Na_2O_2 = Na_4[UO_2(OO)_3] + 2NaOH + H_2O. \quad (24)$$

Reaction (24), like reaction (12) for the carbonates, is a total reaction. The total picture of the dissolution, given the present level of knowledge on this process, is difficult to sketch out, but we may feel safe in assuming, to a fair degree of certainty, the formation of the following intermediary complexes:

$$Na_6[(UO_2)_2(OO)_5(H_2O)_2],$$
$$Na_2[UO_2(OO)_2(H_2O)_2],$$

as well as others containing in their coordination sphere, in addition to the peroxo groups, also aquo groups and hydroxyl groups.

In technological practice, the need may arise to bring into solution not only uranium oxides but also some other difficultly water-soluble uranium compounds such as $[UO_2CO_3]$, $[UF_4]$, and others. When they are dissolved with the aid of alkali peroxides, an important role is played by the formation of mixed uranyl complexes containing, along with the peroxo group, other acidic residues, $CO_3^{=}$, F^-, $SO_4^{=}$, and the aquo groups $[UO_2(OO)(CO_3)(H_2O)_2]^{=}$, $[UO_2F_2(OO)(H_2O)_2]^{=}$, $[UO_2(OO)(SO_4)(H_2O)_2]^{=}$, etc.

Acid-free dissolution of uranium metal and uranium compounds is not exhaustively covered solely by the two cases discussed: carbonates and peroxides. We might also cite many examples of an essential enhancement of the solubility of comparatively difficultly soluble uranyl compounds as a result of complexing reactions with neutral salts. We shall limit our survey to a consideration of some of these reactions. As will be demonstrated below, precipitation of the neutral complex triaquo oxalato uranyl $[UO_2(C_2O_4)(H_2O)_3]$ is sometimes resorted to in operations based on affinity. Its solubility is ~0.5 g in 100 ml solution. The interaction between triaquo oxalato uranyl ion and ammonium oxalate through the reaction

$$[UO_2(C_2O_4)(H_2O)_3] + (NH_4)_2C_2O_4 = (NH_4)_2[UO_2(C_2O_4)_2(H_2O)_2] + H_2O, \quad (25)$$

results in the formation of ammonium diaquo dioxalato uranylate, possessing the very high solubility ~500g in 100 ml, i.e. the solubility is improved about 1000 times. Approximately the same solubility values characterize the reactions of triaquo oxalato uranyl with sodium fluoride and ammonium carbonate, which take place with the formation of the chemical compounds sodium monoaquo trifluoro oxalato uranylate and ammonium diaquo carbonato oxalato uranylate [8, 9]:

$$[UO_2(C_2O_4)(H_2O)_3] + 3NaF = Na_3[UO_2(C_2O_4)F_3(H_2O)] + 2H_2O, \quad (26)$$

$$[UO_2(C_2O_4)(H_2O)_3] + (NH_4)_2CO_3 = (NH_4)_2[UO_2(C_2O_4)(CO_3)(H_2O)_2] + H_2O. \quad (27)$$

An interesting example illustrating the possibility of complexing reactions as a tool for obtaining uranyl compounds of the most varied properties and highly specific compositon is the interaction of the practically water-insoluble monoaquo dihydroxylaminedihydroxo uranyl ion and potassium carbonate [10]:

$$[(UO_2(OH)_2(NH_2OH)_2(H_2O)] + 2K_2CO_3 = K_3[UO_2(OH)(CO_3)_2(H_2O)] + KOH + 2NH_2OH. \quad (28)$$

The potassium monoaquo dicarbonato hydroxo uranylate then forming has very high solubility and stability in alkaline solutions.

In concluding this section, we may cite the comparatively well known reaction involving diaquo diacetato uranyl and ammonium acetate:

$$[UO_2(CH_3COO^-)_2(H_2O)_2] + NH_4CH_3COO = NH_4[UO_2(CH_3COO)_3] + 2H_2O. \quad (29)$$

The solubility (in 100 ml solution) of the ammonium triacetato uranylate formings is about 50 g, and the solubility of the original compound, in contrast, is 7.7 g.

Complexing Reactions in the Precipitation of Uranyl Salts

Precipitation reactions of various uranyl compounds are widely used in the chemical processing of uranium-bearing materials, even though mastery of extraction and sorption techniques has somewhat narrowed down their sphere of applications. It is therefore feasible to discuss the most characteristic precipitation reactions involving uranyl compounds in use at the present time.

In processing uranium concentrates containing significant quantities of phosphorus, vanadium, iron, and silicic acid, recourse is sometimes had to the reaction of precipitating a complex salt which is virtually insoluble either in water or in dilute acids, viz. ammonium triaquo phosphato uranyl complex [3]:

$$[UO_2(H_2O)_6](NO_3)_2 + NH_4H_2PO_4 = \\ = [UO_2(NH_4PO_4)(H_2O)_3] + 2HNO_3 + 3H_2O. \quad (30)$$

The complex so forming is a neutral complex. The central acceptor ion, the uranyl ion, is surrounded by aquo groups and residues of singly substituted phosphoric acid. The ammonium ion is bound solely to the phosphoric acid. On account to the low pH value at which this complex precipitates (1.9-2.5), satisfactory purification of the uranium from many elements is achieved.

In the previous section, we discussed reactions leading to a solution of uranyl carbonate complexes. Under certain conditions, viz. in the presence of an excess of alkali carbonate (most often ammonium carbonate), the uranium is successfully converted, to an adequately complete extent, into a precipitate in the form of a crystalline easily filtrated powder. The combination of the dissolution and precipitation steps of uranyl carbonate complexes makes it possible to rid the latter of most of the accompanying impurities. The reaction of the formation and precipitation of ammonium tricarbonato uranylate, e.g. from an aqueous solution of hexaaquo uranyl nitrate, is a multistage process and may be represented by the following equations:

$$[UO_2(H_2O)_6](NO_3)_2 + 3(NH_4)_2CO_3 = 2NH_4[UO_2(OH)(CO_3)(H_2O)_3] + 4NH_4NO_3 + CO_2 + 5H_2O, \quad (31)$$

$$2NH_4[UO_2(CO_3)(OH)(H_2O)_3] + (NH_4)_2CO_3 = (NH_4)_3[(UO_2)_2(CO_3)_3(OH)(H_2O)_5] + NH_4OH + H_2O, \quad (32)$$

$$(NH_4)_3[(UO_2)_2(CO_3)_3(OH)(H_2O)_5] + (NH_4)_2CO_3 = 2(NH_4)_2[UO_2(CO_3)_2(H_2O)_2] + NH_4OH + H_2O, \quad (33)$$

$$2(NH_4)_2[UO_2(CO_3)_2(H_2O)_2] + (NH_4)_2CO_3 = (NH_4)_6[(UO_2)_2(CO_3)_5(H_2O)_2] + 2H_2O, \quad (34)$$

$$(NH_4)_6[(UO_2)_2(CO_3)_5(H_2O)_2] + (NH_4)_2CO_3 = 2(NH_4)_4[UO_2(CO_3)_3] + 2H_2O, \quad (35)$$

$$2[UO_2(H_2O)_6](NO_3)_2 + 7(NH_4)_2CO_3 = 2(NH_4)_4[UO_2(CO_3)_3] + 4NH_4NO_3 + 2NH_4OH + CO_2 + 11H_2O. \quad (36)$$

The reaction of the precipitation of ammonium tricarbonate uranylate is usually represented as:

$$UO_2(NO_3)_2 + 3(NH_4)_2CO_3 = (NH_4)_4[UO_2(CO_3)_3] + 2NH_4NO_3. \quad (37)$$

Clearly, Eqs. (36) and (37) are essentially different. From Eq. (36), the formation of one mole of ammonium tricarbonato uranylate requires 3.5 moles of ammonium carbonate, whereas, according to Eq. (37), only 3 moles would be required. According to Eq. (36), we must also anticipate a vigorous release of carbon dioxide gas from the solution as the first portions of ammonium carbonate are added. Experiments have shown that vigorous evolution of carbon dioxide actually takes place in the first stages of the reaction, in amounts of ~0.5 mole per gram-mole of uranyl nitrate, and that more ammonium carbonate than 3 gram-moles per gram-mole of nitrate are required for the reaction to go to completion. Consequently, the total equation (36) not only takes into account all the phenomena observed in practice and occurring in the solution when these reactions are carried out, but also justifies the higher amount of carbonates consumed over that computed from Eq. (37).

As pertains to the precipitation of practically water-insoluble aquo-hydroxo uranyl complexes, this process is not a selective operation, but it is very widely employed, e.g. in producing concentrates after leaching uranium-bearing ores. The comparatively widespread use of aquo-hydroxo complexes is due primarily to the fact that they are very sparingly soluble in water, are readily decomposed by mineral acids, and in the case of ammonium complexes, uranium oxides may be obtained by directly calcining the precipitate.

The reaction of precipitation of "ammonium diuranate" from aqueous solutions of uranyl nitrate should be presented as follows:

$$[UO_2(H_2O)_6](NO_3)_2 + 3NH_4OH = NH_4[UO_2(OH)_3(H_2O)_3] + 2NH_4NO_3 + 3H_2O. \quad (38)$$

The reaction, and most other reactions involving the uranyl ion, is the terminal stage of the stepwise formation of the compounds in question. As intermediary steps, we may consider those reactions ending in the formation of the following series of genetically associated complexes

$$[UO_2(OH)(H_2O)_5]NO_3,$$
$$[UO_2(OH)_2(H_2O)]$$

and

$$NH_4[(UO_2)_2(OH)_5(H_2O)_6].$$

The real "diuranate" with which the chemical engineer works is most often a mixture of two compounds: ammonium hexaaquo pentahydroxo diuranylate $(NH_4)[(UO_2)_2(OH)_5(H_2O)_6]$ and ammonium triaquo trihydroxo uranylate $NH_4[UO_2(OH)_3(H_2O)_3]$ with the first predominating.

In operations involving affinity, in uranium purification, precipitate of uranium oxalate compounds is frequently resorted to. For example, isolation of uranyl triaquo oxalato complexes (containing free HNO_3) from uranyl nitrate solutions makes it possible to free the uranium from several impurities, in particular from many rare earths. The equation of the reaction has the following form:

$$[UO_2(H_2O)_6](NO_3)_2 + H_2C_2O_4 = [UO_2(C_2O_4)(H_2O)_3] + 2HNO_3 + 3H_2O. \quad (39)$$

The solubility of the product forming as a result is ~0.5 g in 100 ml. Many available data testify to the fact that triaquo oxalato uranyl is a typical neutral complex in which the aquo groups are coordinated around the uranyl ion. In the operations of refined chemical purification of natural uranium, and likewise in the processing of any number of irradiated materials, peroxide precipitation is frequently employed. This reaction is highly specific for uranium. Its selective action makes it possible to rid uranium of many impurities. The precipitation reaction of tetraaquo peroxo uranyl complex corresponds to the following equation:

$$[UO_2(H_2O)_6](NO_3)_2 + H_2O_2 = [UO_2(OO)(H_2O)_4] + 2HNO_3 + 2H_2O. \quad (40)$$

The solubility of peroxo uranyl complex $[UO_2(OO)(H_2O)_4]$ (or $UO_4 \cdot 4H_2O$) in water amounts to ~8 mg/liter at 20° C. This product constitutes a neutral complex in which the peroxo and aquo groups act as ligands [2].

The enormous significance of neutral complexes of various elements in the production of ultrapure materials is a long established fact in the chemistry of coordination compounds. Because of the absence of any electric charge in the external sphere (cation or anion), these complexes rarely take up foreign impurities. In this context, it is interesting to point to one more reaction of the uranyl ion, viz. to the reaction consisting of the interaction between the uranyl ion and hydroxylamine hydrochloride and alkali:

$$[UO_2(H_2O)_6](NO_3)_2 + 2NH_2OH \cdot HCl + 4NaOH = [UO_2(OH)_2(NH_2OH)_2(H_2O)] + 2NaCl + 2NaNO_3 + 7H_2O. \quad (41)$$

When caustic soda is added to a solution containing a mixture of uranyl nitrate and hydroxylamine hydrochloride, crystallization of the practically water-insoluble neutral monoaquo dihydroxylamine dihydroxo uranyl complex is observed at pH ~6.0-6.5. This reaction is specific for uranium and, thanks to the formation of a precipitate which is readily filtrable and readily convertible to oxides, may find suitable application in the production of pure metal preparations. There are literature references to the possibility of satisfactorily separating uranium and thorium from their fluoride solutions with the aid of hydrogen peroxide, by isolating from the solution the mixed aquo peroxo fluoride solutions with the aid of hydrogen peroxide, by isolating from the solution the mixed aquo peroxo fluoride complex:

$$Na_3[UO_2F_5] + H_2O_2 + 3H_2O = Na[UO_2(OO)F(H_2O)_3] + 2HF + 2NaF. \quad (42)$$

The sodium triaquo fluoro peroxo uranylate so forming is readily passable through filters and is practically water-insoluble.

In conclusion, consider still other reactions leading to the formation of comparatively difficultly soluble uranyl complexes of specific composition:

$$NH_4[UO_2(CH_3COO)_3] + NH_4F = \downarrow NH_4[UO_2(CH_3COO)_2F] + NH_4CH_3COO, \quad (43)$$

$$[UO_2(H_2O)_6](NO_3)_2 + 3NaCH_3COO = \downarrow Na[UO_2(CH_3COO)_3] + 2NaNO_3 + 6H_2O, \quad (44)$$

$$[UO_2(SO_4)(H_2O)_3] + KF = \downarrow K[UO_2SO_4F] + 3H_2O, \quad (45)$$

$$(NH_4)_4[UO_2(CO_3)_3] + 2[Co(NH_3)_6](NO_3)_3 = [Co(NH_3)_6]_2[UO_2(CO_3)_3](NO_3)_2 + 4NH_4NO_3. \quad (46)$$

Reaction (46), used in analytical chemistry, displays the possible applications of compounds having complex cations and anions in the extraction and purification of uranium. Reactions (43) and (45) describe the formation of mixed uranyl fluoride acetates and uranyl fluoride sulfates, while reaction (44) describes the formation of sodium triacetato uranylate, a familiar compound in analytical chemistry. The examples mentioned embrace virtually all the most important reactions involving precipitation of uranyl salts as used in chemical technology. The compositon of the complexes forming are complicated, as a rule, by the fact that their internal sphere (and, in some cases, even

the external sphere) consists of unlike substituents. It is precisely this variety in the compositions of the possible compounds, due to the nature of the uranyl ion, which allows us to rely on the production of new complexes with interesting and valuable properties for chemical processing practice.

Complexing Reactions in Extractive Processes

In the technology of processing of uranium-bearing materials, extraction processes have maintained a firm place through the years. These processes are based on the properties of various organic reagents to selectively form, with tetravalent uranium salts or uranyl salts, complex compounds which are soluble in an excess of extractant or other organic products which do not mix with water. Extractants in question are various alcohols, simple and complex ethers, ketones, aldehydes, organophosphorus oxygen-containing compounds, organic amines, etc. [11, 12].

These extractant may be either neutral, acidic (organic acids or inorganic salts of organic acids) and basic (as a rule, the salts of inorganic acids with organic bases). In this connection, all extraction reactions in use at the present time in chemical processing of uranium materials may be divided into three basic types.

1. Reactions involving neutral organic reagents, occurring for the most part in line with the following scheme:

$$[UO_2(H_2O)_nA_2] + 2R \longrightarrow [UO_2R_2(H_2O)_{n-2}A_2] + 2H_2O, \quad (47)$$

where A is the univalent residue of a mineral acid, and R is an organic radical.

2. Reactions involving acidic organic reagents (or inorganic salts of organic acids):

$$[UO_2(H_2O)_nA_2] + 2HR \longrightarrow [UO_2R_2] + 2HA + nH_2O, \quad (48)$$

$$[UO_2(H_2O)_nA_2] + 3BR \longrightarrow B[UO_2R_3] + 2BA + nH_2O, \quad (49)$$

where B is an inorganic univalent cation.

3. Reactions involving alkaline organic reagents (principally salts of inorganic salts and organic bases):

$$[UO_2(H_2O)_nA_2] + RHA \longrightarrow RH[UO_2A_3] + nH_2O. \quad (50)$$

Combinations of these reactions are possible, e.g. in the extraction by a mixture of neutral and acidic organic extractants (synergistic mixtures, or extraction, e.g. by alkylphosphates). The equations mentioned above for extraction reactions are given in their general form. The interaction occurring between neutral organic reagents may ensue not only with neutral uranyl complexes, as demonstrated in reaction (47), but also with the cationic and anionic forms of the complexes. In addition, one, two, or all the water molecules present in the inner sphere of the complex may be displaced, thereby bringing about a direct linkage to the uranyl ion of a different number of moles of extractant. However, the gist of these reactions remains the same: displacement of water molecules from the inner sphere of the complex and attachment of neutral organic molecules with the formation of a complex compound of new composition, dissolving in an excess of extractant. The gist of the second type of reaction consists in the complete displacement of inorganic acidic residues and the formation of new neutral (possibly, chelating) or anionic uranyl complexes with organic ligands, soluble in an excess of extractant or, what would amount to the same thing, in any other organic liquid suitable for these purposes. The third type of reaction is characterized by the formation of an anionic uranyl complex (with inorganic inner-sphere substituents), having, in the outer coordination sphere, a large organic cation soluble in an excess of extractant or other organic reagent. All of these reactions involve complexing of the uranyl ion and organic ligands. An important consequence is the subordination of these reactions to the laws governing reactions involving the formation of uranyl complexes in general, as confirmed by available factual information.

Consider in brief various typical complexing reactions employed in extraction operations in the processing of uraniferous materials.

Of the neutral organic extractants for uranium, we note two: diethyl ether $(C_2H_5)_2O$ and tributylphosphate $(C_4H_9O)_3PO$. The diethyl ether extraction processes: at the present time, extraction by diethyl ether is carried out on a small scale primarily because of the extensive danger of explosion on the part of the extractant. In operations involving affinity in the processing of natural uranium, processing of any number of nuclear reactor by-products and wastes of gaseous diffusion plants, solvent extraction of uranium by tributylphosphate or, rather, by solutions of TBP in inert organic diluents (e.g. in the high-boiling fraction of saturated hydrocarbons) is frequently resorted to.

As a large fund of experimental data has shown, extraction by diethyl ether and tributylphosphate proceeds successfully not only from solutions of uranium containing ligands situated in the second half of the series arranged by displacing power:

$$CO_3^{2-} \geqslant OO^{2-} \geqslant OH^- > F^- \geqslant CH_3COO^- \geqslant \geqslant C_2O_4^{2-} > SO_4^{2-} > H_2O \geqslant NO_3^- \geqslant$$
$$\geqslant Cl^- > CNS^- > Br^- \quad \text{etc.}$$

For example, diethyl ether is very efficient in extracting uranium from nitrate, chloride, thiocyanate, and other solutions. On the other hand, extraction virtually comes to a standstill in the case of solutions containing ions which are the first terms of the series: carbonates, peroxides, hydroxides, fluorides, acetates, oxalates. This fact is a direct indication of a relationship between the extractive power of a neutral organic reagent and the stability of the initial uranyl complex. One of the most reliable classical techniques for estimating the relative stability of complex compounds is measurement of the molar electrical conductivity of the complexes in aqueous solution. If we consider the molar electrical conductivity of a series of the simplest uranyl salts situated with respect to the series of displacing power of the ligands, then the electrical conductivity values will enable us to present the formulas of these compounds in the form*:

$$[UO_2(CO_3)(H_2O)]^0, \quad [UO_2(OO)(H_2O)_3]^0, \quad [UO_2F_2(H_2O)_3]^0,$$
$$[UO_2(CH_3COO)_2(H_2O)_2]^0, \quad [UO_2C_2O_4(H_2O)_3]^0, \quad [UO_2SO_4(H_2O)_3],$$
$$[UO_2(H_2O)_6](NO_3)_2, \quad [UO_2(H_2O)_6]Cl_2, [UO_2(H_2O)_6](CNS)_2 \quad \text{etc.}$$

Carbonate, peroxide, fluoride, acetate, and oxalate complexes in aqueous solution are dissociated to an insignificant degree and may be regarded as nonelectrolytes, a fact which is reflected in the manner of representing their formulas, whereas nitrate, chloride, and thiocyanate complexes are practically completely dissociated, i.e. they exist in the form of cationic aquo complexes in aqueous solutions of intermediate concentration. Uranyl sulfate is not completely dissociated, and in solution it probably exists in the form of both cationic and neutral complexes. The dependence of extraction efficiency on the degree of dissociation of uranyl aquo complexes is quite obvious. It demonstrates that a necessary element of the extraction mechanism in the case of neutral organic reagents is the substitution of aquo groups by these reagents in the inner coordination sphere of the complexes. The interaction between hexaaquo uranyl nitrate and tributylphosphate may be conceived as occurring in two stages.

The first reaction, occurring in the aqueous phase saturated with tributylphosphate, tentatively corresponds to the following equation:

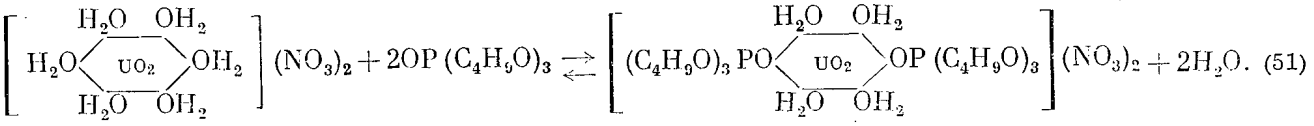

$$\left[H_2O(OH_2)UO_2(OH_2)OH_2\right](NO_3)_2 + 2OP(C_4H_9O)_3 \rightleftarrows \left[(C_4H_9O)_3PO(H_2O)(OH_2)UO_2(OH_2)OP(C_4H_9O)_3\right](NO_3)_2 + 2H_2O. \quad (51)$$

The conversion of the tetraaquo ditributylphosphate uranyl nitrate complex to the organic phase is probably accompanied by the following reaction (as terminal stage):

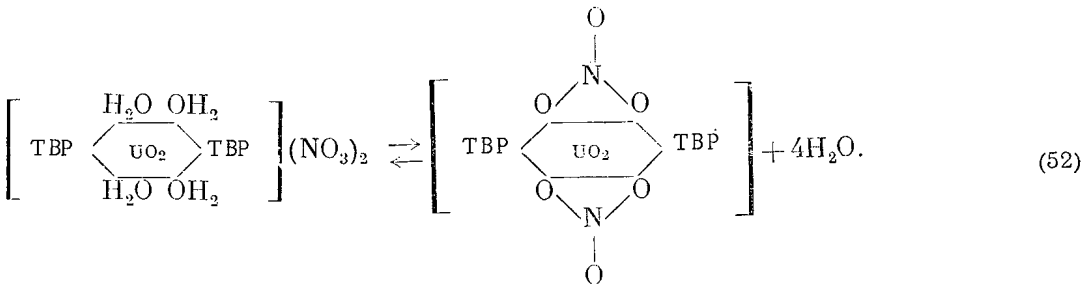

$$\left[TBP(H_2O)(OH_2)UO_2(H_2O)(OH_2)TBP\right](NO_3)_2 \rightleftarrows \left[TBP\,UO_2(NO_3)_2\,TBP\right] + 4H_2O. \quad (52)$$

As for the values of the coordination number of uranyl in the last compound, there are different views in currency, but it may be considered proven (by measurements of the electrical conductivity of the compound in the organic phase) that nitrato groups are included in the inner sphere of the compound. For the diethyl ether extraction process, the reactions are depicted by similar equations. For the water-ether phase:

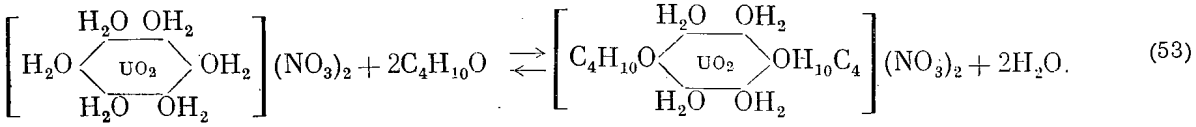

$$\left[H_2O(OH_2)UO_2(OH_2)OH_2\right](NO_3)_2 + 2C_4H_{10}O \rightleftarrows \left[C_4H_{10}O(H_2O)(OH_2)UO_2(OH_2)OH_{10}C_4\right](NO_3)_2 + 2H_2O. \quad (53)$$

* The values of molar electrical conductivity for carbonate and peroxide were not determined because of the negligible solubility, although indirect data point to a low value in each case.

And for the ether-water phase:

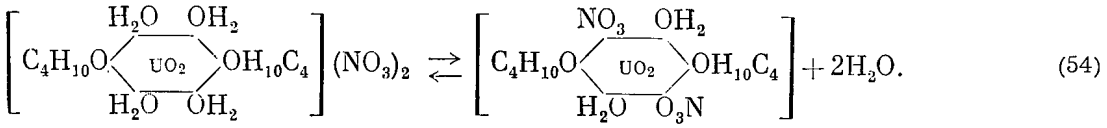

$$\left[C_4H_{10}O\left\langle \begin{matrix} H_2O & OH_2 \\ UO_2 & \\ H_2O & OH_2 \end{matrix} \right\rangle OH_{10}C_4\right](NO_3)_2 \rightleftarrows \left[C_4H_{10}O\left\langle \begin{matrix} NO_3 & OH_2 \\ UO_2 & \\ H_2O & O_3N \end{matrix} \right\rangle OH_{10}C_4\right] + 2H_2O. \quad (54)$$

Because of the slight difference in the stability of the uranyl-water bonds and the organic molecules selected as examples, the compositions of the compounds may vary somewhat depending on conditions prevalent.

The reactions discussed here render possible, at least qualitatively, a displacement of TBP and diethyl ether in series of displacing power for ligands. They will fall somewhere in the immediate vicinity of water in the series. In complex compounds where the position of the aquo groups is strengthened by ligands which are among the first members of the displacement series, organic molecules will not be able to displace water from the inner sphere, and no extraction will occur. On the other hand, such ligands as NO_3^-, Cl^-, CNS^-, Br^-, etc. which under ordinary conditions are incapable of competing with water contribute to extraction. In essence, in compounds of the $[UO_2(H_2O)_6]X_2$ type, organic molecules need compete only with coordinated water molecules, since the acidic residue is found in the outer sphere and fails to exert any appreciable influence on the strength of the attachment of the aquo groups.

Now let us attempt, on the basis of what has been said here, to account for some specific phenomena observed in the course of extraction. For example, in TBP solvent extraction of uranium, the distribution coefficient varies inversely with the concentration of metal in the aqueous phase, dropping sharply as the concentration is increased. At 10 g/liter uranium content, the distribution coefficient is ~5.7, while it is only 0.39 at ~40 g/liter uranium content. Bearing in mind the fact that uranyl nitrate is markedly associated at high concentrations, we might find one satisfactory explanation for that phenomenon. The association of uranyl nitrate means that molecules of neutral compounds, e.g. $[UO_2(H_2O)_4(NO_3)_2]^0$, are found in the solution together with the cationic aquo complex of composition $[UO_2(H_2O)_6](NO_3)_2$. The stability of the inner sphere and, consequently, the stability of the bond linking the aquo groups to the central atom, increases slightly, while the capacity of organic molecules to compete with water molecules decreases correspondingly.

The effect contributed by salting-out agents (some nitrates) is readily accounted for in that they depress the concentration of free water. The stability of the inner sphere of aquo complexes is diminished, while the extracting power of neutral organic reagents increases. The effect of the nitrato groups as ions of like sign in these cases (in the first stage of the reaction) is of no essential significance, although the role is enhanced nevertheless depending on conditions (large concentrations of NO_3^-). Properly speaking, this is a possible explanation for the complex relationship between the distribution coefficient and the concentration of various salting-out agents when, e.g. the acidity of the solution and the concentration of metal in the aqueous phase are varied. The abrupt increase in distribution coefficient as acidity is heightened, particularly near the neutral point, is readily explained by the existence of aquohydroxo complexes, possibly of the type $[UO_2(OH)(NO_3)(H_2O)_4]^0$ at comparatively high pH values. The presence of hydroxo groups in the inner coordination sphere of complexes adds significantly to the stability of the complexes. The mobility of the aquo groups is lowered, and with it the extraction efficiency.

Extractants having a high distribution coefficient for uranium are relied upon in the extractive processing of clarified slurries or pulps in the acidic extraction of uranium from ores. A necessary requirement imposed on these extractants is the possibility of extracting uranium from sulfate solutions, and sometimes from solutions containing appreciable quantities of phosphates. These requirements are satisfied by the two groups of extractants which are best known at the present time: alkylphosphates and alkylamines.

The chemical mechanism involved in extraction by alkylphosphates consists in the formation of mono- and di-alkylphosphoric acids of highly stable complexes with uranyl ions and the dissolution of complexes in the organic phase (in a mixture of extractant and diluent). It may be assumed, to a satisfactory degree of reliability, that the chemical mechanism behind the interaction of these acids and the uranyl ion will prove similar to that involved in the interaction between the latter and the customary singly and doubly substituted ortho- and pyrophosphates. Although uranyl phosphate compounds have been studied only to a slight extent so far from the vantage point of coordination theory and the position of the phosphato groups in the series of displacing power of ligands has not been established with any precision, it is possible to place PO_4^{3-} and $P_2O_7^{4-}$ between the first members of this series. At least, they are capable of readily displacing such groups as H_2O, Cl^-, NO_3^-, $SO_4^{=}$, etc. from the inner sphere of uranyl compounds, completely converting them to phosphate compounds. The reactions involving interaction between alkyl-

phosphoric acids and uranyl salts may be written only in the most general form, since the complicated structure of the acids (at the basis of which lies, probably, the oxygen tetrahedron with a phosphorus atom at the center) and their high basicity allow the widest variety in variants of reacting, in particular, the formation of mono-, di-, tri- and tetranuclear compounds, as well as products of polymeric structure.

The reaction involving hexaaquo uranyl nitrate and dialkylorthophosphoric acid proceeds in line with the schematized equation:

$$[UO_2(H_2O)_6](NO_3)_2 + 2R_2HPO_4 = [UO_2(R_2PO_4)_4] + 2HNO_3 + 6H_2O, \quad (55)$$

but the neutral complex forming a di-dialkylorthophosphato uranyl is probably not a monomer. The reactions between uranyl salts and alkylpyrophosphates does not differ in principle from those described above.

Back-extraction of uranium, as might be expected in view of the great stability of the resulting uranyl complexes with alkylphosphoric acids, proceeds only under rigidly fixed conditions. As back-extractants, 10 M hydrochloric acid, hydrofluoric acid, or solutions of the alkali carbonates are used. Readily water-soluble chloride, fluoride, or carbonate complexes, respectively, are formed in the back-extraction.

Extraction by means of organic ammonia derivatives, i.e. by alkylamines, has also met with applications in industry in recent years, as for instance in the processing of clarified sulfate solutions after sulfuric acid treatment of uraniferous ores. Most of the tertiary aliphatic amines with a normal chain and high molecular weight are extractants of a most satisfactory nature for uranium. They feature high distribution coefficients and slight solubility in the aqueous phase.

For the organic amines, as well as ammonia, the proton attachment reaction is quite typical:

$$R_3N + HX = [R_3NH]X. \quad (56)$$

In the case of sulfuric acid and a tertiary amine

$$2R_3N + H_2SO_4 = (R_3NH)_2SO_4. \quad (57)$$

Any further interaction between an amine sulfate and uranyl salts will not differ in any way from the well known complexing reactions:

$$(NH_4)_2SO_4 + [UO_2(SO_4)(H_2O)_3] = (NH_4)_2[UO_2(SO_4)_2(H_2O)_2] + H_2O, \quad (58)$$

$$(R_3NH)_2SO_4 + [UO_2(SO_4)(H_2O)_3] = (R_3NH)_2[UO_2(SO_4)_2] + 3H_2O. \quad (59)$$

Taking into account the nature of the cation which stabilizes the complex, as well as data available on the number of amine moles required per mole of uranium in the organic phase (from 4 to 6), we may logically suppose that a complex richer in sulfato groups than the disulfato uranylate

$$2(R_3NH)_2SO_4 + [UO_2(SO_4)(H_2O)_3] = (R_3NH)_4[UO_2(SO_4)_3] + 2H_2O \quad (60)$$

enters the organic solution. And, taking into account the possibility of opening up the $SO_4^{=}$ group in this cycle, and, consequently, having it occupy a single coordination site

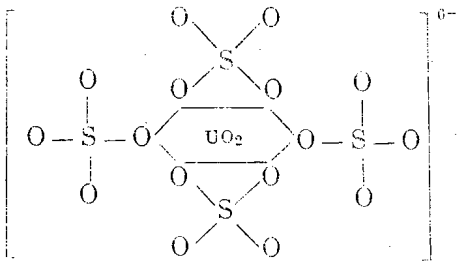

we are also free to assume the probability of such a reaction as:

$$3(R_3NH)_2SO_4 + [UO_2(SO_4)(H_2O)_3] = (R_3NH)_6[UO_2(SO_4)_4] + 2H_2O. \quad (61)$$

The trialkylamine sulfato uranylates then forming dissolve in excess of amine in the organic diluent. For extraction mixtures containing up to several percent amine in the diluent are employed. As in the case of any other complexing reactions involving the uranyl ion, the reactions with amines are stepwise in nature, and the direction of

the reactions depends on many reactors, chief among which are the concentrations of the reagents, the acidities of the solutions, and the temperature (cf., e.g. [13]). The best back-extractants for uranium in solvent extraction by means of amines are aqueous solutions of soda and nitric-acid solutions of ammonium nitrate.

Back-extraction reactions of uranium, from an organic phase, are illustrated by the following equations: back-extraction by soda:

$$(R_3NH)_2[UO_2(SO_4)_2(H_2O)_2] + 4Na_2CO_3 = 2R_3N + Na_4[UO_2(CO_3)_3] + 2Na_2SO_4 + CO_2; \quad (62)$$

back-extraction by aqueous nitric-acid solutions of ammonium nitrate:

$$(R_3NH)_2[UO_2(SO_4)_2(H_2O)_2] + 4NH_4NO_3 + 4H_2O = [UO_2(H_2O)_6](NO_3)_2 + 2R_3NHNO_3 + 2(NH_4)_2SO_4. \quad (63)$$

The complexing reactions (62) and (63) are quite involved and reflect only the terminal stages of these processes.

In concluding this final section, it would be fitting to state one further remark on the synthesis of new uranium extractants. At the present time, great efforts are being centered on researches into the extractive power of a series of organic ligands containing phosphorus and nitrogen in their composition. By taking into due account the great affinity of the uranyl ion to fluorine ions, it might be possible, in all likelihood, to find extractants which are highly suitable in their properties from among the well-populated class of organofluorine compounds.

LITERATURE CITED

1. V. P. Markov and I. V. Tsapkina, Zh. neorgan. khim., 4, No. 10, 2255 (1959).
2. I. I. Chernyaev et al., Geneva conference 1958, P/2138.
3. N. P. Galkin, A. A. Maiorov, and U. D. Veryatin, Uranium concentrates processing technology [in Russian], Atomizdat, Moscow (1960).
4. V. B. Shevchenko and B. N. Sudarikov, Uranium technology [in Russian], Gosatomizdat, Moscow (1961).
5. A. N. Zelikman, Metallurgy of rare earths, thorium, and uranium [in Russian], Metallurgizdat, Moscow (1961).
6. I. I. Chernyaev, V. A. Golovnya, and G. V. Ellert, Zh. neorgan. khim., 6, No. 4, 790 (1961).
7. A. M. Gurevich, Radiokhimiya, No. 3, 322 (1961).
8. I. I. Chernyaev, V. A. Golovnya, and R. N. Shchelokov, Zh. neorgan. khim., 6, No. 3, 549 (1961).
9. I. I. Chernyaev and R. N. Shchelokov, Zh. neorgan. khim., 6, No. 3, 557 (1961).
10. I. I. Chernyaev, V. A. Golovnya, and G. V. Ellert, Zh. neorgan. khim., 5, No. 7, 1481 (1960).
11. V. M. Vdovenko, Chemistry of uranium and the transuranium elements [in Russian], Publ. by USSR Academy of Sciences (1960).
12. V. V. Fomin, Chemistry of extractive processes [in Russian], Atomizdat, Moscow (1960).
13. V. P. Markov and V. V. Tsapkin, Zh. neorgan. khim., 4, No. 10, 2261 (1959).

All abbreviations of periodicals in the above bibliography are letter-by-letter transliterations of the abbreviations as given in the original Russian journal. *Some or all of this periodical literature may well be available in English translation.* A complete list of the cover-to-cover English translations appears at the back of this issue.

AN INVESTIGATION OF THE REACTION OF $UO_2(NO_3)_2$ WITH Na_2HPO_4 IN AQUEOUS SOLUTION

I. V. Tananaev and G. V. Rodicheva

Translated from Atomnaya Énergiya, Vol. 14, No. 4,
pp. 395-399, April, 1963
Original article submitted June 6, 1962

The system $UO_2(NO_3)_2-Na_2HPO_4-H_2O$ was investigated by determining the solubility, pH, electrical conductivity and apparent volume of the precipitates. It was found that the reaction in this system takes place in three stages, with successive formation of $(UO_2)_3(PO_4)_2$, a mixed sodium uranyl acid phosphate $UO_2H_XNa_{1-X}PO_4$ and, finally, $NaUO_2PO_4 \cdot nH_2O$.

Conclusions are drawn regarding the possibility of titrimetric determination of the uranyl ions and the free acidity in its salts, also the conditions for obtaining the most closely compacted uranyl phosphate precipitate.

As a result of their low solubility, uranyl phosphates are of practical interest in the analytical chemistry and processing of uranium. The following phosphates are described in the literature: $(UO_2)_3(PO_4)_2 \times nH_2O$ (n = 4 and 6), $UO_2HPO_4 \cdot 4H_2O$, $UO_2 \times (H_2PO_4)_2 \cdot nH_2O$, $MUO_2PO_4 \cdot nH_2O$ (M = K, Na, NH_4), $M_4UO_2(PO_4)_2 \cdot nH_2O$, $M(UO_2PO_4)_2 \cdot nH_2O$ (M = = Mg, Ca and other metals), some information on these being given in [1]. But, in general, only data (sometimes incomplete) on the composition of phosphates obtained by the preparative method are given. But this gives no indication of the conditions of formation of the individual compounds and the limits of their existence: concentration and ratio of the reagents and the role of the acidity of the medium. This is not altogether true for [2] and the investigations of Victor I. Spitsyn and his co-workers[3], but even in these the emphasis is on the individual stages of the reaction between UO_2^{2+} and PO_4^{3-} ions.

This article gives the results of an investigation of the precipitation of uranyl phosphates in the system $UO_2(NO_3)_2-Na_2HPO_4-H_2O$ by determining the solubility, pH, specific electrical conductivity and apparent volumes of the precipitate. Our aim was to obtain more detailed information on the characteristics of formation of solid phases in this system and their mutual conversions.

The initial components were used in the form of aqueous solutions of $UO_2(NO_3)_2 \cdot 6H_2O$ and Na_2HPO_4. All the investigations were carried out at 25 ± 0.1° C, and measurements of the precipitate volumes at room temperature. The mistures used (100 ml) contained 0.025 M $UO_2(NO_3)_2$ and gradually increasing amounts of Na_2HPO_4. The mixtures were stirred in a thermostat at 25 deg C until equilibrium was established (6 hours). The molar ratio of the components in the initial mixtures was n = $Na_2HPO_4 : UO_2(NO_3)_2$ between 0.1 and 6.0

Uranyl (by precipitation with ammonia), phosphate (by precipitation of $MgNH_4PO_4 \cdot 6H_2O$) and sodium (by flame photometry) contents in the equilibrium solution were determined respectively. Since the composition of the initial mixture was known exactly, that of the solid phases formed could be determined from the analytical data of the solution, with the exception of the hydrate water whose content was determined separately.

The results of an investigation of the system $UO_2(NO_3)_2-Na_2HPO_4-H_2O$ by the solubility method are given in the table and Fig. 1, which show that the compositon of the precipitate is not the same in all cases, but depends on the ratio of the reacting components. Three reaction stages in the system may be noted:

1. n = 0-0.67. In this section the system is characterized by an excess of the uranyl ion in the solution; phosphate is not detected. The reaction takes place with formation of normal uranyl phosphate:

$$3UO_2(NO_3)_2 + 2Na_2HPO_4 = (UO_2)_3(PO_4)_2 + 4NaNO_3 + 2HNO_3. \quad (1)$$

2. n = 0.67-1.0. The UO_2^{2+} concentration decreases systematically, PO_4^{3-} ions are absent. The $PO_4^{3-} : UO_2^{2+}$ ratio increases steadily from 0.67 to 1.0. The process with formation of a solid phase of mixed composition takes place via two successive reactions:

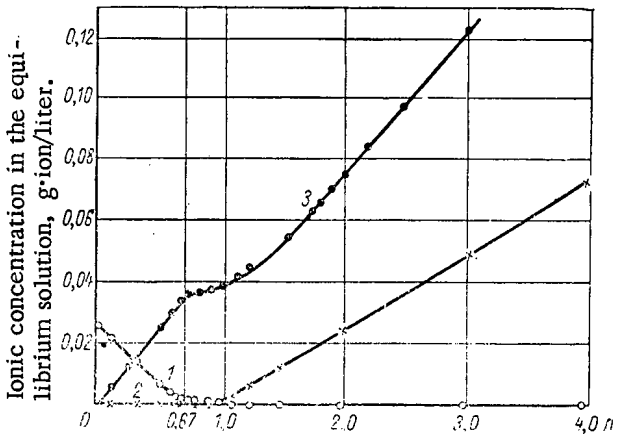

Fig. 1. Variation of the concentration of UO_2^{2+} (1), PO_4^{3-} (2), and Na^+ (3) ions in the system $UO_2(NO_3)_2-Ba_2HPO_4-H_2O$.

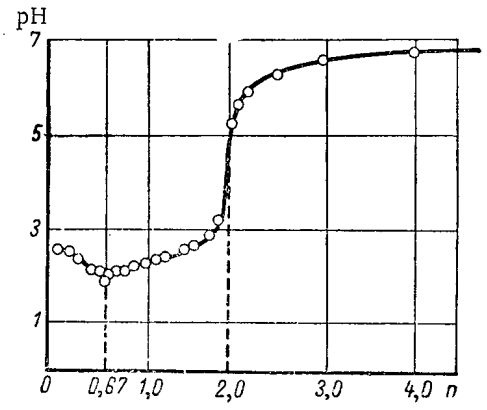

Fig. 2. pH variation in the system $UO_2(NO_3)_2-Na_2HPO_4-H_2O$.

$$(UO_2)_3(PO_4)_2 + 2HNO_3 + Na_2HPO_4 = 3UO_2HPO_4 + 2NaNO_3; \quad (2)$$

$$UO_2HPO_4 + x\,Na^+ = UO_2Na_xH_{1-x}PO_4 + x\,H^+. \quad (3)$$

Where n = 0.67-1 the solid phase is a mixture of $(UO_2)_3(PO_4)_2nH_2O$ and the mixed sodium uranyl acid phosphate, with a gradually increasing proportion of the latter. At n = 1, normal uranyl phosphate is no longer present; the composition of the solid phase may then be expressed by the formula $UO_2H_{0.54}Na_{0.46}PO_4 \times nH_2O$.

Data on the Determination of the Solubility, pH, Specific Electrical Conductivity and Volume of the Precipitate in the System $UO_2(NO_3)_2-Na_2HPO_4-H_2O$.

n	Na_2HPO_4 in the initial mixture, M.	Found in the equilibrium solution, g·ion/liter			Solid phase			pH	Specific electrical conductivity $\varkappa \cdot 10^3$, $ohm^{-1} \cdot cm^{-1}$.	Vol. of ppt. after 24 hrs., ml.		Composition of the solid phase (anhydrous).
		UO_2^{2+}	PO_4^{3-}	Na^+	PO_4^{3-}/UO_2^{2+}	Na^+/UO_2^{2+}	H^+/UO_2^{2+}			Observed	Per g·ion of UO_2^{2+} in precipitate	
0.1	0.0025	0.0214	Not detected	0.0050	0.69	0.0	0.0	2.60	5.67	1.3	14560	
0.3	0.0075	0.0139	Same	0.0150	0.68	0.0	0.0	2.30	7.03	2.0	7264	$(UO_2)_3(PO_4)_2$
0.5	0.0125	0.0064	"	0.0252	0.67	0.0	0.0	2.10	8.64	2.7	5832	
0.67	0.0168	0.00143	"	0.0337	0.70	0.0	0.10	1.90	9.65	4.0	6400	
0.75	0.0188	0.00113	"	–	0.785	0.16	0.29	2.08	9.20	3.4	5440	$(UO_2)_3(PO_4)_2 +$
0.9	0.0225	0.00098	"	0.0378	0.94	0.30	0.51	2.12	8.64	3.1	4960	$+ UO_2H_xNa_{1-x}PO_4$
1.0	0.0250	0.00079	"	0.0387	1.02	0.46	0.54	2.25	7.79	2.9	4640	
1.1	0.0275	Not detected	0.00309	0.0435	0.98	0.46	0.54	2.30	7.54	2.9	4640	
1.5	0.0375	Same	0.0135	0.0565	0.96	0.74	0.26	2.60	6.84	2.9	4640	$UO_2H_xNa_{1-x}PO_4$
1.8	0.0450	"	–	0.0670	–	0.92	0.08	2.85	6.82	4.6	7360	
2.0	0.0500	"	0.0257	0.0757	0.97	0.97	0.03	5.35	6.89	6.1	9760	
2.1	0.0525	"	–	0.0796	–	1.01	0.0	5.80	7.33	5.7	9120	
3.0	0.0750	"	–	0.1247	–	1.01	0.0	6.70	10.20	4.2	6720	
4.0	0.1000	"	0.0750	0.1739	1.0	1.04	0.0	6.90	13.50	4.0	6400	$NaUO_2PO_4$
6.0	0.1500	"	–	0.2739	–	1.04	0.0	7.20	17.90	–	–	

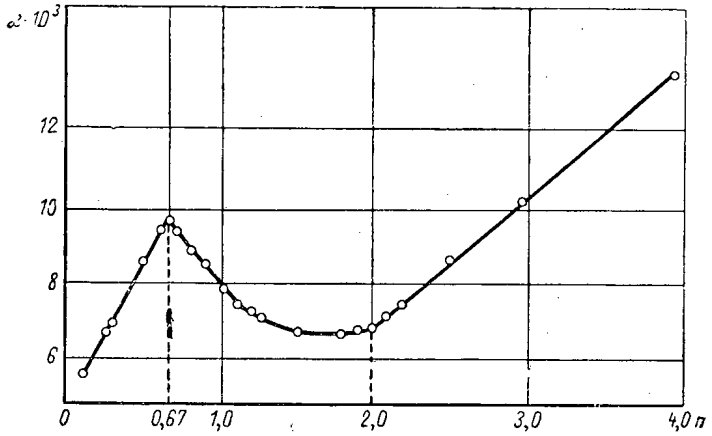

Fig. 3. Change in specific electrical conductivity in the system $UO_2(NO_3)_2 - Na_2HPO_4 - H_2O$.

3. n = 1-2. The process of replacement of hydrogen ions by sodium ions in the solid phase continues:

$$UO_2H_{1-x}Na_xPO_4 + (1-x)\,Na^+ = NaUO_2PO_4 + (1-x)\,H^+. \quad (3')$$

At n = 1, phosphate ions (more accurately, $H_2PO_4^-$ ions) appear in the solution.

At n > 2 the composition of the solid phase ($NaUO_2PO_4$) is practically constant.

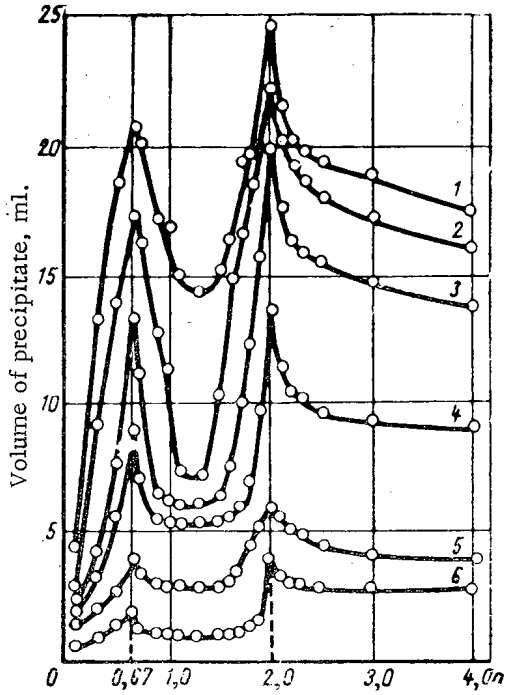

Fig. 4. Change in the apparent volume of the precipitate in the system $UO_2(NO_3)_2 - Na_2HPO_4 - H_2O$ at t = 18-20° C. Settling time: 1) 15 min; 2) 30 min; 3) 1 hour; 4) 2 hours; 5) 24 hours; 6) 48 hours.

An investigation of this system by pH measurement (see table and Fig. 2) showed that the pH of the equilibrium solution decreases initially (to a minimum at n = 0.67) and then slowly increases. But at $n \simeq 2$ there is a sudden increase of 3 in the pH, after which its variation is asymptotic. This pattern of pH change agrees exactly with the above reactions. Thus, the increase in hydrogen ion concentration in the first section of the curve is due to reaction (1), which leads to formation of free nitric acid. Then at n > 0.67, in accordance with equation (2) the hydrogen ion concentration decreases as a result of formation of insoluble sodium uranyl acid phosphate. Reaction (3), which takes place in the solid phase, does not lead to an appreciable increase in hydrogen ion concentration because these ions are neutralized by disubstituted sodium phosphate: $HPO_4^{2-} + H^+ \rightleftharpoons H_2PO_4^-$. After this process, which is completed at n = 2, the excess Na_2HPO_4 causes a marked increase in the pH of the solution.

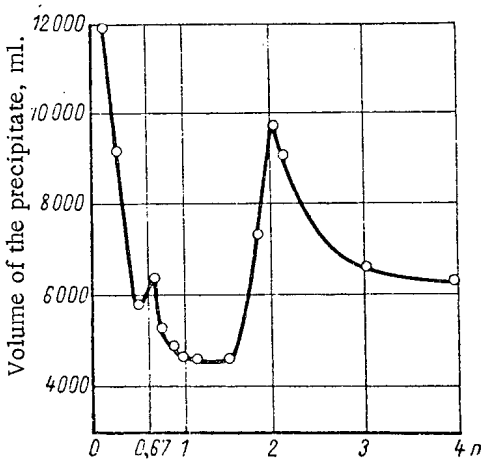

Fig. 5. Volume of the precipitate, calculated per g-ion of UO_2^{2+} in the solid phase. Settling time 24 hours.

The results of an investigation of the specific electrical conductivity show (see table and Fig. 3) that at n = 0.67 the curve has a maximum, due to maximum hydrogen ion concentration. The subsequent decrease in conductivity is due to the ion-exchange process in the solid phase, discussed above. At n > 2 another increase in conductivity is observed, increasing in proportion to the excess Na_2HPO_4 concentration, because no further chemical reaction takes place.

The results obtained by measuring the volume of the precipitate in the solution are given in the table and Fig. 4. The procedure was the same as in [4]. The results show that two distinct maxima are present when the volume of the precipitate changes (at n = 0.67 and 2.0), corresponding to the formation of normal uranyl phosphate by reaction (1), and $NaUO_2PO_4$ by reaction (3). The section of the curves with minimum values of the precipitate volume correspond to solid phases with ion-exchange functions.

Investigations of the reaction in the system $UO_2(NO_3)_2 - Na_2HPO_4 - H_2O$ by different methods gave the same results. We noted above that

normal uranyl phosphate is formed in the first stage of the reaction, despite the increasing acidity of the solution. During this stage, precipitation of uranyl ions is not complete; about 4% of the initial uranyl content remains in solution.

Since phosphate ions are not detected in the solution, the precipitate evidently contains an admixture of the acid salt, $UO_2HPO_4 \cdot nH_2O$. It is only when this stage is completed that all the added phosphate reacts, with formation of UO_2HPO_4 and $NaUO_2PO_4$ simultaneously. We did not determine the nature of the mixed sodium uranyl acid phosphate, but we consider that in this stage of the reaction the precipitate is not a mechanical mixture of the two compounds and is probably not a solid solution with the general compositon $(UO_2HPO_4)_X(NaUO_2PO_4)_Y$, but a compound of variable composition $UO_2H_XNa_{1-X}PO_4 \cdot nH_2O$ in which the H^+ and Na^+ ions can undergo mutual substitution. To solve this problem, further physicochemical investigations of the corresponding solid phases must be carried out. But if our conclusion is correct, it follows from the data of the table that the strength of the hydrogen ion bonds in the molecule of the mixed salt is considerably greater than that of the sodium ions. This follows from the fact that at n = 1 the Na^+ concentration in the solution is five times greater than that of H^+, but that the content of the latter in the precipitate is higher (H^+: Na^+ = 0.54 : 0.46). Further substitution of H^+ by Na^+ ions in the precipitate does not take place by an increase in Na^+ concentration, but as a result of the marked reduction in the H^+ ion concentration (to $6 \cdot 10^{-6}$ at n = 2). Therefore, this ion-exchange reaction must be interpreted as a consequence of ion exchange. Considered separately, this phenomenon depends on the pH of the medium, which is typical of ion exchange in general.

Be that as it may, at n = 2 the precipitate corresponds exactly to the formula $NaUO_2PO_4 \cdot nH_2O$* and the composition does not change with a six-fold excess of Na_2HPO_4. The pH change at this point is so appreciable that it is possible to carry out titrimetric determination of UO_2^{2+} ions by means of Na_2HPO_4, and at a certain UO_2^{2+} content the free acid in a solution of a number of uranyl salts can be determined. Where free acid content is not very high, the uranium and acidity determinations can probably be carried out in the same sample by either potentiometric (see Fig. 2) or conductometric (Fig. 3) methods, because either method allows one to determine the primary equivalent point corresponding to the uranyl ion content of the solution.

As was stated above, the curves of the change in volume of the precipitates (see Fig. 4) indicate the existence of the same equivalent points, but, as regards the compactness of the precipitate, which is of practical interest, Fig. 4 gives only a partial idea. In this connection however, the curve of the change in precipitate volume, calculated on the same amount of precipitate (Fig. 5), is more informative. This curve was calculated for a series of precipitates settling out in 24 hours, but the general picture is the same for any settling time. It should be noted that the least compact precipitate is not $NaUO_2PO_4$ (as might be expected from Fig. 4), but $(UO_2)_3(PO_4)_2$. But the apparent specific volume of the latter decreases rapidly with an increase in the amount of added Na_2HPO_4 as a result of the increase in acidity, which increases markedly the solubility of the precipitate.

The marked increase in the volume of the precipitate as one approaches complete substitution of H^+ ions by Na^+ ions ($NaUO_2PO_4$ solid phase) is due to the substantial increase in the pH of the medium, as a result of which the solubility of the precipitate and its particle size decrease.

Minimum volume is obtained in the region of existence of mixed sodium uranyl acid phosphate, where the curve of the change in precipitate volume is table shaped. From the practical aspect, precipitation of uranyl ions by phosphate would be most effective under these conditions (n = 1-1.5; pH $\simeq$ 2.5).

LITERATURE CITED

1. V. M. Vdovenko, Chemistry of Uranium in Transuranium Elements [in Russian], Goskhimizdat, Moscow (1960) page 171.
2. A. Chretien and G. Kraft, Bull. Soc. Chim., 5, 373 (1938).
3. Investigations in the Field of Uranium Chemistry, Symp. of Articles, Edited by Victor I. Spitsyn [in Russian], Izd-vo MGU (1961) pp. 233, 240.
4. I. V. Tananaev, Izv. sektora fiz.-khim. analiza, 20, 288 (1950).

*We did not determine the exact water content in the solid phases, and literature data on this subject are not clear.

SPECTRA AND INELASTIC SCATTERING CROSS SECTIONS OF NEUTRONS IN THE 0.2–1.2 MeV ENERGY RANGE SCATTERED BY NUCLEI OF V, Th, Hg, W, Sb, Cd, Mo, Nb, Fe

N. P. Glazkov

Translated from Atomnaya Énergiya, Vol. 14, No. 4,
pp. 400-402, April, 1963
Original article submitted June 18, 1962

To measure the spectra of inelastically scattered neutrons in the 0.4-1.2 MeV range we used a simple spherical chamber of small dimensions (ϕ 40 mm), filled with He^3 to 40 atm. The energy resolution of the chamber (~100-150 keV) was mainly determined by the recombination effect, which was very noticeable at this pressure. Experience has shown [1] that the He^3 spherical chamber is as good as the proportional counter in energy resolution; it is isotropic and a more effective neutron detector. In the present work the inelastic scattering of neutrons was studied by the method of inverse spherical geometry. The scattering specimens were prepared from substances with a natural content of isotopes in the form of spherical layers of 30 mm thickness (external and internal diameters 100 and 40 mm respectively). For most of the scatterers the initial material was selected in the form of powders which were poured into specially prepared containers of thin (0.2 mm) steel. The neutron source was a tritium target bombarded by a

Cross Sections of Neutrons Inelastically Scattered by Various Nuclei, b

Energy of neutron, MeV	Partial cross sec. corr. to var. energies of excited residual nucleus		Total cross section
	(0,26–0,30)	(0,56–0,62)	
Cd			
0,4	0,11±0,01		0,10±0,01
0,6	0,24±0,02		0,24±0,02
0,8	0,15±0,02	0,37±0,03	0,50±0,05
1,0	0,12±0,01	0,78±0,10	0,90±0,10
	0,15	(0,50–0,57)	
Sb			
0,4	0,10±0,02		0,10±0,02
0,6	0,09±0,02		0,10±0,02
0,8	0,08±0,02	0,20±0,02	0,30±0,03
1,0	0,07±0,02	0,20±0,02	0,30±0,03
	(0,05–0,12)	(0,21–0,26)	
W			
0,4	1,03±0,10	0,10±0,05	1,10±0,15
0,6	1,01±0,10	0,20±0,05	1,20±0,15
0,8	1,60±0,15	0,25±0,05	1,85±0,20
1,0	1,80±0,20	0,70±0,20	2,50±0,30
	~0,74	~(0,8–0,99)	
Nb			
0,4			<0,1
0,6			<0,1
0,8	0,20±0,02		0,20±0,02
1,0	0,15±0,03	0,50±0,05	0,65±0,06
1,2	0,35±0,04	0,85±0,10	1,20±0,10

Energy of neutron, MeV	Partial cross section corresponding to various energies of excited residual nucleus				Total cross section
	0,20	0,53	(0,66–0,75)		
Mo					
0,4	0,10±0,02				0,1±0,02
0,6	0,10±0,02	0,03±0,01			0,15±0,03
0,8	0,30±0,02	0,16±0,02			0,45±0,04
1,0	0,10±0,02	0,10±0,02	0,7±0,1		0,90±0,10
	(0,16–0,20)	~(0,38–0,43)	~0,90		
Hg					
0,4	0,12±0,02				0,12±0,02
0,6	0,15±0,02	0,42±0,04			0,55±0,05
0,8	0,15±0,02	0,48±0,05			0,60±0,05
1,0	0,15±0,02	0,48±0,05	0,27±0,03		0,90±0,10
	0,044	0,145	0,300	~0,700	
U					
0,4	1,15±0,10	0,20±0,04			1,35± 0,15
0,6	1,50±0,15	0,35±0,04	0,10±0,05		1,95± 0,20
0,8	1,20±0,20	0,35±0,07	0,15±0,05	0,30±0,03	2,00± 0,30
1,0	0,80±0,10	0,30±0,03	0,15±0,02	0,70±0,07	1,95± 0,20
	0,055	0,17	0,30	~0,8	
Th					
0,4	1,25±0,10	0,30±0,20			1,5±0,3
0,6	1,20±0,10	0,40±0,20			1,6±0,3
0,8	1,23±0,10	0,45±0,20			1,7±0,3
1,0	1,23±0,10	0,50±0,20	0,10±0,05	0,65±0,20	2,4±0,3

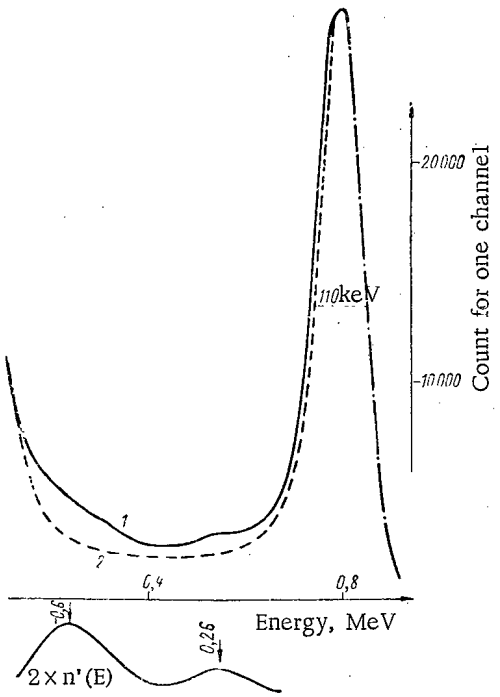

Fig. 1. Spectrum of neutrons with an energy of 0.8 MeV inelastically scattered by cadmium: 1) with scatterer; 2) without scatterer.

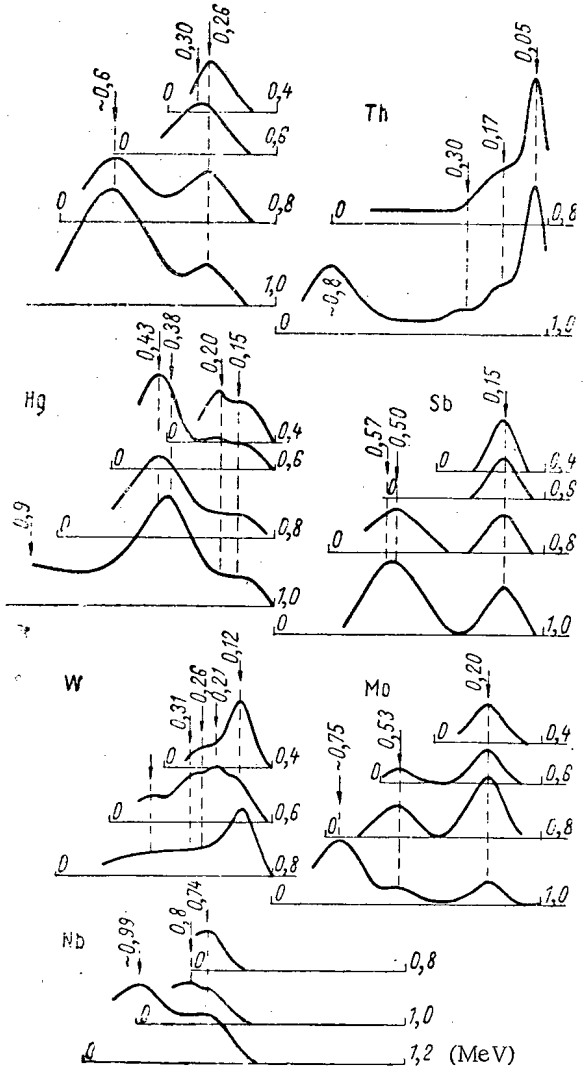

Fig. 2. Spectra of neutrons inelastically scattered by various nuclei.

proton beam from the ÉG-2.5 Van de Graaf accelerator. The energy scattering due to the target was ~ 60 keV. The distance from the target of the accelerator to the scatterer was 350 mm. The chamber was covered by a cadmium hood (thickness 0.2 mm) for protection against thermal neutrons. After amplification, the pulse spectrun of the chamber was recorded by a 128-channel amplitude analyzer.

To obtain the effect of inelastic scattering we measured the neutron spectra in turn: without a scatterer and with a scatterer. The difference between these spectra, standardized from the maximum in the hard part, is due to inelastic scattering. The spectrum of inelastically scattered neutrons n'(E) was obtained by numerical subtraction separately for each channel with a correction for the efficiency of the He^3-chamber as a function of the energy.

The form of the obtained spectrum was determined by the position of the energy levels of the nuclei of the scatterer and their partial excitation cross sections during inelastic scattering of neutrons and the energy resolution of the chamber. By a simple summation for all channels or some of the channels of the spectrum n'(E) we can obtain the total or partial effects of inelastic neutron scattering respectively; these are related to the corresponding cross section $\sigma_{n'}$ in the following way:

$$\frac{\Sigma n'}{\Sigma K N_1 + \Sigma n'} = 1 - e^{-n\sigma_{n'}\bar{l}},$$

where n is the density of nuclei in a given scattering specimen; $\bar{l}$ is the mean path of incident neutrons in the specimen; $\Sigma(KN_1) + \Sigma(n')$ is the standardized total flux of the incident neutrons.

Data on the transport cross sections σ_{tr}, used for the calculation of $\bar{l}$ were mainly taken from [2]. These data are not very accurate (~ 15-20%); the indefiniteness in $\bar{l}$ and $\sigma_{n'}$ therefore reaches 4-5%. The accuracy of $\sigma_{n'}$ also depends on the accuracy in the measurements of this effect. We will analyze certain errors in the measurement of the total and partial inelastic scattering effects. Since the absorption of neutrons in the material of the scatterer was

not recorded and therefore not taken into account in the total flux of incident neutrons, the cross section $\sigma_{n'}$ due to this effect will be approximately 1% high. The presence in the scattering specimen of a hole to take the chamber, occupying about 8.5% of the total volume of the scatterer leads to a reduction in the measured effect. A correction to $\bar{l}$ should therefore be introduced into the calculation formula. In the case of incomplete resolution of the close-lying neighboring levels their partial excitation cross sections were determined by the method of successive subtractions. The mean accuracy in the separation of partial effects by this method is ~10%. The partial inelastic scattering cross sections may be determined with less accuracy than the total inelastic scattering cross sections.

Additional difficulties arise in the separation of partial effects of inelastic scattering with excitation of levels with an energy < 0.1 MeV, since in this case it is essential to allow for the effect of softening of the incident neutrons due to elastic scattering. This effect was allowed for but the errors can be large. The statistical error in one measurement of the inelastic scattering effect was less than 3%.

The analysis and evaluation of the above errors and corrections makes it possible to obtain total inelastic scattering cross sections with an accuracy of 10% and partial cross sections with an accuracy of 10-15%. By way of illustration, Fig. 1 gives the results for the measurement of the spectrum of neutrons with an energy of 0.8 MeV inelastically scattered by cadmium. The difference spectrun n'(E) with a resolution of 110 keV is the spectrum of inelastically scattered neutrons (without a correction for the efficiency of the chamber). Figure 2 gives the spectra of inelastically scattered neutrons. From the obtained spectra, with an allowance for the energy resolution of the chamber, we determined the inelastic scattering cross sections shown in the table. When the effects of inelastic scattering with excitation of separate levels were well resolved experimentally, the table gives the partial cross sections corresponding to them. In the case where, due to the closeness of the levels, the effects of the latter were not resolved, the table gives partial cross sections for the whole group of unresolved levels with an indication of the assumed excitation energies of these levels according to [3]. The last column of the table shows the total inelastic scattering cross sections $\sigma_{n',\Sigma}$ as the sum of all partial cross sections.

As a control experiment we measured the cross sections of neutrons with energies of 1.0 and 1.2 MeV, inelastically scattered by iron. The cross sections obtained for iron, equal to 0.28 ± 0.04 and 0.55 ± 0.05 b, agree well with the data of other papers within the limits of the errors.

LITERATURE CITED

1. N. P. Glazkov, PTÉ, No. 4, 96 (1957); A. I. Abramov, PTÉ, No. 4, 56 (1959).
2. I. V. Gordeev, D. A. Kardashev, and A. V. Malyshev. Handbook on Nuclear Physical Constants for Reactor Designs [in Russian], Atomizdat, Moscow (1960).
3. B. S. Dzhelepov and L. K. Peker, Decay Schemes of Radioactive Nuclei [in Russian], Izd. AN SSSR, Moscow (1958).

A METHOD FOR CALCULATING THE NEUTRON FLUX IN A SHUT – DOWN REACTOR WITH A PHOTONEUTRON SOURCE

L. V. Konstantinov and B. I. Kochetov

Translated from Atomnaya Énergiya, Vol. 14, No. 4,
pp. 402-404, April, 1963
Original article submitted June 9, 1962

Repeated starts of nuclear reactors involve difficulties in the measurement of the neutron flux in the subcritical state, caused by the influence of γ-radiation of fission fragments on the instruments recording the neutrons. In repeated starts artificial neutron sources are therefore used to increase the neutron flux to a value needed for reliable operation of the apparatus.

Po-α-Be-sources should not be used because the preparation of these sources with an intensity of 10^9-10^{10} neutrons/sec is complex and expensive. These sources with an intensity of 10^7-10^8 neutrons/sec are only used for the initial physical starts of reactors.

Another type is the photoneutron source in which beryllium or heavy water are used. The γ-quanta sources can be radioactive isotopes Na^{24}, Sb^{124}, Mn^{26}, etc. The decay of these sources after the reactor has been shut down will be compensated by their activation by thermal neutrons during further operation of the reactor. A fault of photoneutron sources is the fact that they introduce an additional negative reactivity into the reactor; this can be reduced by the (γ, n) reaction for beryllium or heavy water due to γ-quanta of fission fragments.

A method is given below for the calculation of a photoneutron source, the γ-radiator of which is provided by fission fragments formed during operation of the reactor. Photoneutron sources using radioactive isotopes are calculated from analogous formulas but with an allowance for the relative arrangement of the beryllium and source of γ-quanta. Furthermore, corrections must be made for the additional yield of neutrons due to the γ-radiation of the fission fragments.

The essential amount of beryllium is calculated for a point source of neutrons placed in the active zone of a cylindrical reactor in which the effect of the reflector is allowed for by effective additions.

According to [1], the neutron flux in the active zone of a subcritical reactor in the presence of a neutron source will be represented in the form of an expansion in eigenfunctions of the reactor using the notations used in [1]:

$$\Phi_n(r; z) = \sum_{m, n}^{\infty} \frac{A_{m\,n} J_0(\alpha_m r) \cos \frac{n\pi z}{H^*} \overline{P}_{\infty}(B^2_{mn})}{\Sigma_a (1 - K_{mn\ \mathrm{eff}})(1 - B^2_{mn} L^2)}, \quad (1)$$

where $H^* = H_0 + 2\delta$ is the extrapolated height of the active zone (δ is the effective addition of the reflector); $\alpha_m = \xi_m / R^*$ (here the ξ_m are the roots of the zero order Bessel function; $R^* = R_0 + \delta$ is the extrapolated radius of the active zone).

The coefficients A_{mn} are determined in the expansion of the function of a source placed at the point with coordinates r_1, z_1 in the active zone, from the eigenfunctions of the cylindrical reactor:

$$S_n \delta(r_1; z_1) = \sum_{m=1}^{\infty} \sum_{n=1}^{\infty} A_{mn} J_0(\alpha_m r) \cos \frac{n\pi z}{H^*}, \quad (2)$$

where S_n is the intensity of a point source of neutrons (neutrons/sec). Later we will only consider the first approximation; according to the evaluation conducted for the reactor of the First Atomic Power Station for $\Delta k \leq 2\%$, this approximation gives an error in the determination of the coefficient A_{mn} of not more than 2%.

To determine the power of the subcritical reactor the flux is integrated over the whole volume of the active zone:

$$P = P_0\eta = \int\limits_{V_{a.z.}} \Phi(r_1 z_1)\,\Sigma_a\,\frac{K_{\infty}}{\varphi\nu\omega}\,dv, \tag{3}$$

where P is the power of the subcritical reactor; P_0 is the nominal power of the reactor; $w = 3{,}1\cdot10^{-10}$ fissions/W·sec.

Substituting the value $\Phi(r_1, z_1)$ in formula (1) and integrating, we obtain

$$S_n = \frac{\pi\nu w\xi_1(1-K_{\text{eff}})\,H^*J_1^2(\xi_1)\,\eta P_0}{8K_{\text{eff}}\,R_0J_1\left(\xi_1\frac{R_0}{R^*}\right)\sin\frac{\pi H_0}{2H^*}\,J_0^2\left(\xi_1\frac{r_1}{R^*}\right)\cos^2\frac{\pi z_1}{H^*}}, \tag{4}$$

This expression determines the intensity of the point neutron source placed in the active zone needed to increase the power of the reactor in the subcritical state to the required quantity P, depending on the subcriticality of the reactor.

By similar discussions, we can obtain formulas for the intensity of a linear source of neutrons, the volume source of neutrons distributed according to the eigenfunction of a cylindrical reactor, and for other cases.

The formula for the calculation of intensity of a volume source distributed according to the eigenfunction of the reactor (which corresponds to uniform arrangement of beryllium over the active zone) has the simplest form

$$S_n = \frac{\nu w(1-K_{\text{eff}})}{K_{\text{eff}}}\,\eta P_0. \tag{5}$$

Having found the required intensity of the neutron source we determine the required amount of beryllium. In the calculation we should allow for the decay in time of the flux of γ-quanta with energy above the threshold of the (γ, n)-reaction for beryllium (E_n = 1.67 MeV). According to [2, 3] the flux of γ-quanta with energy greater than E_n is split up into three energy groups: 1.8-2.2 MeV, 2.2-2.6 MeV, and 2.8 MeV. In the center of the active zone of the reactor at time t after its shut-down, according to [2], the γ-quanta flux

$$\Phi_{\gamma_k}(0t) = \frac{P_0\xi_1\bar{J}_{\gamma_k}(t)\,\gamma_k}{4R_0R^*H^*J_1\left(\xi_1\frac{R_0}{R^*}\right)\sin\frac{\pi H_0}{2H^*}\,E_k\mu_{a.z.k}}, \tag{6}$$

where E_k is the energy of the k-th group; γ_k is the self-absorption coefficient of the γ-quanta of the k-th group in the fuel. (The other notations are given in [2].) The neutron intensity due to beryllium being carried into the center of the active zone of the reactor is determined by the formula

$$S_{nk}(r_1z_1) = \Phi_{\gamma_k}(0t)\,\sigma_k(\gamma, n)\,N_{\text{Be}}J_0\times\left(\xi_1\frac{r_1}{R^*}\right)\cos\frac{\pi z_1}{H^*}, \tag{7}$$

where N_{Be} is the total number of beryllium nuclei and $\sigma_k(\gamma, n)$ is the effective cross section of the (γ, n)-reaction by beryllium. Substituting the value of the γ-quanta flux in formula (7), from formula (6) we obtain

$$S_n = \frac{P_0\xi_1N_{\text{Be}}J_0^2\left(\xi_1\frac{r_1}{R^*}\right)\cos^2\frac{\pi z_1}{H^*}}{4R_0R^*H^*J_1\left(\xi_1\frac{R_0}{R^*}\right)\sin\frac{\pi H_0}{2H^*}}\times\sum_{k=1}^{3}\frac{\sigma_k(\gamma n)\,\bar{J}_{\gamma_k}(t)\,\gamma_k}{E_k\mu_{a.z.k}}, \tag{8}$$

where k is the number of groups of γ-quanta able to cause a photoneutron reaction.

Substituting the values of S_n in expressions (4) and (5), we obtain formulas for the calculation of the reactor power with an artificial neutron source and given subcriticality in its active zone:

1) for a point source

$$\eta = \frac{P}{P_0} = \frac{2K_{\text{eff}}N_{\text{Be}}J_0^2\left(\xi_1\frac{r_1}{R^*}\right)\cos^2\frac{2\pi z_1}{H^*}}{\pi\nu wR^{*2}H^*(1-K_{\text{eff}})\,J_1^2(\xi_1)}\sum_{k=1}^{3}\frac{\sigma_k(\gamma n)\,\bar{J}_{\gamma_k}(t)\,\gamma_k}{E_k\mu_{a.z.k}}; \tag{9}$$

2) for a linear source

$$\eta=\frac{P}{P_0}=\frac{2K_{\text{eff}}\,N_{\text{Be}}J_0^2\left(\xi_1\frac{r_1}{R^*}\right)\left(\frac{H_0}{2}+\frac{H^*}{2\pi}\sin\frac{\pi H_0}{2H^*}\right)}{\pi v w R^{*2}H^*(1-K_{\text{eff}})\,J_1^2(\xi_1)\,H_1}\sum_{k=1}^{3}\frac{\sigma_k(\gamma n)\,\bar{J}_{\gamma_k}(t)\,\gamma_k}{E_k\mu_{\text{a.z.k}}}, \tag{10}$$

where H_1 is the length of a linear source placed symmetrically with respect to the central plane;

3) for a volume source distributed according to the eigenfunction of the reactor,

$$\eta=\frac{P}{P_0}=\frac{K_{\text{eff}}\,N_{\text{Be}}}{vwV_{\text{a.z.k}}(1-K_{\text{eff}})}\sum_{k=1}^{3}\frac{\sigma_k(\gamma n)\,\bar{J}_{\gamma_k}(t)\,\gamma_k}{E_k\mu_{\text{a.z.k}}}. \tag{11}$$

The method for the calculation of the photoneutron source was checked with the reactor of the First Atomic Power Station. Before the routine start-up of the reactor at subcriticality $\Delta K = 0.093$, 8 kg of beryllium oxide was introduced into one of the central cells in the form of a rod. The neutron flux in the experiment was measured by an instrument with a sensitivity of 10^{-12} A/fission; a high-sensitivity compensated KNK-54 ionization chamber and a fission chamber were used as the detectors.

Introducing beryllium oxide into the active zone of the reactor increased the neutron flux by a factor of 2.3-2.5; the difference between the calculated and experimental data did not exceed 10%. To increase the efficiency of the photoneutron source the beryllium is best placed in the active zone at the points of maximum flux of the γ-quanta of the fission fragments.

LITERATURE CITED

1. S. Glasstone and M. Edlund, Principles in the Theory of Nuclear Reactors [Russian translation], Izd. inostr. lit., Moscow (1954).
2. T. Rockwell, Nuclear Reactor Shielding [Russian translation], Izd. inostr. lit., Moscow (1958).
3. V. Crocer and K. Henry, Reports RP/m 72 (1956).

THE ENERGY DISTRIBUTION OF SCATTERED NEUTRONS IN WATER

V. A. Dulin, Yu. A. Kazanskii, and I. V. Shugar

Translated from Atomnaya Énergiya, Vol. 14, No. 4,
pp. 404-405, April, 1963
Original article submitted July 18, 1962

This article deals with the experimental determination of the neutron spectrum in water at distances of 20-90 cm from a neutron source with an energy of ~15 MeV.

The neutron source was the reaction $H^3(H^2, n)He^4$ with a deuteron energy of 400 keV. The measurements were made along the direction of the deuteron beam under conditions of infinite geometry. We used a single-crystal scintillation fast-neutron spectrometer with discrimination of the γ-radiation during fluorescence [1]. During measurements at greater distances from the source the ratio between the neutron flux and γ-radiation flux reached 0.02. To ensure satisfactory statistics in the measurement of neutron spectra it was essential to have a pulse count rate of not less than 50 cps. The pulse count rate from the γ-radiation was $\sim 2.5 \cdot 10^3$ cps. The established and periodically checked level of discrimination was such that the degree of attenuation of γ-radiation with an energy of ~2.5 MeV was $\sim 3 \cdot 10^{-4}$. The spectroscopic threshold was then 1.9 MeV.

The amplitude distributions were measured with a 128-channel analyzer [2]. The measurements were conducted for two different amplification factors. The energy scale of the spectrometer with low amplification was estab-

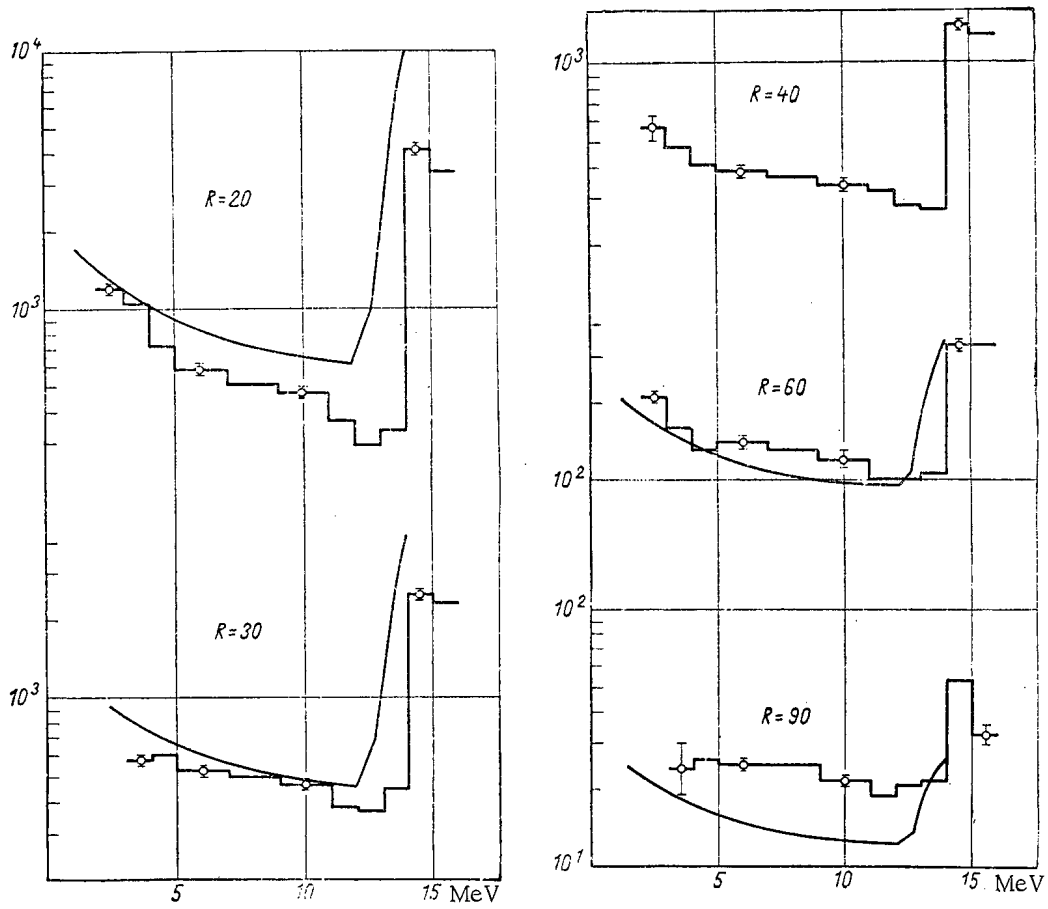

Histograms of Measured Energy Distributions.

lished from the amplitude distribtuion of neutrons with an energy of 15 MeV and for high amplification from the γ-radiation of ThC"(E_γ = 2.62 MeV), which corresponds to a neutron energy of 6.1 MeV. For various amplifications the neutron spectra agreed within the limits of the errors.

The measured amplitude distributions $\Phi[V(E)]$ were converted to the neutron spectrum $N(E_n)$ from the formula

$$N(E_n) = -\frac{E_n}{1-\exp[-\Sigma(E_n)\,d]} \times \frac{d}{dE}\left\{\Phi[V(E)]\,\frac{dV}{dE}\right\}_{E=E_n},$$

where $\Sigma(E_n)$ is the macroscopic neutron cross section for scattering by the hydrogen of the crystal; d is the thickness of the crystal; $V(E)$ is the dependence of the pulse amplitude on the energy.

The amplitude distributions were measured four to six times for all values of the distance R_i. The figure gives the neutron spectra related to unitary energy range, multiplied by $(R_i/20)^2$ (histograms). The mean-square errors are shown. For comparison, the results are given for calculations by the method of moments for the energy spectrum of neutrons from a point isotropic source with an energy of 14 MeV [3] (smooth curve). The calculation curve and the results of the measurements are standardized over the area for R = 20 cm. As can be seen from the figure, the measured spectra agree well with the calculated spectra. The difference in the absolute value extends beyond the limits of error in the measurements; it may be due to the different primary energy of the neutrons.

From the measured spectra we can determine the relaxation length for a group of neutrons with energies of 14-16 MeV. At distances of 30-60 and 60-90 cm it is 15.0 ± 0.8 and 14.7 ± 0.9 cm respectively, which agrees well with measurements of the relaxation length by the indicator Cu^{63}·(n, 2n)Cu^{62}, performed by B. I. Sinitsyn.

The authors would like to thank S. G. Tsypin for useful discussions and V. G. Dvukhsherstnov for helping with the work.

LITERATURE CITED

1. V. A. Dulin et al., Pribory i tekhnika éksperimenta, No. 2, 35 (1961).
2. L. A. Matalin et al., Pribory i tekhnika éksperimenta, No. 1, 64 (1957).
3. The Shielding of Atomic-Powered Transportation Units [Russian translation], Collection of translations edited by V. V. Orlov and S. G. Tsypin, Izd. inostr. lit., Moscow (1961).

All abbreviations of periodicals in the above bibliography are letter-by-letter transliterations of the abbreviations as given in the original Russian journal. *Some or all of this periodical literature may well be available in English translation.* A complete list of the cover-to-cover English translations appears at the back of this issue.

THE BREMSSTRAHLUNG RADIATION OF β-PARTICLES AND SHIELDING AGAINST IT

V. S. Eliseev

Translated from Atomnaya Énergiya, Vol. 14, No. 4,
pp. 405-407, April, 1963
Original article submitted July 7, 1962

In various branches of industry extensive use is made of β-radiators, the activity of which often reaches hundreds of millicuries. The operating personnel are protected against radiation by screens of plexiglas, aluminum, glass, plastics, and other materials, with a thickness equal to the path length of the β-particles in the material. However, this does not take into account bremsstrahlung radiation which occurs when β-particles are absorbed by the protective screens.

At present certain authors [1, 2] recommend the following formula for the determination of the yield of bremsstrahlung radiation

$$B = 1.23 \cdot 10^{-4} (\underline{Z} + 3) E_\beta^2 \text{ MeV/β-particle},$$

where E_β is the maximum energy of the β-particle, MeV; $\underline{Z} = \Sigma_i Z_i^2 / \Sigma_i Z_i$ is the effective atomic number of the retarding material (i is the fraction of atoms of the retarding material with atomic number Z_i of the total number of atoms); 3 is a number which takes into account the internal bremsstrahlung radiation.

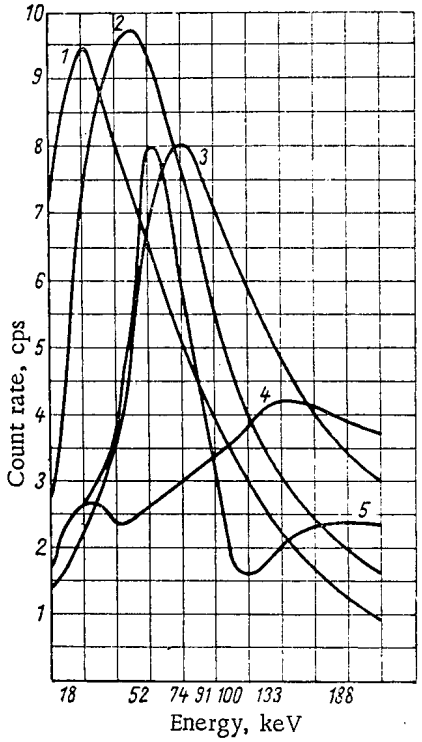

Fig. 1. Bremsstrahlung radiation spectra of Sr^{90}-Y^{90}, formed in targets of various materials with thickness equal to the path length of the β-particles: 1) Plexiglas; 2) aluminum; 3) copper; 4) tin; 5) lead.

However, this formula does not provide a complete evaluation of the spectral distribution of bremsstrahlung radiation with energies up to 100 keV.

From an overall evaluation of the spectral distribution of intensity of bremsstrahlung radiation obtained from this formula, it follows that the energy of much of the radiated quanta will be up to 100 keV. Experimental investigations of the effect of the material of the protective screen on the energy of the maximum of the bremsstrahlung radiation yield in the 0-200 keV range will therefore be of considerable interest. For this purpose, quanta radiated by particles during slowing down in the screen were recorded by a standard scintillation spectrometric NaI(Tl) crystal (30 mm in diameter and 14 mm in height) in combination with the FÉU-29 photoelectron multiplier, the signal from which was passed to an AADO-1 ampli-

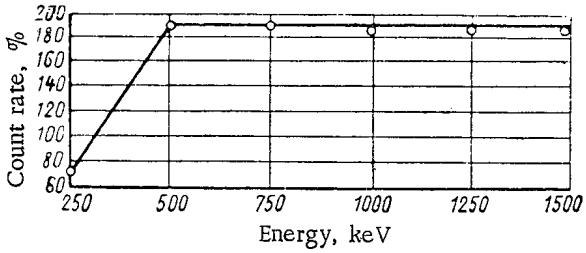

Fig. 2. Ratio of the yield of bremsstrahlung radiation from a lead screen to the yield of radiation from a plexiglas screen (for screen thicknesses equal to the path lengths of the β-particles).

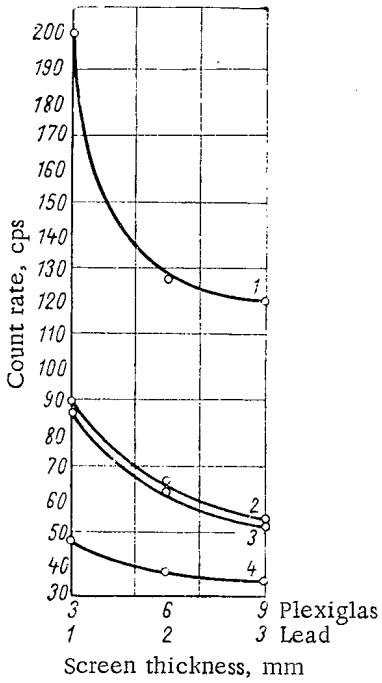

Fig. 3. Dependence of the intensity of bremsstrahlung radiation on the screen thickness: 1) Plexiglas; 2) lead; 3) compound screen (lead + + plexiglas); 4) combined screen (plexiglas + lead).

tude differential analyzer and fed to a PS-5M scaling device. As the source of β-particles we used Sr^{90}-Y^{90} with an activity of 5 μCi with respect to strontium, applied in the form of a 3-mm dia. spot on cellophane by the evaporation of strontium chloride. In order to make the cellophane rigid, it was glued into a plexiglas frame (1 mm thick with 5-mm dia. holes over the source), placed in a 1-mm thick cardboard support. The distance between the source of β-particles and the lower plane of the crystal in all experiments was 50 mm along the central axis of the source and crystal. The accuracy of the experiments was 2-5%.

In the processing of the curves an allowance was made for the absorption coefficient of the γ-quanta in the NaI(Tl) crystals [3].

Figure 1 gives curves for the spectral distribution of intensity of bremsstrahlung radiation in the protection of a source by uniform targets of various materials with a thickness equal to the path length of the β-particles. The curves show that the maximum of intensity of the radiation is inversely proportional and the energy of the maximum of intensity is directly proportional to the atomic number of the material of the protective screen.

Materials with high atomic numbers give several intensity maxima, the energy of one of which corresponds to the calculated value [4]. For materials with low atomic numbers a characteristic feature is one intensity maximum corresponding to the calculated value of energy. The appearance of additional maxima may be due to the characteristic radiation and to impurities in the materials of the screens. A certain reduction in the intensity maximum of the radiation with a plexiglas screen is due to the absorption of low-energy quanta (18 keV) by the lid of the container.

When screens of materials with low atomic numbers are used for shielding against β-particles there is therefore very intense radiation of low-energy quanta; the use of heavy materials involves the formation of quanta with higher energies but lower intensity.

Figure 2 gives the dependence of the spectral distribution of intensity of bremsstrahlung radiation on the atomic number of the material of the screen for quanta with energies higher than 250 keV. It follows from these data that with increase in the atomic number of the material of the screen there is an increase in the yield of quanta with high energies.

Consequently, for shielding against β-particles we must use compound screens for which the material with the low atomic number is placed near the source and the material with the high atomic number is placed behind it. In this case quanta with low energy, formed in the first material with a thickness equal to the path length of the β

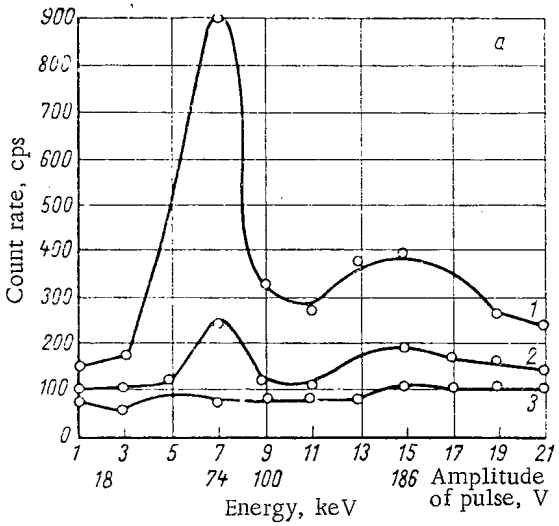

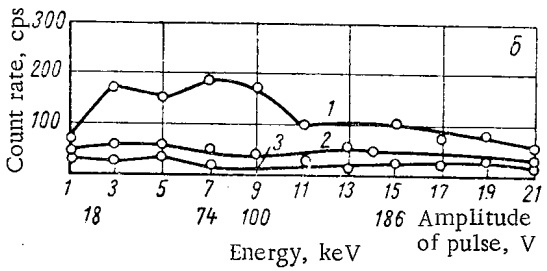

Fig. 4. Spectral distribution of intensity of bremsstrahlung radiation in protection by compound screens: a) Lead is placed near source [1) 1 mm lead + 3 mm plexiglas; 2) 2 mm lead + 6 mm plexiglas; 3) 3 mm lead + 9 mm plexiglas]; b) plexiglas is placed near source [1) 3 mm plexiglas + 1 mm lead; 2) 6 mm plexiglas + 2 mm lead; 3) 9 mm plexiglas + 3 mm lead].

particles, are absorbed in the material with the high atomic number. Experiments showed that the intensity of bremsstrahlung radiation behind compound screens is almost a half of that behind uniform materials of the same thicknesses (Fig. 3). Curves of the spectral distribution of intensity of bremsstrahlung radiation using compound screens (Fig. 4) show that the intensity is mainly reduced due to absorption of the low-energy quanta.

LITERATURE CITED

1. G. V. Gorshkov, Gamma-Radiation of Radioactive Bodies and Elements in the Design of Radiation Shields [in Russian], Izd. AN SSSR, Moscow (1959).
2. N. Gusev, V. Mashkov, and G. Obvintsev, Gamma-Radiation of Radioactive Isotopes and Fission Products [in Russian], Fizmatgiz, Moscow (1958).
3. W. Price, The Recording of Nuclear Radiation [Russian translation], Izd. inostr. lit., Moscow (1960).
4. Levek, Martinelli, and Shoven, Reports of the International Conference on the Peaceful Uses of Atomic Energy (Geneva, 1955), Vol. 15, Mashgiz, Moscow (1957).

CERTAIN DOSIMETRIC CHARACTERISTICS OF THE SBM-10 SMALL-SIZE COUNTER

A. M. Panchenko

Translated from Atomnaya Énergiya, Vol. 14, No. 4,
pp. 408-409, April, 1963
Original article submitted July 11, 1962

In measuring the intensity of γ-radiation which has a complex spectral-angular distribution, the sensitivity of the radiation detector, as a rule, must not heavily depend on the radiation energy (the "behavior with hardness" with respect to intensity must be absent), and the detector must have isotropic sensitivity and small dimensions.

We have investigated the possibility of using as a detector of γ-radiation the SBM-10 small-size halogen β-counter with a screen, which has been recently developed by the industry. The schematic diagram of the counter and its basic dimensions are given in Fig. 1. The counter's rated operating voltage is 400 V, the Geiger plateau is not less than 100 V, the natural background level does not exceed 8 pulses/min, and the thickness of the steel cathode is 40 mg/cm^2 ($\sim 50\mu$).

The best results with respect to the behavior with hardness (Fig. 2) were obtained for a counter with a screen selected on the basis of data from [1, 2], which consisted of three layers: tin (0.12 mm), aluminum (1 mm), and lead (0.22 mm).

The counter's mean sensitivity was determined experimentally; it was equal to $8.2 \cdot 10^{-3}$ pulses·cm^2/MeV ± 11% in the energy range from 0.1 to 1.25 MeV.

For sources of γ-radiation, we used the following isotopes: Hg^{203} (0.28 MeV), Cr^{51} (0.33 MeV), Cs^{137} (0.661 MeV), Cs^{134} (0.72 MeV), Zn^{65} (1.12 MeV), and Co^{60} (1.25 MeV), and also filtered x-ray radiation.

The intensity of the incident γ-radiation was determined by means of a Bakelite ionization chamber, the inside walls of which were covered with a conducting layer. It was assumed that such a chamber with air-equivalent walls is not characterized by behavior with hardness with respect to intensity. The chamber was calibrated by means of a standard Co^{60} source.

The investigation results given above pertain to the case of the normal incidence of γ-quanta. The angular dependences of the counter's sensitivity with and without the screen are shown in Fig. 3. The values of the ratio of the counting rate $n(\psi)$ for the incidence of γ-quanta at the angle φ with respect to the counter's axis to the counting rate $n(\varphi = 90$ deg) for the normal incidence of γ-quanta are laid off on the axis of ordinates. The maximum difference in the counting rate was equal to 11% for γ-quanta with the energy E_γ = 0.28 MeV. The asymmetry of the counter hardly affects the angular sensitivity.

Thus, SBM-10 counters with screens can be considered as sufficiently isotropic detectors without the behavior with hardness with respect to intensity in the energy range under consideration, so that they can be used for measuring the intensity of γ-radiation characterized by a complex spectral-angular distribution.

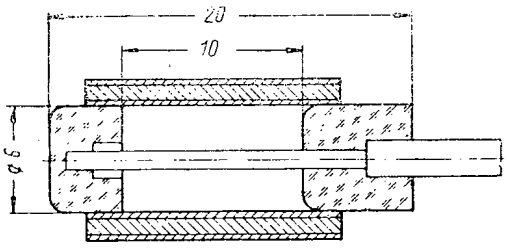

Fig. 1. Diagram of the SBM-10 counter with the screen.

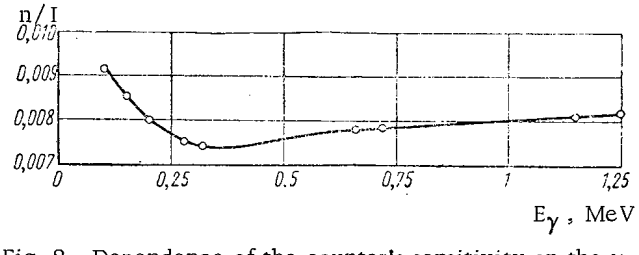

Fig. 2. Dependence of the counter's sensitivity on the γ-radiation energy [I is the radiation intensity (MeV/cm^{2}sec); n is the counting rate (pulses/sec)].

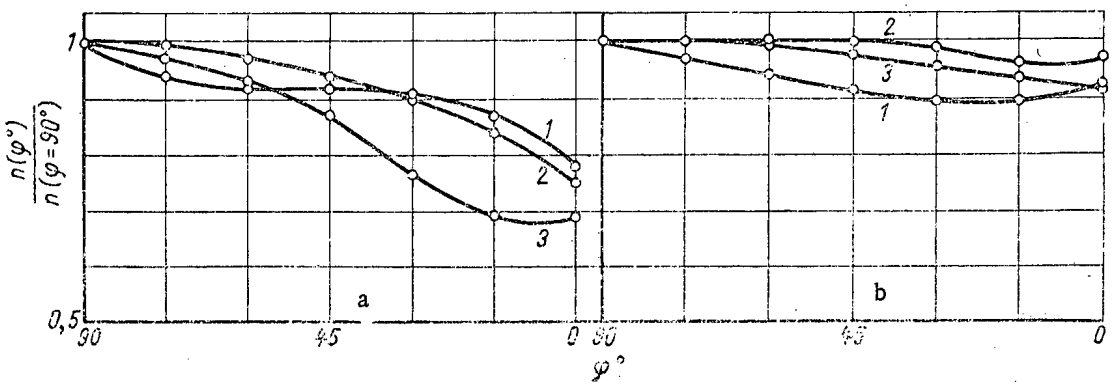

Fig. 3. Dependence of the counter's sensitivity [a) without the screen; b) with the screen] on the angle of incidence of γ-quanta.

The author hereby expresses his gratitude to O. I. Leipunskii for the valuable remarks he offered in discussing this paper.

LITERATURE CITED

1. V. N. Sakharov, Atomnaya Énergiya, 3, No. 7, 61 (1957).
2. B. P. Bulatov, Atomnaya Énergiya, 6, No. 3, 332 (1959).

DETERMINATION OF THE CONTENT OF α-RADIATORS WHOSE ENERGIES ARE CLOSE TO EACH OTHER IN ISOTOPE MIXTURES

L. S. Gorn and B. I. Khazanov

Translated from Atomnaya Énergiya, Vol. 14, No. 4,
pp. 409-411, April, 1963
Original article submitted May 31, 1962

The determination of the isotope composition by using the method of α-spectrometry constitutes one of the interesting problems in the practice of radiometric analysis.

The similar intensities of the lines of isotopes which are in equilibrium and the well-defined correspondence between the amplitude of the electric signal and the radiation energy constitute definite advantages of the described method in comparison with γ-β-measurements. In particular, this method can be used for determining the ratio of the isotopes of elements of the natural radioactive series [1, 2].

For the elements found at the beginning of the uranium and thorium series, the α-decay energy lies within the range from 4 to 5.7 MeV, while individual lines are spaced at several hundreds of kiloelectron volts. Therefore, requirements for a sufficiently high energy resolution (of the order of 1%) are imposed on spectrometric α-detectors.

The recent development of the technology of semiconductor detectors [3, 4] made it possible to design α-spectrometric instruments for laboratory and industrial mass inspection which do not require complex vacuum devices and whose resolving power exceeds the resolving power of ionization chambers. However, detectors with a small transition area, i.e., with low efficiency, have the best spectrometric properties. This is very important if one takes into account the low specific counting rates in measuring natural radioactive specimens.

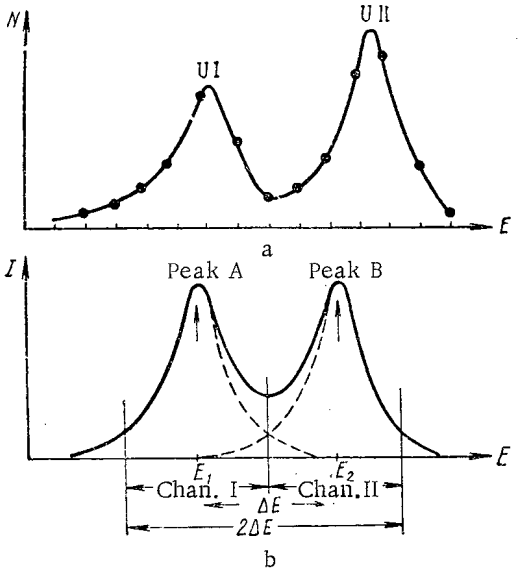

Fig. 1. Uranium spectrum obtained by means of a semiconductor detector (a) and the diagram of the position of energy channels (b).

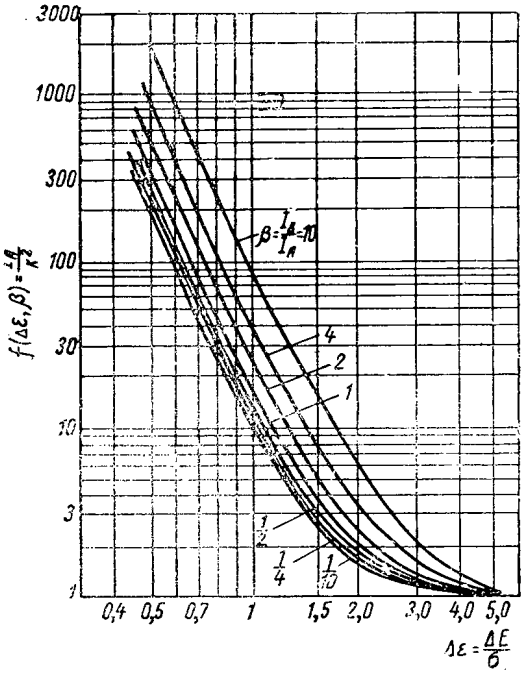

Fig. 2. Increase in the measurement time in dependence on the intensity ratio of lines and their overlapping.

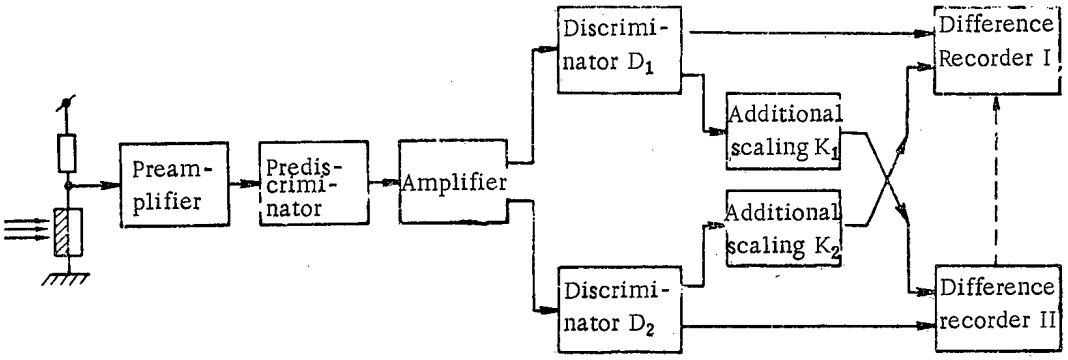

Fig. 3. Block diagram of the measuring device.

The increase in the detector area as a consequence of an increase in its volume and the deterioration of the signal-to-noise ratio unavoidably leads to a deterioration of the spectrometric properties, so that the distributions of the amplitudes from two lines begin to overlap. This seen in Fig. 1a, which shows the uranium spectrum (UI and UII) which was obtained by means of a semiconductor detector with an area of about 0.8 cm^2. Moreover, if the ratio of the isotope percentages differs considerably from unity, even the overlapping of lines which are relatively far removed from each other begins to play a considerable role, as it introduces errors in measurements.

In connection with this, it would be of interest to devise a simple mathematical operation (calculation of spectral distributions) with the aim of effectively improving the resolution and increasing the sensitivity and accuracy in using semiconductor α-detectors for isotope analysis. This method will be considered here for the case of two overlapping lines. Obviously, it would not be difficult to extend this method to the case of several overlapping distributions.

The measurements were performed in two energy channels, I and II (see Fig. 1b). If I_I and I_{II} are the numbers of pulses recorded in channels I and II, I_A and I_B are the actual numbers of pulses due to the corresponding radiators (the areas under the peaks A and B), and the coefficients α_1, α_2, α_3, and α_4 are the shares of peaks that contribute to the count in the corresponding channels, then,

$$\left.\begin{aligned} I_I &= \alpha_1 I_A + \alpha_2 I_B; \\ I_{II} &= \alpha_3 I_A + \alpha_4 I_B. \end{aligned}\right\} \tag{1}$$

The values of I_I and I_{II} are determined experimentally. The values of the α coefficients can be found from measurements with monochromatic lines. However, if the specimen under investigation is sufficiently thin, the shapes of the lines approach the normal curve of errors with a sufficiently high degree of accuracy, so that the coefficients α can be calculated. This is the case if the broadening of the lines caused by the specimen's finite thickness is much less than the dispersion due to the detector, i.e., $d/R \ll \sigma$ (where d is the specimen thickness, R is the range of α-particles and σ is the line's dispersion). In the opposite case, the symmetry of the curve is disturbed, and the coefficients α must be determined experimentally.

By solving system (1) with respect to the unknowns I_A and I_B, we find

$$\left.\begin{aligned} I_A &= \frac{\alpha_4}{\alpha_1\alpha_4 - \alpha_2\alpha_3} I_I - \frac{\alpha_2}{\alpha_1\alpha_4 - \alpha_2\alpha_3} I_{II}; \\ I_B &= \frac{-\alpha_3}{\alpha_1\alpha_4 - \alpha_2\alpha_3} I_I + \frac{\alpha_1}{\alpha_1\alpha_4 - \alpha_2\alpha_3} I_{II}. \end{aligned}\right\} \tag{2}$$

If the energy difference $E_1 - E_2$ is small in comparison with the E_1 and E_2 values, the dispersions of both lines are practically the same, and the shape of each line can be described in analytical form:

$$I(E) = \frac{I_0}{\sqrt{2\pi}\sigma} e^{-\frac{1}{2}\frac{\Delta E^2}{\sigma^2}}, \tag{3}$$

where $I_0 = I(E_0)$ is the line intensity at the maximum, and $\Delta E = E_0 - E$ (E_0 is the probable energy value). For convenience in further calculations, we shall introduce the dimensionless energy $\varepsilon = E/\sigma$; then, the difference $\Delta E = E_1 - E_2$ between the energy values of both lines, expressed in σ units, will be $\Delta\varepsilon = \Delta E/\sigma$.

For the symmetric position of the channels shown in Fig. 1b, the values of the α_i coefficients can be written thus:

$$\alpha_1=\alpha_4=2\int_0^{\varepsilon/2}\frac{1}{\sqrt{2\pi}}e^{-\frac{1}{2}\xi^2}d\xi=\Phi\left(\frac{\Delta\varepsilon}{2}\right)=\alpha;\quad \alpha_2=\alpha_3=\frac{1}{2}\left[\Phi\left(\frac{3}{2}\Delta\varepsilon\right)-\Phi\left(\frac{\Delta\varepsilon}{2}\right)\right]=\frac{1}{2}(a-\alpha), \tag{4}$$

where

$$2\int_0^{x}\frac{1}{2\sqrt{\pi}}e^{-\frac{1}{2}\xi^2}d\xi=\Phi(x);\quad \Phi\left(\frac{3}{2}\Delta\varepsilon\right)=a.$$

The values of the $\Phi(x)$ function are tabulated and can be used in calculations. The factor α in the above equations characterizes the degree of line overlapping.

The ratio of the percentages of both isotopes in the mixture can be found from the relationship

$$\frac{I_A}{I_B}=\frac{\alpha_1 I_{\mathrm{I}}-\alpha_2 I_{\mathrm{II}}}{-\alpha_3 I_{\mathrm{I}}+\alpha_1 I_{\mathrm{II}}}=\frac{I_{\mathrm{I}}-\frac{1}{2}\left(\frac{a}{\alpha}-1\right)I_{\mathrm{II}}}{-\frac{1}{2}\left(\frac{a}{\alpha}-1\right)I_{\mathrm{I}}+I_{\mathrm{II}}}=\frac{I_{\mathrm{I}}-kI_{\mathrm{II}}}{-kI_{\mathrm{I}}-I_{\mathrm{II}}},$$

where $k=\frac{1}{2}\left(\frac{a}{\alpha}-1\right)$ is a factor which depends only on the overlapping of lines.

For instance, in determining the concentration of U^{238} (E = 4.18 MeV) and U^{235} (E = 4.38 MeV) with a spectrometer resolution of approximately 3%, the values of the coefficients will be $\alpha_1=\alpha_4=0.93$; $\alpha_2=\alpha_3=0.035$ and $k=0.038$.

In principle, the above method makes it possible to resolve any lines, no matter how close to each other they are. However, this cannot be done in practice for a number of reasons. In order to achieve the same statistical accuracy as in recording separable lines, it is necessary to increase the measurement time, which becomes so large if the lines are sufficiently close to each other that the measurements become a practical impossibility.

The root-mean-square error in determining the value of I_A is

$$(\Delta I_A)^2=[\Delta(c_1 I_{\mathrm{I}})]^2+[\Delta(c_2 I_{\mathrm{II}})]^2=c_1^2 I_{\mathrm{I}}+c_2^2 I_{\mathrm{II}},$$

where

$$c_1=\frac{\alpha_4}{\alpha_1\alpha_4-\alpha_2\alpha_3}\ \text{and}\ c_2=\frac{\alpha_2}{\alpha_1\alpha_4-\alpha_2\alpha_3},$$

or

$$\Delta I_A=\sqrt{c_1^2(\alpha_1 I_A+\alpha_2 I_B)+c_2^2(\alpha_3 I_A+\alpha_4 I_B)}.$$

For the criterion, we shall use the factor $m=I_A^0/\Delta I_A^0$, which makes it possible to estimate the necessary amount by which the measured quantity should exceed the level of statistical fluctuations. Consequently, in order to achieve the required accuracy, the measured value of I_A must satisfy the relationship

$$I_A\geqslant I_A^0=m\Delta I_A^0=m\sqrt{I_A^0(c_1^2\alpha_1+c_2^2\alpha_3)+I_B^0(c_1^2\alpha_2+c_2^2\alpha_4)}.$$

Hence, we find

$$I_A^0=m^2c_1^2\left[\left(\alpha_1+\frac{c_2^2}{c_1^2}\alpha_3\right)+\frac{I_B}{I_A}\left(\alpha_2+\frac{c_2^2}{c_1^2}\alpha_4\right)\right]=m^2 f(\alpha,\beta),$$

where $\beta=I_B/I_A$. Thus, the I_A^0 value depends on the required statistical accuracy (factor m), the factor α of line overlapping, and the ratio β of line intensities. By substituting in the latter expression the values of the coefficients α from Eqs. (4), we shall determine the form of the functional dependence $f(\alpha,\beta)$:

$$f(\alpha,\beta)=\frac{16\alpha^2}{(\alpha+a)^2+(3\alpha+a)^2}\left[\alpha+\frac{(a-\alpha)^2}{8\alpha^2}+\frac{(a^2-\alpha^2)}{4\alpha}\beta\right]. \tag{5}$$

It is readily seen that, in the particular case where $\alpha=1$, i.e., where the lines are separated, we also have $f(\alpha,\beta)=1$, i.e., we obtain the ordinary result $I_A^0=m^2$.

Figure 2 shows a family of the curves $f(\Delta\varepsilon, \beta)$, which characterize the increase in the measurement time (β is the parameter). It is obvious from these curves that, for equal line intensities, the separation of lines which differ by $\Delta\varepsilon = 2$ (i.e., $\Delta E = 2\sigma$) requires that the measurement time be doubled in comparison with the time necessary for measuring separate lines. If $\Delta\varepsilon = 1$, the measurement time increases by a factor of about 17.

A two-channel device (Fig. 3) was constructed for checking the above method. This device was designed for the separate determination of the percentages of two isotopes whose energies were close to each other (with overlapping amplitude distributions). The fact that transistors were exclusively used in constructing the units of the device made it possible to use it in field laboratories.

In the semiconductor detectors which we used, the signal level corresponding to an energy of 5 MeV was equal to 100 μV. The transistor preamplifier was designed so as to secure the minimum noise level, which, when reduced to the circuit input, was equal to 2-3 μV [5]. After preamplification, the signals are transmitted to the discriminating device, after which only the pulse peaks that exceed a certain given threshold are additionally amplified (the range from 0 to 3-3.5 MeV is thereby excluded).

The discrimination levels of the two differential discriminators D_1 and D_2 were set so that the maxima of the amplitude distributions coincided with the channel centers. The pulses were recorded by means of two difference recorders, where the signals to the summation inputs of both recorders were supplied directly from their own discriminators, while the signals transmitted to the subtraction inputs were supplied from another discriminator after additional scaling.

In order to adjust the system for recording the intensity of two certain radiators, the additional scaling factors K_1 and K_2 must be secured in correspondence with the calculated values. If one of the recorders is used as the master recorder, i.e., if it stops recording after completing a certain count volume N_0, the other recorder can be used for directly determining the ratio of the isotopes under investigation. The coefficients in the equations relating the number of pulses recorded to the actual number of pulses that corresponds to the peak area are taken into account in choosing the N_0 value.

It should be noted that, in principle, the above method can be used for the separate determination of not only two, but also a larger number of isotopes in a mixture. The measurements must be performed by means of several single-channel discriminators, followed by a very simple computer. This method may also be convenient in using scintillation α-detectors (thin CsI(Tl) crystals), which, although their energy resolution is worse, make it possible to secure a high counting efficiency due to their larger area [6]. The curves given in Fig. 2 make it possible to determine the scope of a certain detector in solving actual problems with the aim of reducing the measurement time to a minimum.

In conclusion, we hereby express our gratitude to V. L. Shashkin and Yu. A. Yuzvuk for their continued interest in the work, and also to M. I. Krapivin, B. V. Fefilov, and Yu. R. Nosov, who kindly supplied the semiconductor α-detectors for the experiments.

LITERATURE CITED

1. Yu. A. Surkov et al., Atomnaya Énergiya, 9, No. 6, 477 (1960).
2. V. V. Cherdyntsev et al., Geokhimiya, No. 10, 840 (1961).
3. A. Chetham-Strode et al., IRE Trans. Nucl. Sci., 8, No. 1, 59 (1961).
4. S. M. Ryvkin et al., Atomnaya Énergiya, 11, No. 3,217 (1961).
5. A. D. Verevkin et al., In the book: Transactions of the Fifth Scientificotechnical Conference on Nuclear Radio Electronics [in Russian] Gosatomizdat, Moscow (1962).
6. V. F. Bolotin et al., Collection of Papers on Certain Dosimetry Problems [in Russian] Vol. II, Edited by Yu. V. Sivintsev, Gosatomizdat, Moscow (1961) p. 154.

DEVICE FOR RADIATION–CHEMICAL INVESTIGATIONS IN THE CHANNEL OF THE IRT–2000 REACTOR

A. A. Akhundov, G. S. Karumidze, G. M. Krasavtseva, and V. T. Popov

Translated from Atomnaya Énergiya, Vol. 14, No. 4,
pp. 412, April, 1963
Original article submitted June 11, 1962

A continuous-flow device for radiation-chemical investigations in gaseous, vapor, and liquid phases at temperatures of 400-600 deg C and under pressures of 1-30 atm, designed for the IRT-2000 reactor of the Institute of Physics, Academy of Sciences, Geor. SSR, was constructed in collaboration with three institutes–the Institute of Petroleum-Chemical Synthesis (INKhS), Academy of Sciences, USSR (Moscow), the Yu. G. Mamedaliev Institute of Petroleum-Chemical Processes, Academy of Sciences, Azer. SSR (Baku), and the Institute of Physics, Academy of Sciences, Geor. SSR (Tbilisi)–and brought into operation in February, 1962. The design of the device is based on the engineering calculations performed at INKhS, Academy of Sciences, USSR, in collaboration with the INKhS Special Design Burear (SKB). The experience gained in the construction of the devices described earlier [1-6] was also used in this design. This device considerably differs from those described in the literature by the design features of the loop that is introduced in the nuclear reactor channel and by the fact that the pressure created by the vapor of the substance under investigation can be maintained in the loop and that the work can be performed in a wide range of temperature and pressure values.

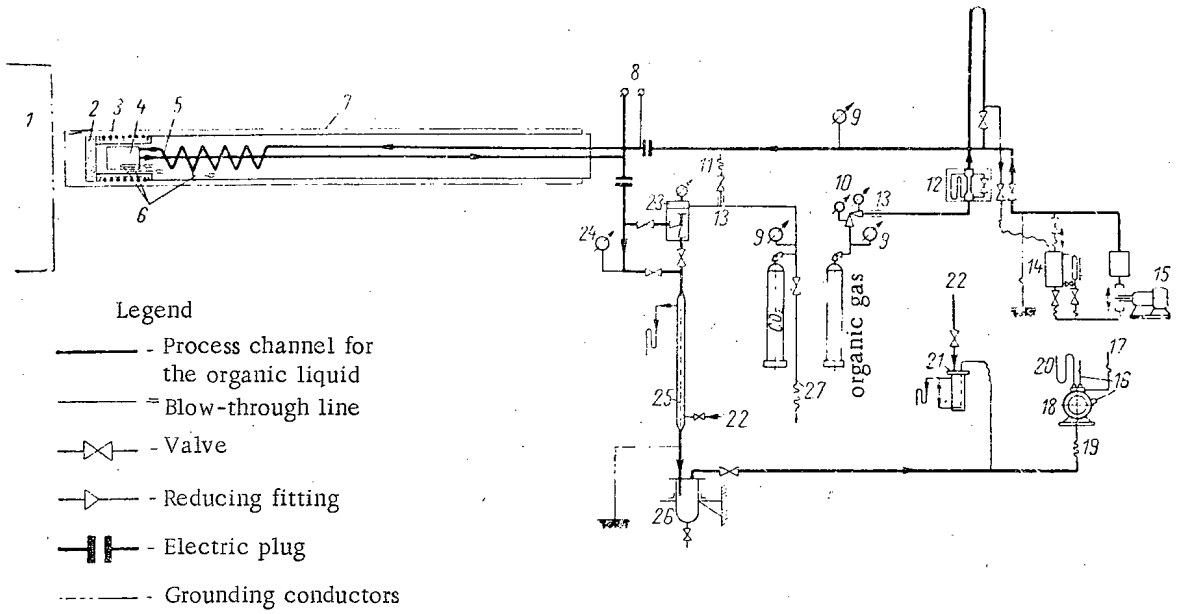

Fig. 1. Technological layout of the device. 1) Reactor core; 2) B_4C filter; 3) electric furnace; 4) reaction zone; 5) current-conducting evaporator tube; 6) thermocouples; 7) reactor channel; 8) electric supply; 9) and 24) standard pressure gauges (p = 1-60 atm); 10) reducing pressure regulator (from 0-150 to 0-60 atm); 11) breather; 12) flowmeter with capillary (p = 100 atm); 13) capillary; 14) tank with raw material (1.5 liters); 15) liquid pump; 16) thermometer (0-50 deg C); 17) to ventilation system; 18) 1-GSB-400 gas meter; 19) line for conveying samples to KhT-24 chromatograph; 20) U-shaped differential pressure gauge (p = 600 mm of water); 21) hydroseal (p = = 600 mm of water); 22) water; 23) "check" pressure regulator; 25) cooler; 26) gas separator; 27) scavenging.

Any type of radiation-chemical investigation with gases, vapors, and liquids which are not corrosive can be performed in this device. Automatic temperature and pressure control and automatic sampling and analysis of gaseous samples are provided.

The device has been tested and used in a series of experiments (80) on the radiation-thermic cracking of vapors of petroleum hydrocarbons.

The technological layout of the device is shown in Fig. 1. Liquid hydrocarbon from the small tank (14) which contains the raw material is conveyed by means of an adjustable pump (15) to a current-conducting stainless-steel communication tube. As it passes through the tube, the liquid evaporates and is overheated as its temperature rises to that of the tube walls, and the vapor enters the electrically heated reaction zone (4). From the reaction zone, the reaction products are conveyed through the current-conducting stainless-steel tube to the "check" pressure regulator (23), which is installed in the hot line, making it possible to create a higher pressure in the system with the hydrocarbon vapor itself without adding inert gases.

Beyond the pressure regulator, the reaction products are conveyed to the gas separator (26) through the cooler (25), which is cooled by running water. The gaseous reaction products are led off to the drum gas meter (18), then conveyed to a KhT-2M chromatograph through the unit for automatic sampling, and finally expelled through the ventilation system. The liquid reaction products are conveyed from the gas separator to calibrated containers, after which they are measured and analyzed.

In work with hydrocarbon gas, the gas is conveyed from the tank through reducing pressure regulator (10) to the flowmeter with capillary (12), after which it passes through the system described above. Standard pressure gauges (9 and 24) are provided at suitable points in the device for measuring the gas supply pressure and the vapor pressure ahead of the pressure regulator.

The temperatures of the walls of the communication supply tube, of the vapor inside the reactor core, and of the core walls are measured by means of chromel-alumel thermocouples (6) and recorded automatically by means of an ÉPP-09 potentiometer. The temperature of the core walls is automatically maintained by means of an ÉPV-11 device.

Carbon dioxide from a cylinder is discharged into the raw-material line between the pump and the supply tube for removing air and remnants of the product from the system. A drainage line is also provided in the device.

Many of the device's structural elements were determined by the parameters of the horizontal channel of the IRT-2000 reactor at the Institute of Physics, Academy of Sciences, Geor. SSR. The channel length is 320 cm, and the diameter is 100 mm.

The characteristics of certain units of the device are the following:

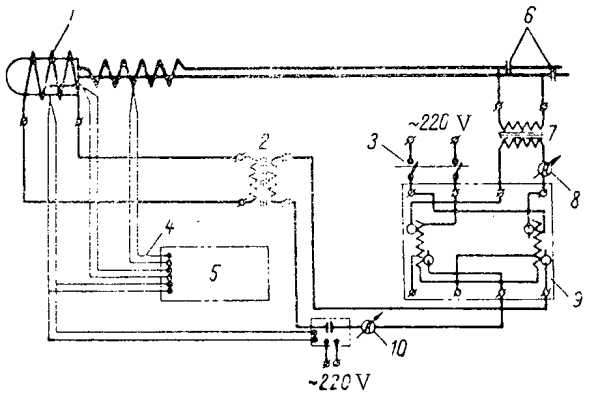

Fig. 2. Wiring diagram of the device. 1) Electric furnace; 2) two parallel-connected transformers; 3) 10-A group switch; 4) thermocouple leads; 5) electronic self-recorder; 6) electric plugs; 7) welding transformer; 8) ammeter; 9) voltage regulator; 10) ammeter.

1. The adjustable liquid pump, designed at SKB INKhS, makes it possible to vary the feed rate of the liquid raw material from 50 to 3000 ml/hr by means of a regulating sleeve.

2. The "check" pressure regulator, designed at SKB INKhS, which has a membrane made of special thermo- and benzine-resistant plastic, makes it possible to regulate in a reliable manner the pressure of hot vapors of organic liquids (up to 300 deg C) in the pressure range from 1 to 30 atm.

3. The electrically insulated disconnection plugs, designed at SKB INKhS, are capable of operation under pressures exceeding 30 atm and at temperatures of up to 300 deg C.

4. The communication tubes (the supply tube, which has a 6×1-mm cross section and a length of 6 m, and the outlet tube with a cross section of 8×1-mm and a length of 5.5 m) are made of 1Kh18N9T stainless steel. Current from an ST-120 welding transformer is transmitted through

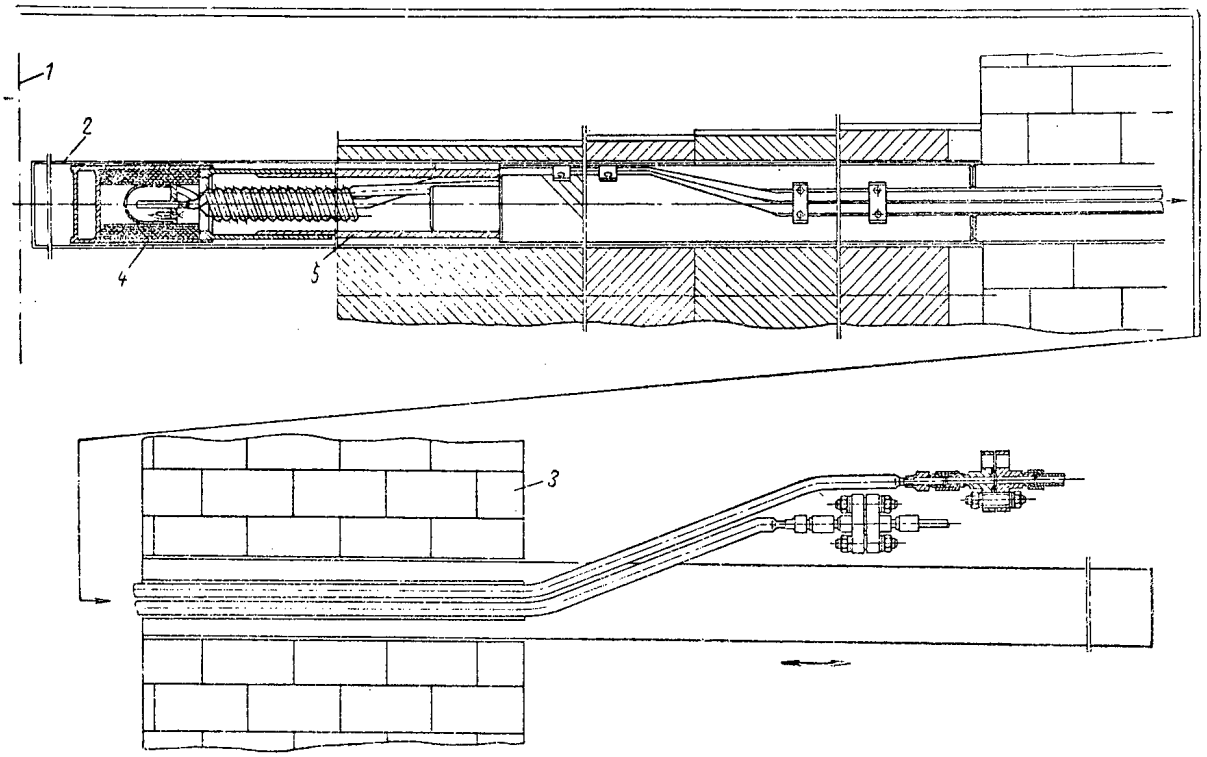

Fig. 3. Diagram of the loop elements in the reactor channel. 1) Plane of the reactor core; 2) reactor channel; 3) biological shield; 4) protective shell; 5) rod.

these tubes (Fig. 2). The over-all ohmic resistance of the tubes up to the joints is equal to 0.51 Ω. With the allowance for the heat loss to the surroundings and the loss due to the overheating of vapor, a power of 1.8 kW with a current of up to 60 A is required for heating the tubes (the supply tube is heated to 480 deg C, while the outlet tube is heated to ~350 deg C). Both communication tubes are insulated by means of a double layer of asbestos rope and several layers of glass tape. The tubes are fitted into the helical groove of the rod (Fig. 3) and are rigidly connected (through the electrical joints) to the supply panel, while their other ends are connected to the reaction zone.

5. The reaction zone is made of 1Kh18N9T stainless steel; it has the shape of a coil with an inside volume of 200 cm^3. On the outside, the coil is wound with insulated nichrome wire with a diameter of 0.8 mm, which has an ohmic resistance of 4 Ω. This electric heater uses a power of 300 W for a current of 9 A. In order to reduce the heat loss, the coil is insulated on the outside with several layers of asbestos rope and glass tape. A protective aluminum shell whose end is provided with a boron carbide filter with a thickness of 25 mm for the complete absorption of thermal neutrons is fitted on the coil. The shell is fastened on a threaded aluminum tube, which is fitted onto the end of the rod.

6. The rod is made of duralumin; on the outside, it is provided with two helical grooves, one of which serves for fastening the communication tubes, while the other is used for the thermocouples and the cable (insulated with porcelain) which supplies the reaction zone with electric power. The length of the rod is 1.6 m, while its diameter is 98.5 mm; the rod is rigidly fastened to the supply panel, and it can be moved in the horizontal position through the required distance in the reactor channel on a special trestle bridge. The supply panel moves on small wheels along rails which are mounted next to the trestle bridge.

The rod serves as a good biological protection from the direct radiation from the reactor. An additional biological shield consisting of lead and paraffin blocks is provided between the supply panel and the downstream end of the channel for a more reliable protection from scattered radiation in work with the device.

By testing the device in operation, it was found that experiments can be performed while observing all the safety rules.

The authors are deeply grateful to the SKB INKhS staff for the development of the initial version of the device, to the collaborators of the Institute of Physics, Academy of Sciences, Geor. SSR, V. M. Likholetov, B. G. Buda,

and M. E. Tinikashvili for their help in adjusting the device, to L. S. Polak for the organization of work and overall supervision, and to É. L. Andronikashvili and M. M. Melik-Zade for their interest in the work.

LITERATURE CITED

1. J. Martin, Chem. Engng. Progr., 54, No. 2, 66 (1958).
2. P. Lucchesi et al., Ind. Eng. Chem., No. 6, 879 (1958).
3. M. A. Mokul'skii et al., Dokl. AN SSSR, 125, No. 5, 1007 (1959).
4. P. Ya. Glazunov, Yu. A. Kolbanovskii, and V. D. Timofeev. In the book: Transactions of the Second All-Union Conference on Radiation Chemistry [in Russian] Izd. AN SSSR, Moscow (1962) p. 725.
5. A. V. Zimin, In the book: Transactions of the Second All-Union Conference on Radiation Chemistry [in Russian] Izd. AN SSSR, Moscow (1962) p. 729.
6. B. S. Gudkov et al., In the book: Transactions of the Second All-Union Conference on Radiation Chemistry [in Russian] Izd. AN SSSR, Moscow (1962) p. 733.

All abbreviations of periodicals in the above bibliography are letter-by-letter transliterations of the abbreviations as given in the original Russian journal. *Some or all of this periodical literature may well be available in English translation.* A complete list of the cover-to-cover English translations appears at the back of this issue.

DETERMINATION OF THE RELATIONSHIP BETWEEN THE COEFFICIENTS OF THE TURBULENT TRANSFER OF HEAT AND MOMENTUM

V. I. Subbotin, M. Kh. Ibragimov, and E. V. Nomofilov

Translated from Atomnaya Énergiya, Vol. 14, No. 4,
pp. 414-416, April, 1963
Original article submitted July 9, 1962

In this paper, we used the results of the processing of temperature fields in turbulent flow of liquid metal (Pr = 0.025) for Re = 20,000-450,000. The experiments were performed with a 34×2.35-mm tube. The design of the experimental section and its basic characteristics were described in [1]. The results were obtained by means of the graphical differentiation of time-averaged experimental data concerning the temperature distribution in turbulent flow of a liquid metal (mercury).

We found the values of the coefficient ε_a of turbulent heat transfer as a result of the measurements and processing of temperature fields in a flow of liquid metal according to the method described in [2]. The maximum ε_a value along the tube's radius in the range Re = $2\cdot10^4$-$4.5\cdot10^5$ can be approximated by the formula

$$\left(\frac{\varepsilon_a}{a}\right)_{\max} = 7{,}5\cdot10^{-5}\,Re. \qquad (1)$$

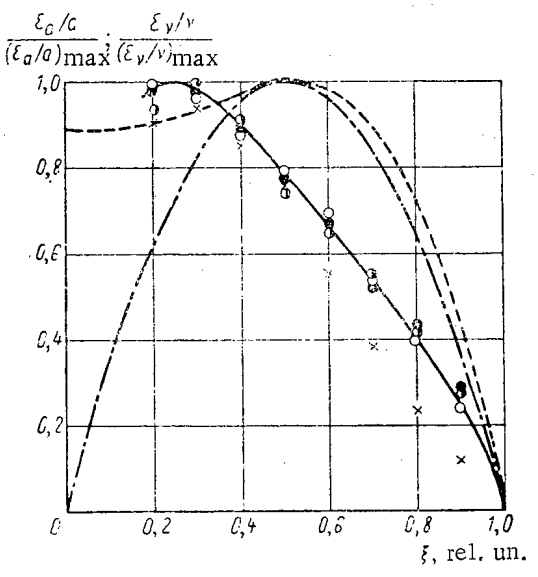

Fig. 1. Relative variation of the coefficients of turbulent transfer of heat and of momentum along the tube's radius. ——) Curve which averages the calculated points for $\frac{\varepsilon_a/a}{(\varepsilon_a/a)_{max}}$; – –) and –·–) curves for $\frac{\varepsilon_\nu/\nu}{(\varepsilon_\nu/\nu)_{max}}$, calculated by using Reichardt's and Prandtl's formulas, respectively; ×) Re = 20,000; ○) Re = 88,000; ◑) Re = 270,000; ●) Re = 430,000.

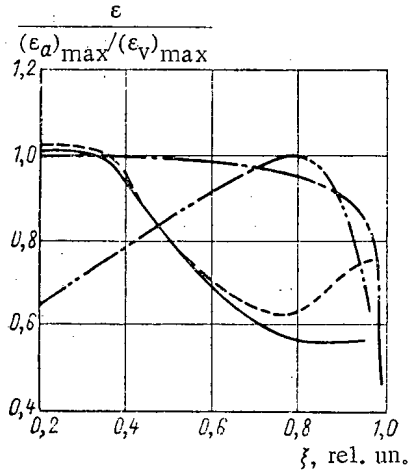

Fig. 2. Variation of the coefficient ε along the tube's radius. ——) and – –) for $\frac{\varepsilon_\nu/\nu}{(\varepsilon_\nu/\nu)_{max}}$ calculated according to Reichardt's and Prandtl's formulas, respectively; ··–··) data borrowed from [5]; –·–) data borrowed from [6].

The ratio $\frac{\varepsilon_a/a}{(\varepsilon_a/a)_{max}}$, that characterizes the variation of turbulent heat transfer along the tube's radius, is shown in Fig. 1. For Reynolds numbers Re = $2\cdot10^4$-$4.5\cdot10^5$, this ratio can be described by a unique dependence with a sufficient degree of accuracy; certain deviations are observed only for low Reynolds numbers (~20,000).

The results of the further processing of experimental data depend on the accepted velocity distribution in the turbulent core of the flow. Therefore, for the sake of comparison, we used two expressions for the velocity distribution in the turbulent core in our calculations:

1) the expression proposed by Prandtl [3]:

$$\frac{u}{u^*}=5{,}5+2{,}5\ln\frac{yu^*}{\nu} \quad \text{and} \tag{2}$$

2) the expression proposed by Reichardt [4]:

$$\frac{u}{u^*}=2{,}5\ln\left[(1+0{,}4y^+)\frac{1{,}5\,(1+\xi)}{1+2\xi^2}\right]+7{,}8\left[1-\exp\left(-\frac{y^+}{11}\right)-\frac{y^+}{11}\exp\left(-\frac{y^+}{3}\right)\right]. \tag{3}$$

By using these formulas for the velocity distribution, we obtain different values of the coefficient ε_ν of turbulent transfer of momentum. The variation of the ε_ν coefficient along the tube's radius is shown in Fig. 1. The maximum values of ε_ν/ν for both velocity distribution formulas are observed for the relative radius ξ = 0.5; however, these values considerably differ from each other: according to Prandtl's formula, we have

$$(\varepsilon_\nu/\nu)_{max}=1\cdot10^{-2}\,Re^{0{,}875}, \tag{4}$$

while according to Reichardt's formula,

$$(\varepsilon_\nu/\nu)_{max}=0{,}75\cdot10^{-2}\,Re^{0{,}875}. \tag{5}$$

It should be mentioned that the velocity distribution in the flow given by Reichardt's formula is more reliable than the distribution given by Prandtl's formula, since the latter used data by Nikuradze, who performed measurements not inside the tube, but in the free stream at the tube's outlet. The maximum values of ε_a/a are observed for ξ = 0.2-0.3. This indicates that there is apparently no complete similarity between the turbulent transfers of heat and of momentum over the entire flow cross section. A comparison of the maximum values of ε_a/a and ε_ν/ν, obtained by using formulas (1), (4), and (5), indicates that the relationship between the coefficients of the turbulent transfer of heat of momentum depends on the Re number.

The value of the coefficient of dissimilarity between the turbulent transfers of heat and of momentum can be expressed in the following manner:

$$\varepsilon=\frac{(\varepsilon_a/\varepsilon_a)_{max}}{(\varepsilon_\nu/\varepsilon_\nu)_{max}}\cdot\frac{(\varepsilon_a)_{max}}{(\varepsilon_\nu)_{max}}. \tag{6}$$

The first factor in this formula is a function of the coordinate and is independent of the flow velocity of liquid metal for Re > $2\cdot10^4$ (see Fig. 1); the second factor is a function of only the Re number; its value can be determined by using formulas (1), (4), and (5) and choosing a suitable Pr value for the liquid metal's average temperature under the given experimental conditions (≃ 30 deg C).

In using the velocity distribution given by Prandtl's formula, we have

$$\frac{(\varepsilon_a)_{max}}{(\varepsilon_\nu)_{max}}=0{,}3Re^{1/8}; \tag{7}$$

in using the distribution given by Reichardt's formula, we have

$$\frac{(\varepsilon_a)_{max}}{(\varepsilon_\nu)_{max}}=0{,}4Re^{1/8}. \tag{8}$$

It is obvious from formulas (7) and (8) that the turbulent transfer of momentum and, consequently, the ε values depend on the velocity distribution formula used. At the same time, the velocity distribution does not greatly influence the variation of ε along the tube's radius (Fig. 2); larger deviations are observed only in the boundary region (ξ > 0.8), where the accuracy with which the experimental data can be processed is relatively low due to the small values of ε_a and ε_ν. The obtained experimental data indicate that the value of ε varies appreciably along the tube's radius.

Isakoff and Drew [7] have observed the maximum values of ε for $\xi = 0.8$, while Brown et al. [8] have found that the value of ε remains approximately constant throughout the entire turbulent core of the flow. The cause of these discrepancies in the variation of ε along the tube's radius has not yet been explained.

As is known, the region $\xi = 0.5$-0.9 determines the heat exchange in liquid metals ($Pr \ll 1$). Therefore, the weighted mean values of $\bar{\varepsilon}$ in dependence on Re numbers were calculated for this region:

$$\bar{\varepsilon} = \frac{\int_{0,5}^{0,9} \varepsilon \xi \, d\xi}{\int_{0,5}^{0,9} \xi \, d\xi}.$$

The results obtained are shown in Fig. 3. The value of $\bar{\varepsilon}$ also depends on the velocity distribution: according to Prandtl's formula, $\bar{\varepsilon} = 0.205\ Re^{1/8}$; according to Prandtl's formula, $\bar{\varepsilon} = 0.254\ Re^{1/8}$.

Figure 3 shows the values of ε obtained in [7, 8], which were averaged in a similar manner. It should be mentioned that the authors of these papers used their own data on the velocity distribution in the turbulent core of the flow, which were in good agreement with Prandtl's law [2].

Although the experimental data differ from each other, a general tendency of the ε value to increase with an increase in the Re number is observed. For large Re values, the value of ε becomes larger than unity, which indicates that the coefficient of turbulent heat transfer is higher than the coefficient of the turbulent transfer of momentum.

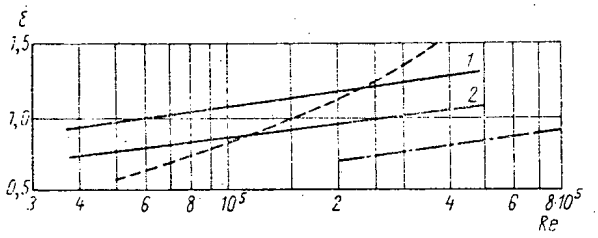

Fig. 3. Values of $\bar{\varepsilon}$, averaged along the radius ($\xi = 0.5$-0.9), in dependence on Re numbers. ——) Our data (1 and 2 — for velocity distributions according to Reichardt's and Prandtl's formulas, respectively); – –) data borrowed from [5]; –·–) data borrowed from [6].

The quantity ε plays an important role in semiempirical heat exchange theories, since it makes it possible readily to determine the temperature field using the known velocity distribution. Experimental determinations of the ε value make it possible to check the validity of the assumptions used in semiempirical theories. However, the physical nature of the heat exchange process cannot be thereby explained. In our opinion, the semiempirical theories of heat exchange for liquid metals [7-9] where the value of ε assumes the maximum value (equal to unity) only for $Pe \to \infty$, although it is assumed that it depends on velocity, and also those theories [10-12] where it is assumed that the value of ε does not depend on the velocity are not entirely substantiated. The satisfactory agreement between experimental data and some theoretical solutions that is observed in a certain range of Re and Pr numbers indicates only the validity of the formulas derived for calculating the heat transfer, but the mechanism of turbulent heat transfer that is assumed in these theories is thereby by no means confirmed. A heat exchange theory which would be substantiated from the physical point of view could be postulated only on the basis of direct investigations of the quantities that characterize turbulent heat transfer, i.e., it can be postulated by investigating velocity and temperature fluctuations and their statistical relationships.

LITERATURE CITED

1. V. I. Subbotin et al., Atomnaya Énergiya, 11, No. 2, 133 (1961).
2. V. I. Subbotin et al., Atomnaya Énergiya, 10, No. 4, 384 (1961).
3. Turbulence Problems [in Russian], Collection of articles, edited by M. A. Velikanov and N. G. Shveikovskii, ONTI, Moscow (1936).
4. H. Reichardt, Z. angew. Math. und Mech., 31, Nr. 7, 208 (1951).
5. K. D. Voskresenskii and E. S. Turilina, Coll.: Heat Transfer and Thermal Simulation [in Russian], Izd. AN SSSR, Moscow (1958), p. 87.
6. R. Deissler, Trans. ASME, 73, 2 (1951).
7. S. Isakoff and T. Drew, General discussion on Heat Transfer, London (1951), p. 405.
8. H. Brown, B. Amstead, and B. Short, Trans ASME, 79, 2, 279 (1957).

9. P. Lykoudis and I. Touloukian, Trans. ASME, 80, 3, 653 (1958).
10. R. Martinelli, Trans. ASME, 69, 8, 947 (1947).
11. R. Lyon, Chem. Engng. Progr., 47, 2, 75 (1951).
12. N. I. Buleev, In the Coll.: Problems of Heat Transfer [in Russian], Izd. AN SSSR, Moscow (1959), p. 208.

All abbreviations of periodicals in the above bibliography are letter-by-letter transliterations of the abbreviations as given in the original Russian journal. *Some or all of this periodical literature may well be available in English translation.* A complete list of the cover-to-cover English translations appears at the back of this issue.

SPECIFIC HEAT OF HEAVY WATER AT HIGH TEMPERATURES AND PRESSURES

S. L. Rivkin and B. N. Egorov

Translated from Atomnaya Énergiya, Vol. 14, No. 4,
pp. 416-418, April, 1963
Original article submitted September 1, 1962

The results obtained in measuring the specific heat of heavy water in the liquid phase under pressures of up to 100 kg/cm^2 and at temperatures of up to 300 deg C were published earlier [1]. The present article provides the results of further investigations of the specific heat of heavy water in the liquid and vapor phases and in the supercritical region of the state parameters. The measurements were performed by means of a continuous-flow adiabatic calorimeter in a closed-loop circulation system, using a new experimental device, the diagram of which is shown in the figure*. In contrast to the device described earlier [1], liquid thermostats with very accurate (± 0.01 deg C) temperature regulation were used for the temperature control of the calorimeters in the new device. Along with other improvements, this made it possible to simplify to a considerable extent the measurement technique and to increase the accuracy.

Specific Heat of Heavy Water, kcal/kg·deg

Temperature, ° C	Pressure, kg/cm^2										
	50	100	150	175	200	225	240	250	260	275	300
20	1,002	0,999	0,996	0,995	0,993	0,991	0,990	0,989	0,988	0,988	0,986
40	1,000	0,997	0,995	0,993	0,992	0,991	0,990	0,990	0,989	0,988	0,987
60	0,997	0,994	0,992	0,991	0,989	0,988	0,988	0,987	0,987	0,986	0,985
80	0,996	0,994	0,991	0,990	0,989	0,988	0,988	0,987	0,987	0,986	0,985
100	0,996	0,993	0,991	0,990	0,988	0,987	0,987	0,986	0,986	0,985	0,984
120	0,997	0,994	0,992	0,991	0,990	0,988	0,987	0,987	0,986	0,986	0,985
140	1,001	0,998	0,995	0,993	0,992	0,990	0,989	0,989	0,988	0,987	0,986
160	1,006	1,002	0,999	0,997	0,995	0,993	0,992	0,992	0,991	0,990	0,989
180	1,016	1,011	1,006	1,004	1,002	1,000	0,999	0,998	0,997	0,996	0,994
200	1,032	1,027	1,020	1,017	1,014	1,012	1,010	1,009	1,008	1,007	1,004
220	1,058	1,048	1,039	1,035	1,031	1,028	1,026	1,025	1,024	1,022	1,020
240	1,090	1,078	1,068	1,062	1,057	1,052	1,049	1,048	1,046	1,043	1,040
260	1,139	1,123	1,108	1,100	1,093	1,086	1,081	1,079	1,076	1,072	1,066
280	—	1,182	1,161	1,149	1,142	1,131	1,126	1,122	1,119	1,114	1,106
300	—	1,300	1,251	1,233	1,216	1,200	1,192	1,186	1,180	1,172	1,160
310	—	—	1,320	1,292	1,268	1,246	1,234	1,226	1,220	1,209	1,194
320	—	—	1,418	1,374	1,339	1,308	1,292	1,280	1,270	1,254	1,234
330	—	—	1,576	1,500	1,442	1,395	1,369	1,353	1,337	1,316	1,287
340	—	—	—	—	1,610	1,529	1,486	1,460	1,437	1,406	1,364
350	—	—	1,807	—	1,936	1,757	1,672	1,624	1,582	1,530	1,462
360	—	—	1,450	2,374	3,220	2,250	2,035	1,920	1,826	1,730	1,620
370	—	—	1,240	1,730	3,160	6,148	3,232	2,720	2,425	2,143	1,890
380	—	—	1,112	1,422	2,018	3,905	10,88	12,20	5,28	3,310	2,418
390	—	—	1,014	1,241	1,588	2,293	3,220	4,27	6,35	8,565	3,960
400	—	—	0,939	1,114	1,348	1,755	2,144	2,490	3,030	4,055	5,775
410	—	—	0,882	1,019	1,199	1,470	1,700	1,875	2,095	2,528	3,580
420	—	—	0,837	0,949	1,090	1,286	1,431	1,545	1,675	1,920	2,485
430	—	—	0,802	0,894	1,007	1,150	1,260	1,345	1,435	1,593	1,930
440	—	—	0,774	0,852	0,947	1,062	1,146	1,208	1,277	1,393	1,627
450	—	—	0,750	0,819	0,903	0,997	1,061	1,109	1,162	1,250	1,415

*This device was also used for measuring the specific heat of ethyl alcohol in the supercritical region of the state parameters. The measurement results with a detailed description of the method used were published in [2].

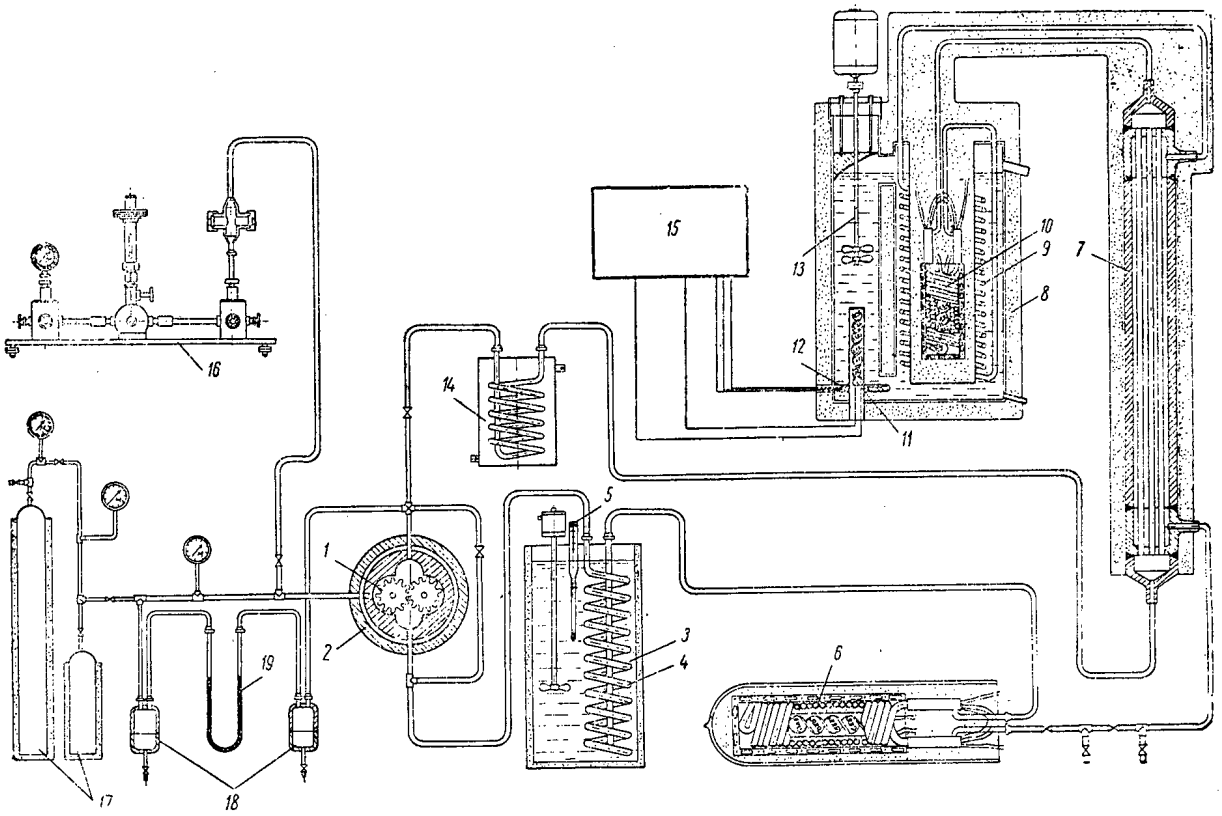

Diagram of the experimental setup for investigating the specific heat of heavy water. 1) Circulation pump; 2) autoclave; 3) water thermostat; 4) and 9) coiled tubes; 5) contact thermometer; 6) calorimeter-flowmeter; 7) heat exchanger; 8) saltpeter thermostat; 10) measuring calorimeter; 11) regulating heater; 12) regulator data transmitter; 13) mixer; 14) cooler; 15) automatic temperature regulator; 16) piston pressure gauge; 17) thermal booster; 18) mercury trap; 19) mercury lock.

Three series of experiments were performed on the new experimental device. In the first series, the specific heat of heavy water in the liquid phase was measured on five isobars: 100, 150, 200, 225, and 250 kg/cm^2 (58 experimental points); in the second series, the specific heat of heavy water in the vapor phase was measured on three isobars: 150, 175, and 200 kg/cm^2 at temperatures of up to 450 deg C (42 experimental points); in the third series, the specific heat of heavy water in the supercritical region of the state parameters was measured on six isobars: 225, 240, 250, 260, 275, and 300 kg/cm^2 at temperatures from 330-360 to 450 deg C (137 experimental points).

The new measurements of the specific heat of heavy water in the liquid phase on the 100-kg/cm^2 isobar agreed with the previous measurements [1] within 0.2-0.7%, i.e., within the limits of the previously determined measurement error. However, in connection with the higher accuracy of the specific heat measurements with the new experimental device, the new experimental data were used in further processing.

According to our estimates, the maximum error in the experimental data on the specific heat of heavy water lies within the limits from 0.35% for the liquid and the vapor phases at a certain distance from the saturation line to 1-2% near the saturation line and the specific heat maximums on the supercritical isobars (with the exception of a few points near the maximum on isobars close to the critical isobar, where the error may be somewhat larger).

The table provides the values of the specific heat of heavy water for rounded-off pressure and temperature values, which were obtained as a result of the graphoanalytical processing of experimental data.

The data given in the present article constitute the only data presently available, and, therefore, we cannot compare them with the results of other independent measurements.

LITERATURE CITED

1. S. L. Rivkin and B. N. Egorov, Atomnaya Énergiya, 7, No. 5, 462 (1959).
2. S. L. Rivkin and B. N. Egorov, Teploénergetika, No. 7, 60 (1961).

NEW TYPE OF NOMOGRAMS FOR γ-FLAW DETECTION*

Slavcho Popov

Laboratory for the Application of Radioisotopes in Machine Construction, Sofia, Bulgaria

Translated from Atomnaya Énergiya, Vol. 14, No. 4,
pp. 418-419, April, 1963
Original article submitted July 31, 1962

Nomograms where the relationship between the thickness d of the part under investigation in millimeters and the exposure in g·eq Ra·hr for the given values of the distance F in centimeters from the radiation source to the photographic film is given in a Cartesian coordinate system are most often used for determining the x-raying time in γ-flaw detection [1-3].

This type of nomogram cannot be used for directly reading the x-raying time t and determining the necessary activity Q of the radiation source.

In connection with this, we suggest the use of a new type of nomogram for determining the x-raying time t for the assigned thickness d of the part under investigation, the activity Q of the radiation source, and the distance F from the source to the photographic film.

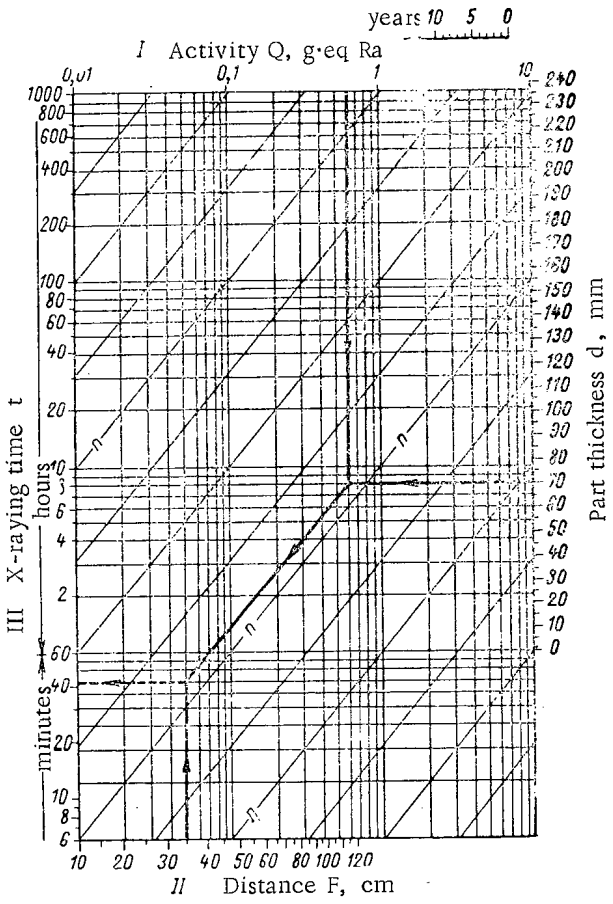

Fig. 1. Nomogram for determining the x-raying time for the assigned part thickness and focal length when Co^{60} is used as the radiation source.

Figure 1 shows such a nomogram for determining the necessary parameters for the inspection of parts made of steel or cast iron by means of the Co^{60} radioisotope. The nomogram is intended for material thicknesses in the range from 0 to 250 mm. The heavy solid line on the scale of thicknesses in the nomogram marks the range of part thicknesses for which the sensitivity of inspection with this source [4] is at the maximum (50-250 mm).

This nomogram was plotted on the basis of the data found in the existing nomograms [1-3]. The values or the source's activity in the range from 0.1 to 10 g·eq Ra are laid off on a logarithmic scale on axis I, the focal lengths F in the range from 10 to 120 cm in divisions of 5 cm are laid off on axis II, and the x-raying time t in the range from 0.1 to 100 hr is laid off on axis III.

The nomogram key is Q dn; nFt. The nomogram is used in the following manner: for the assigned values Q = 0.6 g·eq Ra and d = 70 mm, the point of intersection between the lines of these values is found. From this intersection point, a line parallel to the diagonal is drawn until it intersects with the line corresponding to the assigned value F = 35 cm. The second intersection point determines the x-raying time t = 42 min = 0.7 hr (see Fig. 1).

Moreover, a scale, every division of which corresponds to the logarithm of the annual reduction in the source intensity, is given in the upper right corner of the nomogram. Thus if the initial source intensity and the

*Translation from the Bulgarian.

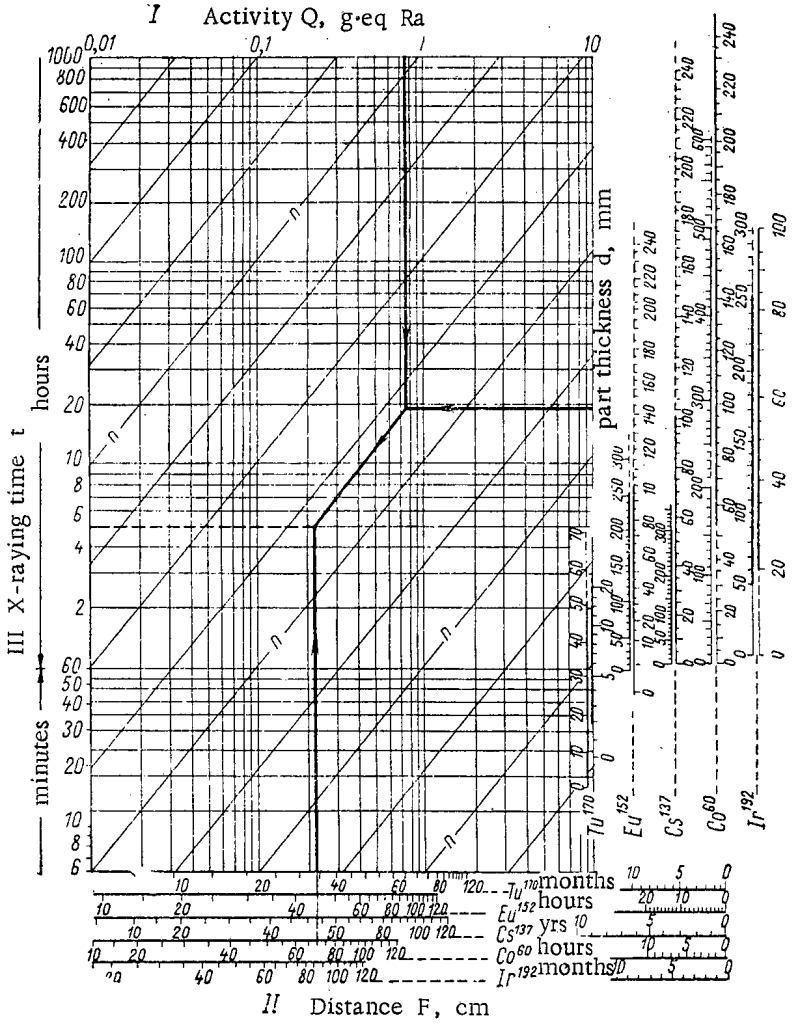

Fig. 2. Combined nomogram for determining the x-raying time when Ir^{192}, Tu^{170}, Eu^{152}, Cs^{137}, and Co^{60} radiation sources are used.

time that has elapsed from the initial measurement of the intensity of this source are known, the given scale can be used for determining the intensity of the source at a certain moment and using the actual source intensity in determinations.

Nomograms for the Ir^{192}, Tu^{170}, Eu^{152}, and Cs^{137} radioisotopes, which are used most often in the γ-detection of flaws in steel and cast iron, can also be plotted in a manner similar to that used in plotting the nomogram for Co^{60}.

In practice, flaw-detection methods are most widely used for inspecting parts made of ferrous metals and aluminum. Therefore, for practical purposes, it is convenient to use a single combined nomogram (Fig. 2).

LITERATURE CITED

1. S. V. Rumyantsev, Application of Radioactive Isotopes in Flaw Detection [in Russian], Atomizdat, Moscow (1960).
2. U. Wightshire, Industrial Radiography [Russian translation], Atomizdat, Moscow (1960).
3. S. V. Rumyantsev and L. N. Matsyuk, Transactions of the Second International Conference on the Peaceful Uses of Atomic Energy (Geneva, 1958), Reports by Soviet scientists [in Russian] Vol. 6, Atomizdat, Moscow (1959) p. 160.
4. V. I. Postnikov and V. A. Letenko, Efficiency of Radioactive Inspection in Machine Construction [in Russian], Mashgiz, Moscow (1960).

PHOTOGRAPHIC HEALTH MONITORING WITH RESPECT TO β- AND γ-IRRADIATION

V. F. Kozlov

Translated from Atomnaya Énergiya, Vol. 14, No. 4,
pp. 419-422, April, 1963
Original article submitted October 11, 1962

Data which indicate the possibility of introducing the dosimetric monitoring of β- and γ-irradiation and of thermal and fast neutron fluxes are given in papers [1-8], which are devoted to the investigation of the physical characteristics of domestically-produced photographic emulsions. However, the problem of the mixed action of β- and γ-irradiation on the photographic emulsion was not considered in these papers. Although it is often necessary to perform photographic health monitoring with respect to comparatively soft and very soft γ-radiation with quantum energies of over 20 keV, the spectral sensitivity of photographic emulsions in the range from 20 to 110 keV was not investigated in the above papers. In connection with the use of these photographic emulsions for the simultaneous measurement of β-irradiation doses, it is absolutely necessary to know the spectral sensitivities of the emulsions in this region.

The present article describes a method which supplements the presently used photographic health monitoring with respect to γ-irradiation (IFK-3) with the measurement of the soft γ-radiation (20-110 keV), which is also of great importance for determining β-irradiation doses in mixed fields of β- and γ-radiation. For this, we first investigated the dependence of the blackening of x-ray films on the γ-radiation energy. Films which were rolled in two layers of lightproof black paper with a thickness of 14 mg/cm^2 were placed in special holders and irradiated by means of standard devices at the D. I. Mendeleev All-Union Scientific Research Institute of Metrology. These holders (Fig. 1) have a 15×20-mm opening and three filters whose thicknesses are 400 mg/cm^2 (micarta), 860 mg/cm^2 (aluminum and micarta), and 1300 mg/cm^2 (lead and micarta); the last filter is identical to that presently used in IFK holders. The results of a theoretical consideration of the action of smoothing-out filters [1, 9, 10] are in sufficiently good agreement with the behavior of the curves given in Fig. 2. Four sections with different photometric densities can be separated on an irradiated and developed film. The experimental curves of Fig. 2 correspond to these sections.

It is obvious from the shape of the curves that the energy of γ-radiation that acts on the holder can be estimated with respect to the ratio of the film blackenings in the four sections. Thus, for instance, if the blackenings of all sections are almost equal, the radiation energy is over 300 keV. In the energy range from 60 to 300 keV, the blackenings of the first, second, and third sections are practically equal to each other, while the blackening of the fourth section is appreciably weaker than that of the first three. In order to estimate the radiation energy in the 20-60 keV range, it is necessary to use the above filters as radiation absorbers and to determine this energy with respect to the ratio of blackenings of the first, second, and third sections.

It was shown in [3] that, with an accuracy to ±20%, the sensitivity of Roentgen XX films with respect to allowable β-radiation doses does not depend on their energy in the region from 0.2-2.0 MeV. This fact greatly simplifies the use of photographic film for dosimetric monitoring, since the necessity of introducing a correction for the spectral composition of β-radiation is thereby eliminated.

A correct estimate of the β-radiation dose is possible only if the contribution of γ-radiation to the blackening formed under the holder's window is known accurately. This difficulty can be successfully eliminated by using the above three filters.

By measuring only β-radiators whose β-particles have a maximum energy of 3.5 MeV, it can be shown that the blackening of the third and the fourth sections of the film is due mainly to γ-radiation. This constraint is entirely admissible in the case of irradiation with β-particles of fragment-origin isotopes and in many other cases. By using tabular values [11] of the material thicknesses required for the complete absorption of β-particles, it is seen that the third filter is penetrated by β-particles whose energies exceed 2.2 MeV, while the fourth filter is penetrated by par-

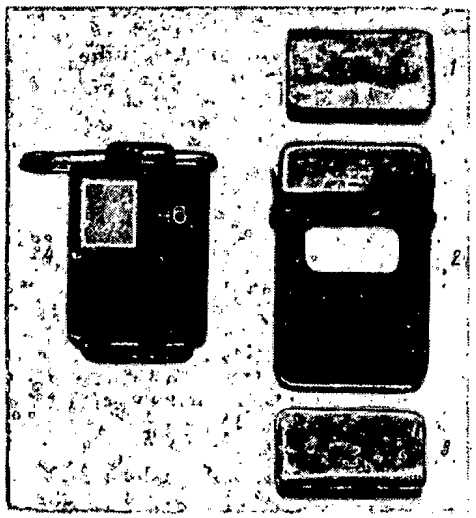

Fig. 1. External view and design of the IFK holder. 1) Lead filter; 2) standard IFK holder; 3) aluminum filter; 4) new holder IFK-2, 3.

ticles whose energies exceed 3.0 MeV. However, it is well known that the number of particles with high energies is small in the continuous spectra of β-radiators. Moreover, by using the equations given in [12], it can be shown that, for the hardest β-radiator, the dose absorbed in the photographic emulsion in the section covered by lightproof paper is more than ten times as large as the dose absorbed in the section beyond the third filter, and even more so in the case of the section beyond the fourth filter.

For determining γ-radiation doses, it is necessary to irradiate several holders by means of a standard source of γ-quanta and to plot control dependences of the photometric densities of all film sections on the γ-radiation doses D_γ. We shall denote these densities by $S_1(D_\gamma)$, $S_2(D_\gamma)$, $S_3(D_\gamma)$, and $S_4(D_\gamma)$, respectively (Fig. 3). After measuring the photometric density of the operating film, the γ-irradiation dose is determined with respect to S_4 and the control curve $S_4(D_\gamma)$ by using the ordinary IFK method. Then, the photometric densities S_1^K, S_2^K, and S_3^K that correspond to the found γ-irradiation dose are determined with respect to the control curves $S_1(D_\gamma)$, $S_2(D_\gamma)$, and $S_3(D_\gamma)$.

These data make it possible to determine approximately the γ-radiation energy in the following cases:

1. If the ratio of the photometric densities S_2, S_3, and S_4 of the operating film is close (within $\pm 10\%$) to the ratio of the S_2^K, S_3^K, and S_4^K values that are determined with respect to the control curves, the γ-radiation energy lies in the range above 300 keV.

2. If the ratio of the photometric densities S_2, S_3, and S_4 of the operating film is larger than the ratio of the values that are determined with respect to the control curves, the γ-radiation energy is equal to 45-300 keV. In this case, in order to determine the energy more accurately, it is neces-

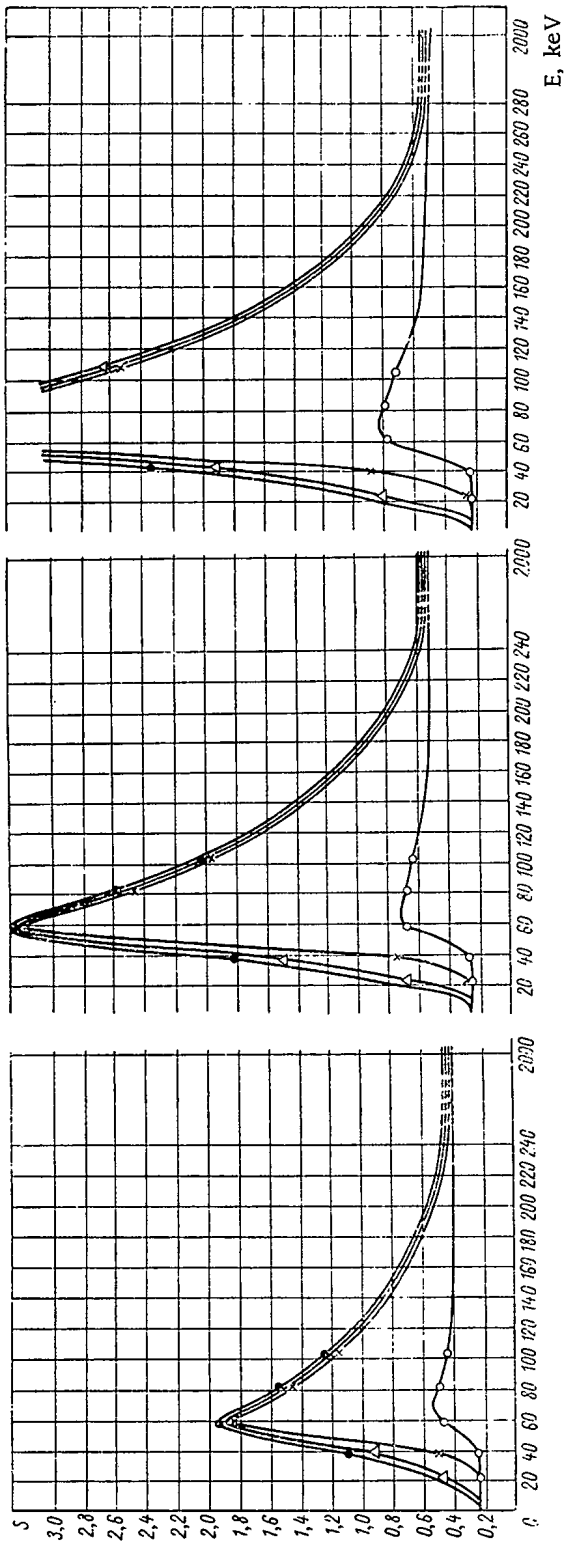

Fig. 2. Dependence of the blackening S of Roentgen XX film on the γ-radiation energy for an irradiation dose of 0.1-0.3 r.

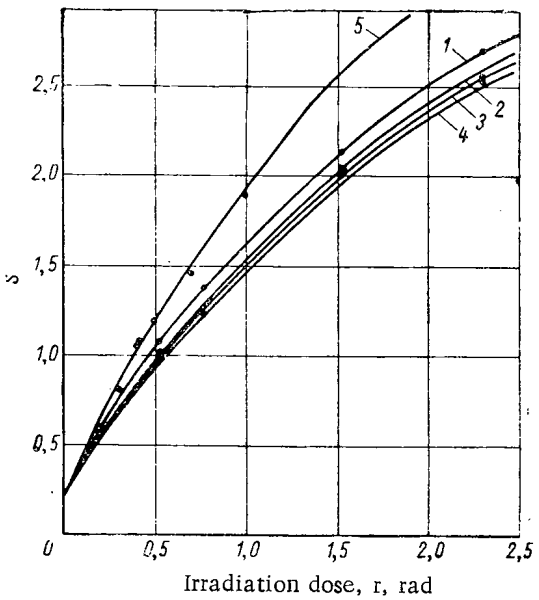

Fig. 3. Dependence of the blackening S of Roentgen XX film on the γ-radiation dose (curves 1, 2, 3, and 4) and on the β-radiation dose (curve 5).

sary to use the standard curves of Fig. 2 and to determine the radiation energy with respect to the ratio of the photometric densities S_2, S_3, and S_4 of the operating film and the ratio of $S_2^{\S}$, $S_3^{\S}$, and $S_4^{\S}$ of the standard curves that correspond to the found dose. In this, if the fogging blackening S_0^K of the control curves does not coincide with the fogging blackening $S_0^{\S}$ of the standard curves, a correction for this difference is introduced into the measured blackening values (in our case, $S_0^{\S}$ was equal to 0.24).

3. If the blackening S_4 of the operating film is equal to the fogging blackening S_0^K, irradiation in the energy range from 20 to 45 keV may have occurred. By comparing the ratio of the blackenings S_2 and S_3 of the operating film and the ratio of the blackenings $S_2^{\S}$ and $S_3^{\S}$ of the standard curves, the energy and the dose of x-ray radiation can be found.

4. If the blackenings S_4 and S_3 of the operating film are equal to the fogging blackening S_0^K, the energy of the x-ray radiation is lower than 25 keV. In this case, the x-ray radiation dose is determined with respect to the blackening S_2 of the operating film by comparing it with the blackenings $S_2^{\S}$ of the standard curves.

5. If the blackenings S_4, S_3, and S_2 of the operating film are equal to the fogging blackening S_0^K, the blackening S_1 of the operating film is caused only by β-irradiation.

In order to increase the accuracy in determining irradiation doses due to soft x rays (20-45 keV) when using the method where the blackenings of operating films are compared with the corresponding standard curves of Fig. 2, it is necessary to reduce the effect of the development factor. For this purpose, the manufacturer's recommendations concerning the conditions under which the operating films are processed must be strictly observed. Doses larger than 0.3 r in the energy range from 45-150 keV cannot be measured by means of Roentgen XX films, since these doses cause such a high degree of blackening that densitometry cannot be applied.

The following formulas must be used for estimating β-irradiation:

$$D_\beta = \frac{S_1 - S_1^K}{B}$$

in the presence of accompanying γ-radiation with E_γ values in excess of 300 keV;

$$D_\beta = \frac{S_1 - S_1^{\S}}{B}$$

in the presence of accompanying x-ray radiation with E_γ values lower than 300 keV;

$$D_\beta = \frac{S_1 - (S_3 + \delta)}{B}$$

in the presence of accompanying β-radiation with E_γ values in excess of 45 keV*.

Here, D_β is the β-irradiation dose in rads, S_1 is the photometric density of the operating film, measured under the holder's window, S_1^K is the photometric density caused by the determined γ-radiation dose under the holder's window, $S_1^{\S}$ is the photometric density under the holder's window which is due to the found dose of x-ray radiation whose energy has been more accurately determined (determined with respect to the standard curves); $\delta = S_1^K - S_3^K$; and B is the blackening factor, the value of which corresponds to a β-irradiation dose of 1 rad.

* This formula is used in order to simplify the calculation of the β-irradiation dose in the presence of soft γ-radiation (in excess of 45 keV) without using calculations with respect to the standard curves. In this case, it is necessary to use only the control curves and introduce the correction $\delta = S_1^K - S_3^K$.

For determining the factor B, the dependence of the photometric density S_β of the film due to the β-irradiation dose is plotted (curve 5 in Fig. 3). This curve can be plotted by means of standard strontium β-sources, which produce the required integral doses within a certain time. The slope of this curve, determined by the S_β/D_β ratio, defines the value of the B factor. If the dose curve can be obtained by means of the β-radiators actually used in work, this possibility should be used [13].

In the case of soft β-radiators (with the maximum energy of the β-spectrum below 0.5 MeV), the value of the factor B must be determined with respect to the β-radiation dose curves which are obtained by means of such radiators.

The control curve of γ-irradiation can be used for the approximate calculation of D_β. For this, its slope $\Gamma = S_4/D_\gamma$ is determined first and then the slope $B = S_\beta/D_\beta$ of the dose curve for β-radiation, after which their ratio $\Gamma/B = P$ is calculated. Considering, with a certain error, that P is constant, the quantity Γ/P can be used instead of the B factor.

The accuracy with which doses of β-radiation in the absence of γ-radiation in the energy range from 0.2 to 3.5 MeV can be measured is ±20%; in the presence of γ-radiation, it is necessary to take into account the error in determining the γ-radiation doses, which added to the above error, yields a value of 40%.

In conclusion, the author hereby extends his thanks to Yu. V. Sivintsev and M. F. Yudin for their help and collaboration, to K. K. Aglintsev and K. S. Bogomolov for their remarks in discussing the paper, and to V. S. Merkulova for her help in the measurements.

LITERATURE CITED

1. N. S. Nikitin, Investigations in the Dosimetry of Ionizing Radiation [in Russian], Izd. AN SSSR, Moscow (1957), p. 123.
2. K. K. Aglintsev, V. V. Smirnov, and M. N. Chubarov, Zh. Nauchn. i Prikl. Fotogr. i Kinematogr., 7, No. 6, 444 (1962).
3. V. F. Kozlov and V. F. Solenkov, In the book: Collection of Papers on Certain Problems in the Dosimetry and Radiometry of Ionizing Radiation [in Russian] Vol. I, Edited by Yu. V. Sivintsev, Atomizdat, Moscow (1960), p. 64.
4. V. F. Kozlov, In the book: Collection of Papers on Certain Problems in the Dosimetry and Radiometry of Ionizing Radiation [in Russian], Vol. I, Edited by Yu. V. Sivintsev, Atomizdat, Moscow (1960), p. 106.
5. V. F. Kozlov and V. S. Merkulova, In the book: Collection of Papers on Certain Problems in the Dosimetry and Radiometry of Ionizing Radiation [in Russian], Vol. II, Edited by Yu. V. Sivintsev, Gosatomizdat, Moscow (1961), p. 23.
6. N. S. Nikitin, Vestn. Rentgenol. i Radiol., No. 4, 59 (1959).
7. L. S. Druskina et al., Atomnaya Énergiya, 12, No. 1, 57 (1962).
8. L. S. Zolin et al., Atomnaya Énergiya, 13, No. 5, 467 (1962).
9. M. Ehrlich, Nucleonics, 9, No. 3, 5 (1951).
10. A. K. Aglintsev, Dosimetry of Ionizing Radiation [in Russian], Second edition, Fizmatgiz, Moscow (1960).
11. N. G. Gusev, Manual of Radioactive Radiations and Protection [in Russian], Medgiz, Moscow (1956).
12. R. Loevinger, Radiology, 66, 55 (1956).
13. T. Clipperley, Health Physics, 4, 173 (1960).

All abbreviations of periodicals in the above bibliography are letter-by-letter transliterations of the abbreviations as given in the original Russian journal. *Some or all of this periodical literature may well be available in English translation.* A complete list of the cover-to-cover English translations appears at the back of this issue.

WORKING CONFERENCE ON WEAK INTERACTIONS

Translated from Atomnaya Énergiya, Vol. 14, No. 4,
p. 423, April, 1963

In December 1962, a working conference on weak interactions was held at the Theoretical Physics Laboratory of the Joint Institute for Nuclear Research. Physicists from the socialist countries were in attendance at the conference.

On the first day of the conference, the questions discussed included the effect of form factors in hyperon and kaon decays and in reactions of the type $\nu + N \rightarrow N + l + \ldots$. It was noted, in the discussion, that, in view of the low statistics in the experiment performed at Brookhaven on the discovery of the μ-meson neutrino, there apparently exists a possible alternative viewpoint to the effect that the neutrino alone exists in nature, while the large number of μ-mesons detected in the experiment are due to the large contribution of the pseudo-scalar form factor. Experiments were proposed to verify this hypothesis. Selection rules in the decay of strange particles were discussed. The view was expressed, in the course of the discussion, that the presence of the selection rules $\Delta S = \pm \Delta Q$ in their totality with data on the measurement of the mass difference between K^0 and $\tilde{K}^0$ apparently clash with the representation of the Hamiltonian in the form of the product of the current with itself (Gell-Mann, Feynman).

Considerable attention was devoted to the cosmological role of the neutrino; a report was heard on a new theory of the evolution of the universe, one in which, in contrast to the Gamow-Alpher theory, the formation of the light elements is forbidden. (The formation of the light elements at an early stage of the evolution of the universe is in contradiction with experimental data.)

A lively discussion was stimulated by a report on a four-component representation of the two-neutrino theory (electron neutrino and muon neutrino). The view was expressed that both formulations of the theory (both the two-component and the four-component) are equivalent and not subject to differentiation in experiments which do not utilize the gravitational field.

In the discussion of radiation effects in weak interactions, it was demonstrated that radiation corrections do not alter the correlation and polarization properties of decay when terms of the order of $\alpha m/M$ are neglected. The role of matrix elements dependent on energy in the radiative capture of muons on nuclei was also established.

V. Belyaev

INTERNATIONAL CONFERENCE ON SECTOR CYCLOTRONS

Based on D. Clark, Physics Today, 15, No. 8, 32 (1962)
Translated from Atomnaya Énergiya, Vol. 14, No. 4,
pp. 423-425, April, 1963

The first conference on spiral-sectored cyclotrons was held in February 1959 at Sea Island (Georgia, USA). In the time elapsed since, interest in these machines has increased, and the need for organizing a subsequent conference was felt. In April 1962, one such conference was organized in Los Angeles, under the auspices of the International Union of Pure and Applied Physics and the University of California, jointly.

178 scientists and engineers from fourteen nations were present at the conference, to hear approximately 60 papers.

G. Richardson described a spiral-sectored proton accelerator in operation since November 1960 at the University of California. The machine had pole diameters of 125 cm, and is designed for 50 MeV energy. The design of the dees is quite interesting in this cyclotron, being situated in the "valleys" of the magnetic field; the design of the dees was discussed in a paper by K. MacKenzie. Because of the design employed, the gap between "ridges" was successfully reduced to 2.5 cm, and a field of 25 kG, averaging at 19 kG, was successfully produced at those points. A high energy for that magnet size was thereby secured, but the energy can only be regulated within 10% limits.

W. Powell reported on a 100-centimeter cyclotron of the Thomas type, built in Birmingham, and capable of accelerating protons (to 11 MeV) and heavier particles. Ions are injected through an opening in the armature at 10 keV energy. At the present time, beam current is about 50 μA. This injection approach is fully applicable to the task of accelerating polarized ions. Powell also rendered an account of phase measurements on the beam.

The tentative operating characteristics of the 224-centimeter spiral cyclotron at Berkeley were reported by E. Kelly. The building of this facility was inaugurated in January 1958. The beam was produced in December 1961. Protons of as much as 50 MeV energy may be produced, and deuterons of up to 60 MeV energy, as well as heavy ions. During the tune-up operations, the intensity was maintained at a level of 10 μA. An interesting peculiarity of this machine, later described by B. Smith, is the retuning of the frequency by means of movable panels rather than by displacing a shorting bar along the dee system. G. Richardson mentioned several experiments on beam extraction from this cyclotron. The beam was completely extracted with no losses in the axial direction by means of coils causing a sinusoidal perturbation of the magnetic field, but the smearing-out of the beam in the horizontal plane proved to be excessive, since the coils were not placed at the optimum radius, and magnetic channels were not used.

R. Worsham described an Oak Ridge facility. This machine is a 193-centimeter spiral-sectored cyclotron with adjustable energy designed to accelerate various particles, and producing protons of energy as high as 80 MeV. Careful preparatory work made it possible to obtain, almost immediately, a beam at maximum radius and current $\sim$250 μA. The threshold voltage across the dees was 13 kV, which indicates excellent adjustment of the magnetic field, plus the fact that the particles make at least 430 circuits. Worsham noted that this accelerator has a vertical magnetic gap, so that the dees feature great mechanical rigidity. However, as pointed out by D. Judd, this design suffers from the drawback that the external beam becomes smeared out in two planes (instead of just one plane) after passing through the deflecting magnets.

Then followed a description of the Colorado 132-centimeter spiral accelerator with control of energy. In this machine, protons of 30 MeV energy and deuterons of 20 MeV energy are to be produced. J. Kraushaar described the first stage of the starting-up operation, noting that the beam was brought out to the maximum radius with only two-fold loss of intensity. The peculiarities of the second stage were the subject of remarks by M. Rickey. The beam of negative ions of 1 μA intensity was accelerated to the maximum radius, where it was stripped of electrons on an aluminum foil and proceeded out of the magnetic field. R. Smith displaced the device blocking positive ions together with the source, to obtain more comprehensive information. Some calculations of the electron stripping process performed by Wright in 1956 at the University of California showed that the acceleration of negative ions to modest energies is entirely possible. The Colorado team was the first to carry out this task in practice. Results depend, in particular, on the chamber vacuum, which should be held at 10^{-6} mm Hg or better.

The last-mentioned paper stimulated a lively discussion among the participants, with its promise of an appreciable simplification in the techniques of beam extraction, since difficulties accompanying beam extraction have a

tendency to increase with energy and beam intensity. The one apparent limitation in principle affecting this beam extraction technique is the break-up of H^--ions brought about by Lorentz forces, which are considerable at high speeds and high field strengths. For example, calculations by D. Judd showed that break-up, at 25 kG, will take place at approximately 50 MeV. For the energies required for meson generation, the critical field would be quite small and, consequently, magnet size would have to be very large. However, for most of the spiral-sectored cyclotrons now in operation or being designed, break-up of ions should not be a great problem.

N. Verster described a controlled-energy accelerator (for various particles) which is being built for completion during 1963, at the Saclay laboratory. It will provide protons of up to 25 MeV energy. The magnet median surface was determined to an accuracy of 1 mm by a floating wire technique.

K. Stnading told of his method of "red hot" shims intended for field adjustments in the Manitoba cyclotron. The shims on the poles are to be made of invar. Each group of shims will be heated to several hundred degrees by means of interior holes. This will vary the magnetic permeability and, accordingly, the magnetic field in the given region. In the author's view, this device will be more effective than the usual correcting coils carrying current.

G. Lawson told of several aspects of the design of the 180-centimeter controlled-energy cyclotron at the Rutherford laboratory in Harwell. Peak proton energy will be 50 MeV. The possibility of electrostatic beam extraction has been under study.

Several papers dealt with the theory of orbits, and computer methods.

Two sessions were devoted to meson production. R. Haddock presented current data on meson formation. He took note of several experiments requiring an intensity characteristic of a cyclotron with azimuthal field variation.

L. Smith compared the possibilities of accelerators of various types. At first, he noted that, from the standpoint of generation of π^--mesons, 800 MeV energy would be much more convenient than 400 MeV, and that interior-target work would require an intensity of 10 μA. The reporter then presented a highly interesting comparison of accelerators which stand good chances of competing with azimuthal-field-variation cyclotrons as meson generators. He noted that FM cyclotrons are capable of yielding 10 μA current at 600-800 MeV energy, with the effective duty cycle increased 100%, if a stochastic acceleration mechanism is resorted to. However the problem of beam extraction still presents some bugs to be ironed out. A strong-focusing 700 MeV synchrophasotron (proton synchrotron) yields 10 μA at 10% effective cycle time, and costs \$7-8 million. Beam extraction is comparatively simple in that case. A constant-field strong-focusing accelerator would give as high as 100 μA. A machine of this type, accelerating to 750 MeV, would cost \$10-12 million, but beam extraction would be a difficult matter. A cyclotron with azimuthal field variation will provide 100-1000 μA at 100% effective duty cycle, but beam extraction here again will meet with severe difficulties. The cost of such a cyclotron would hover around \$5 million, for 400 MeV energy, and around \$10-12 million for 800 MeV. Finally, Smith mentioned a linear accelerator which, in his view, could provide 100 μA at 1-10% duty cycle. Beam extraction would be very simple, of course. Of the entire group of accelerators under discussion, the linear accelerator would be the most expensive machine, and would cost \$15-17 million for 800 MeV.

R. Wallace discussed the problem of shielding and residual radioactivity in facilities designed for meson generation. In his calculation, he assumed that the intensity of the external proton beam would be 100 μA at 600 MeV energy. In order to reduce the activity during operation to a tolerable level at a distance of 15 meters from the target, a wall of concrete about 10 meters thick would be required. The problems associated with the residual activity of the machine itself and of the surrounding equipment would be resolvable, although serious.

J. Blaser told of plans considered by the ETH firm in Zürich. In collaboration with the AEG concern, they propose to construct a 6-sector cyclotron, 430 MeV, in West Germany. Two dees of 90° each, operating at the second harmonic of the frequency of revolution, will be employed. N. Fogge-Nielsen told of work at CERN on designing a sex-sectored machine designed for meson generation. The meson generator project at Oak Ridge, an 800 MeV machine, was presented by R. Livingston. The energy in this machine is so chosen that resonance $\nu_r = 2$ will be achieved at the maximum radius, and the beam may be readily extracted by means of a magnetic deflector.

W. Müller told of the AEG firm's work on a 400-450 MeV accelerator. It is desirable to use 6 sectors for this energy range, since a choice of three or four sectors for energies 190 and 240 MeV, respectively, would lead to an undesirable resonance. A transition to three sectors may be included in the design near the center, in order to increase the field modulation factor. The cost of the machine is estimated at \$5-6 million.

J. Richardson told of his views on the choice of accelerator parameters. The field at the center should be 6 kG for a 700 MeV machine. Dees lying in the "valleys" of the magnetic field and extending to the region of field maxima in the central region should be employed. One interesting feature of the project is the absence of a return path in the magnet yoke.

The Oak Ridge electron analog of the 800 MeV proton cyclotron has been in operation since August 1961. This machine has been described by J. Martin. The field (41 G) is produced by a system of iron-free coils. A special difficulty encountered in running the machine up to speed is the problem of getting the beam over the resonance $\nu_r = 2$. 2600 particle circuits were obtained, while only 800 circuits were required in the simulated proton facility. R. Johns told of an interesting experiment carried out on this machine. 29 circular and 8 sectored coils were arranged randomly. After this, an attempt was made to adjust the cyclotron by means of control levers, while monitoring a beam current indicator. The beam was extracted at maximum radius in eight hours, whereupon it was proved that the cylotron could be adjusted even without benefit of computer techniques.

Experiments to be carried out on new sectored cyclotrons were discussed at a special session. Many experiments belonging to the 10-100 MeV energy range were discussed. These include investigations of nucleon-nucleon interactions, including the p-p and n-p scattering reactions, as well as various experiments on polarized beams, which fall within the realm of practical possibility at the expected high beam intensities. Discussion turned later to elastic and inelastic scattering of nucleons on nuclei, and to nuclear reactions, particularly those involving heavy-ion experiments. Great significance is attached to papers on nuclear spectroscopy as well, particularly from the standpoint of accurate energy level determinations.

Toward the end of the conference, the general view became current among the audience that a huge amount of work has been done on the design and development of sectored cyclotrons, but that there is still quite a lot to be done. 41 machines were discussed at the conference: of these, 11 are already in operation, 12 are under construction, and the remaining ones are in various stages of design and planning.

A. L.

A TWO WEEKS' VISIT TO BRITISH PHYSICISTS

Translated from Atomnaya Énergiya, Vol. 14, No. 4,
pp. 425-427, April, 1963

In the fall of 1962, a delegation of Soviet specialists on nuclear physics and charged-particle accelerators, including authors, visited research centers and physics laboratories of several universities in Great Britain.

During their stay in the country, the delegation visited the Atomic Center at Harwell, the National Nuclear Research Institute (Rutherford High Energies Laboratory), and also familiarized themselves with research on nuclear physics being conducted at universities in Oxford, Birmingham, Manchester, Liverpool, and Glasgow.

Of, course, two weeks cannot possibly present opportunity for detailed acquaintance with the status of nuclear physics and accelerator techniques throughout an entire nation. However, we did obtain some idea of the basic trends in this research, and will render an account of them in this brief note.

At the present time, the level of research in the field of nuclear physics is determined to a considerable extent by the development of accelerator technique, so that we shall start off with a concise description of existing and planned charged-particle accelerators.

The largest accelerator is the proton synchrotron at the University of Birmingham. This machine was made operational in 1953, and can accelerate protons to 1 GeV, deuterons to 650 MeV. The beam intensity is 10^9 particles/burst, at six bursts per minute.

The second largest accelerator is the synchrocyclotron at the University of Liverpool, with a peak energy of 400 MeV for the accelerated protons. The intensity of the extracted proton beam is $3 \cdot 10^{10}$ particles/cm^2·sec, or 10^8 particles/cm^2·sec and $3.5 \cdot 10^3$ particles/cm^2·sec respectively, for π^+- and π^--mesons.

Since 1954, an electron synchrotron (400 MeV) has been in operation at the University of Glasgow.

The basic material of the research conducted on these three accelerators is related to elementary particle physics.

The fourth largest operating accelerator is a synchrocyclotron at Harwell, employed to accelerate protons to 166 MeV.

In speaking of operating accelerators, we must take note that laboratories in the United Kingdom are well equipped with accelerators of energies ranging to several tens of millions of electron-volts, making it possible to perform research on the physics of the atomic nucleus on a broad scale.

Since 1960, a 50 MeV proton linear accelerator has been in operation at the National Nuclear Research Institute. Energies of 30 and 10 MeV may be produced by shutting off individual sections of the accelerator. A source of polarized protons, whose operation is based on separation of a beam of hydrogen atoms in a nonuniform magnetic field (degree of polarization: 32%, intensity: $5 \cdot 10^7$ particles/sec) is present in this accelerator system.

An extensive research program involving the use of electrostatic accelerators is in progress. There are several 6 MeV accelerators and some less powerful ones, as well as tandem accelerators of 12 MeV energy (Harwell, Liverpool, Aldermaston).

At the University of Birmingham, the 10 MeV "Nuffield" cyclotron is being used to accelerate protons, deuterons, α-particles, and He^3 ions. In addition, this university has a varied-field cyclotron (100 cm pole diameter) with an external ion source. Ions from an RF source are focused by lenses, and enter the cyclotron chamber through an opening in the magnet pole. A source of polarized ions will be installed, according to a proposal now being considered.

Of the operational accelerators, we may also note a 27 MeV linear electron accelerator at Harwell with ~1 A current per pulse. At low current values, the electron energy is 35 MeV. Pulse duration varies from $2 \cdot 10^{-6}$ to $5 \cdot 10^{-9}$ sec. The accelerated electrons generate a beam of gamma rays in a mercury target, and the beam is directed to a subcritical U^{235} with multiplication factor 10, placed alongside the facility. The neutron flux is 10^{17} neutrons/pulse.

At the present time, new accelerators of charged particles are being constructed in Great Britain. We shall mention, first of all, the Nimrod accelerator at the National Nuclear Research Institute: a weak-focusing 7 GeV proton synchrotron. The accelerator is to be commissioned in August 1963.

A varied-field cyclotron (1778 cm pole diameter) is being designed at the National Nuclear Research Institute. Protons will be accelerated to 50 MeV on this machine, deuterons, α-particles, and heavy ions to 12 MeV. Currents of about 100 μA are expected for the protons, deuterons, and α-particles. For heavy ions, the extracted beam should exceed 1 μA. The variation of the magnetic field will be achieved by means of three shims on each pole. The magnetic field at the center will be 13 kG for protons, deuterons, and α-particles, and 16-17 kG for ions. The cyclotron will have a single dee at the termination of a coaxial line. The voltage across the dee with respect to ground will be 100 kV in the frequency range 6.5-21 Mc. The principal function of the machine is to facilitate research in the fields of radiochemistry and solid state physics. Plans also call for utilizing the cyclotron for nuclear research. The machine must be built and ready for final adjustments by 1965.

At the present time, Oxford University is constructing a building to house a three-stage tandem accelerator. The basement room will contain a 12 MeV two-stage tandem generator, while the third stage, 8-10 MeV energy, to be fabricated by the university itself, will be set up vertically; the total proton energy will be 24 MeV.

By late 1962, work is to be completed on a three-stage linear heavy-ion accelerator at the University of Manchester. The ions accelerated in the first stage will pass through a thin graphite film into the second accelerator stage (the ion charge being augmented in the process). The second stage will be a linear accelerator operated at 75 Mc frequency. The energy of the ions, after passage through the second stage, will be 4.5 MeV/nucleon. The ions from the second stage will proceed to the third stage (linear accelerator operating at 75 Mc frequency), where the energy will be 10 MeV/nucleon after acceleration. Currents of argon ions and heavier ions at an intensity of several microamperes will be obtained with the accelerator.

At the University of Liverpool, the magnet, vacuum chamber, and other components of a new electron cyclic accelerator, 4 GeV and strong focusing, are in the design stage. Centered around this accelerator, which is to be built in 1966 in a low-population region between Liverpool and Manchester, will be a second laboratory of the National Nuclear Research Institute.

Design work has been commenced at the Rutherford laboratory on a proton linear accelerator using superconducting resonators, and accelerating protons to 600 MeV.

At the present time, investigations relating to the study of the structure of the nucleus, the mechanisms of nuclear reactions, and the physics of elementary particles, are underway in physics laboratories throughout Britain.

Research on elementary particle physics is related to a significant degree to processing of plates obtained fron bubble chambers at CERN, and to the processing of photoemulsions obtained at CERN and at Brookhaven.

Automatic facilities for processing bubble-chamber plates are available at the laboratories of the universities of Oxford, Birmingham, and Glasgow. At present, plates obtained in a hydrogen bubble chamber with a beam of K-mesons and antiprotons are being processed.

The nuclear emulsion team of the Oxford University is devoting serious attention to the study of decay of hypernuclei.

Experimental research conducted on synchrocyclotrons and on the electron synchrotron include the study of nucleon scattering on nucleons and on nuclei to determine the basic characteristics of scattering amplitude; the study of meson production in nucleon-nucleon interactions at 1 GeV; the study of the capture of μ^--mesons by hydrogen; measurement of the differential photoproduction cross section of π^+-mesons on hydrogen near the reaction threshold; measurement of the ratio of photoproduction cross sections of π^-- and π^+-mesons; measurement of the angular distribution of π^0-mesons in photoproduction; measurement of proton polarization in deuteron photodisintegration.

At the present time, an intense preparative labor is underway to set up future experiments on the Nimrod proton synchrotron. Work in this direction is proceeding ahead both at the Harwell laboratories and at various universities. In particular, universities are pooling their efforts in the fabrication of bubble chambers.

The study of the structure of the nucleus, as well as mechanisms of nuclear reactions, is being conducted by teams working with electrostatic accelerators, linear proton accelerators, electron accelerators, the synchrocyclotron at Harwell, and the Birmingham cyclotron.

A considerable fraction of the work being carried on with electrostatic accelerators is related to the study of scattering of charged particles with correlation of the data obtained and results yielded by the optical model of the nucleus. Experiments with polarized particles are also being conducted. Stripping and knock-on reactions with sub-

sequent data analysis by the method of perturbed waves is an important subject of study. Research on coulomb excitation of nuclei, and accurate determination of nuclear mass values from the (pn) reaction thresholds is being performed on the tandem generators.

Electrostatic accelerators operated in pulsed modes are being applied to the study of neutron spectra from various reactions, inelastic scattering of neutrons, and lifetimes of isomeric states.

Pick-up and knock-on reactions and radiative capture of protons in the giant resonance region are being studied on the linear proton accelerator, along with elastic scattering of protons.

The electron linear accelerator is being used primarily in neutron spectroscopy in the energy range from several electron-volts to several tens of kiloelectron-volts. The research program here includes measurement of total cross sections and fission cross sections for heavy nuclei, gamma-ray spectra in the resonance region, the effective number of neutrons emitted in neutron capture by U^{235}, cross sections of (γ, n) reactions, mass spectra of fission fragments.

Experiments on the study of (p, p'), (p, 2p), (p, pn), (p, pα), (p, 3n) reactions are being carried out on the Harwell synchrocyclotron.

In carrying out these experiments, extensive use is made of the technique developed in measuring particle spectra from time-of-flight determinations.

Silicon charged-particle detectors are being employed in practically all the research laboratories. Experimenters find that the use of n-silicon with its resistivity to 17,000 ohm·cm enables them to devise surface-barrier detectors with a large depth of sensitive layer, sufficient to record high-energy protons. In addition to deep-layer detectors, British experiments are also successfully fabricating thin detectors (100 microns thick) convenient for use in measuring the specific ionization of particles.

In speaking of the advances in technique, we must mention use of acoustic spark chambers in which the site where particles impact is determined by the time it takes for sound to propagate from the spark to an ultrasonic detector. At the present time, work on building chambers of this type for subsequent use in magnetic spectrometers, replacing photographic plates in that application, is underway at Harwell.

It is also worthwhile to note the intensive use of available accelerator techniques. As a rule, work on a particular accelerator is attended to not only by the staff of the laboratory in question, but also by guest scientists from other research centers.

S. M. Polikanov and E. S. Lazutkin

Translated from Atomnaya Énergiya, Vol. 14, No. 4,
p. 428, April, 1963

USSR

The research institutes of the State Committee on the Uses of Atomic Energy of the USSR are developing various devices for use as sources of ionizing radiations. For example, in the coming year plans call for fabricating experimental models of 5 MeV linear accelerators, small-size neutron generators, and powerful cascade generators.

The 5 MeV linear accelerator producing a gamma dosage of up to 200 r/min is designed for therapy of malignant tumors. The accelerator design will facilitate both stationary and rotatory therapy.

A small neutron generator of 160 kV voltage and beam current of accelerated particles ~100 μA will be used to carry out activation analysis in the production of pure and ultrapure materials.

The powerful cascade generator, for the production of electron beams to 2.5 μA at a current of 10 mA, is intended for use in the chemical processing industries. Radiation-chemistry research has demonstrated the feasibility of such generators for polymerizing polyethylene, modifying the properties of polymers, vulcanization of rubber, etc.

NEW LITERATURE

BOOKS AND SYMPOSIA

Atomizdat Releases

Plasma v magnitom pole i pryamoe preobrazovanie teplovoi energii v elektricheskuyu [Plasma in a magnetic field and direct conversion of heat energy to electrical energy]. Collection of articles translated from the English, edited by L. I. Dorman. 1962, 472 pages. 1 ruble, 53 kopeks.

This symposium contains theoretical and experimental papers completed prior to 1962. For the most part, the papers deal with the interaction between a moving plasma and a magnetic field, with an eye to applications to the problem of direct conversion and the use of magnetohydrodynamic generators. The articles discuss such questions as: interaction between partially ionized gases and electrical and magnetic fields; flows of conducting media in MHD channels; performance of MHD generators; interaction between moving partially ionized gases and a magnetic field; determination of the electrical properties of ionized gases. The collection also contains some papers which shed light on the prospects of utilizing this approach to generate electrical energy, and various fields of application of MHD generators. The extensive bibliography presented embraces the period from 1956 to January 1962 inclusive.

V. D. Rusanov. Sovremennye metody issledovaniya plazmy [Latest methods in plasma research]. 1962, 184 pages. 64 kopeks.

This book surveys experimental methods used in investigating the physical state of plasma. The first section of the book outlines high-frequency methods in studying the temperature and concentration of charged particles; the second and third sections describe probe techniques and optical techniques in studying plasma parameters; the fourth section deals with investigations of radio-frequency emission of a plasma and the determination of concentration and temperature; the fifth and last section discusses additional techniques in monitoring concentration and temperature. The bibliography for all sections is grouped together at the end of the book.

R. Meghreblian and D. Holmes. Teoriya reaktorov [Nuclear reactor theory, translated from the English (McGraw-Hill)]. 1962, 590 pages. 3 rubles, 13 kopeks.

This book is devoted to a mathematical description of the physical behavior of thermal reactors; it runs through analytical methods in neutron-physics calculations; describes various neutron phenomena in reactors in the light of extensively used mathematical models. The first chapter provides a brief discussion of nuclear chain reactions and general aspects of reactor theory. The second and subsequent chapters are devoted to probability theory, the concept of neutron flux, moderation, diffusion theory, age approximation, transport theory, the theory of reactors with reflectors, reactor kinetics, heterogeneous reactors, the theory of control rods, etc. A list of pertinent literature is appended to the book.

V. S. Balabukha, L. M. Razbitnaya, N. O. Razumovskii, and L. I. Tikhonova. Problema vyvedeniya iz organizma dolgozhivushchikh radioaktivnykh izotopov [Problem of isolating long-lived radioactive isotopes from the organism]. 1962, 168 pages. 69 kopeks.

The book discusses how to prevent the resorption of the long-lived radioisotopes: Cs^{137}, Sr^{90}, Y^{91}, Ce^{144}, Zr^{95}, and Ru^{106}. The current status of the question of using complexing agents as prophylactic and therapeutic media is elucidated. The theoretical foundations of processes involving the complexing of chemical elements and organic compounds is presented, and methods for determining the composition and stability of complexes are discussed. The conditions decisive in the linking of radioisotopes in biological media are examined with a view to their removal. A list of useful literature is appended to each chapter.

The book is intended for scientists and practicing physicians interested in this problem.

Metallurgiya i metallovedenie plutoniya i ego splavov [Metallurgy of plutonium and its alloys, translated from the English]. Edited (original) by W. Wilkinson. 1962, 276 pages. 1 ruble, 41 kopeks.

This book constitutes a symposium of papers presented at the symposium of the American Institute of Mining Engineers (San Francisco, February 1959).

The first portion deals with material on plutonium metallurgy. It discusses such methods of getting plutonium metal as: extraction from salts, recuperation from wastes, reduction by calcium of plutonium halides, etc. The second portion contains papers on the metallurgical behavior of plutonium. It discusses the problems of the behavior of plutonium in alloying and the behavior of various plutonium alloys under elevated pressures; phase diagrams of plutonium-cerium and plutonium-zinc systems are described; methods used in the metallographic study of plutonium and cathodic etching of plutonium and plutonium alloys are investigated; transformation diagrams of α- and β-plutonium are studied; experiments on zone purification of plutonium are described.

A useful supplement to the basic material of the book is the generous annotated bibliography and subject index.

New Releases by Other Publishers

A. N. Holden. Fizicheskoe metallovedenie urana [Physical metallurgy of uranium, translated from the English (Addison-Wesley)]. Metallurgizdat, 1962, 268 pages.

This book is a translation of a monograph appearing in the USA in 1958 on the structure, properties, and engineering applications of uranium and its alloys. It contains 14 chapters, some appendices (diagrams of binary uranium alloys), and a subject index.

The book starts off with a brief discussion of uraniferous ores, production of uranium metal, and some basic information on nuclear physics. Following this are descriptions of the crystal structure of the various allotropic modifications of uranium, and listings of the physical, chemical, and mechanical properties of uranium metal. We then proceed to a discussion of the deformation of uranium in various allotropic modifications, the structure of deformed uranium, and changes in the properties and structure of deformed uranium in annealing. Chapters VIII and IX present the kinetics of phase transformations in uranium and its alloys, and indicate methods for growing uranium single crystals. The next chapter is devoted to diffusion in uranium alloys, which is of unusual interest in the design of fuel elements. Chapters XI and XII deal with the effects of irradiation and thermal cycling on the structure and physical and mechanical properties of uranium metal.

The concluding portion of the book contains a brief description of fuel element design, and the metallography of uranium and uranium alloys.

The book will be a useful asset to metallurgical engineers and metal physicists, as well as students in metallurgical programs.

ARTICLES FROM THE PERIODICAL LITERATURE

I. Nuclear Physics

Neutron physics and reactor physics. Physics of a hot plasma and controlled fusion. Physics of charged-particle acceleration.

Doklady akd. nauk SSSR, 146, No. 5 (1962).

A. P. Komar et al., 1051-53. Fission of U^{238} nuclei by photons of the continuous spectrum with $E_{\gamma\,max}$ 35 MeV and 14 MeV neutrons.

Zhur. prikladn. mekhan. i tekhn. fiz., No. 5 (1962).

V. N. Oraevskii, 39-41. On the stability of ion longitudinal plasma oscillations in a magnetic field.

G. M. Zaslavskii, 42-47. On the relativistic hydrodynamics of a plasma in a magnetic field.

V. M. Eleonskii and Yu. Ya. Polyak, 48-51. Heating electrons in a moving plasma.

K. P. Cherkasova, 144-45. On evolutionary MHD currents.

Zhur. tekhn. fiz. 32, No. 12 (1962).

E. F. Tkalich and V. S. Tkalich, 1418-27. On stationary states of a high-temperature plasma. Plasma pinch in a longitudinal magnetic field.

T. N. Filimonova and A. M. Shmygov, 1438-45. 15 MeV linear electron accelerator.

I. B. Chekmarev, 1477-79. On resonance phenomena in forced oscillations of a layer of incompressible electrically conducting fluid in a transverse magnetic field.

Yu. M. Kagan and V. I. Perel', 1479-82. Contribution to the theory of ion current on a probe.

V. G. Makhan'kov, 1484-86. On excitation of electromagnetic waves in a plasma where the electrons have a directed velocity with respect to the ions.

N. D. Morgulis and Yu. P. Korchevoi, 1487-89. Effect of an interelectrode cesium plasma on the characteristics of a thermionic energy converter.

G. V. Skornyakov, 1494-95. Note on the existence of magnetic surfaces.

Zhur. eksptl. i teoret. fiz., 43, No. 6 (1962).

V. S. Golubev, 1985-90. Investigation of diffusion of charge carriers in ionized gases, by the method of diffusion waves.

A. A. Panov, 1998-99. Probability of ternary fission of Pu^{239} in the 0.05-0.7 eV neutron energy region.

V. F. Apalin et al., 2053-55. On the number of neutrons emitted by U^{234} and Pu^{240} in symmetric fission.

V. I. Pakhomov, K. N. Stepanov, 2152-65. Emission of low-frequency waves by ions and electrons in a magnetoactive plasma.

A. S. Kompaneets, 2185-87. Regularization of classical electrodynamics equations.

B. B. Kadomtsev and V. I. Petviashvili, 2234-44. A weakly turbulent plasma in a magnetic field.

V. I. Pustovoit, 2281-89. Conductivity of plasma media in the presence of drift.

Arkiv Fys., 22, No. 5 (1962).

B. Lehnert, 445-47. Plasma stability in a nonuniform field.

E. Witalis, 375-87. Electrical characteristics of a toroidal high-pressure discharge.

J. Appl. Phys., 33, No. 11 (1962).

T. Tsukishima and S. Takeda, 3290-91. Reflection of microwaves by uniform dense plasmas.

D. Rose and R. Esterling, 3317-18. Calculating energy distribution in plasma flows.

B. Barnes, 3319-22. Probe perturbation of a low-pressure discharge.

R. Redmond et al., 3383-85. Energy spectrum of fission fragments emitted by thin layers of uranium oxide.

Phys. Fluids, 5, No. 8 (1962).

Tamada K., 871-78. Near-sonic flow of an ideally conducting gas with a collinear magnetic field.

I. Shohet, 879-84. Velocity and temperature distribution in a laminar magnetohydrodynamic flow in the entrance region of an annular channel.

I. Fay and W. Hogan, 885-90. Heat transfer to cold electrodes in a moving ionized gas.

G. Miller, 899-907. Propagation of electromagnetic waves in a nonuniform ionized medium.

H. Weitzner, 933-46. The Green's function for the linearized Vlasov equation.

D. Montgomery and D. Gorman, 947-49. The Boltzmann-Vlasov equation in a bounded region.

R. Yaggi, 949-62. Wave motion in a plasma with anisotropic pressure.

R. Liboff, 963-80. Long-wave phenomena in a plasma.

D. Wetstone, 981-87. Coaxial plasmoid source with low clearance to tube diameter ratio.

R. Johnson and D. Jerde, 899-93. Instability of a plasma column in a longitudinal magnetic field.

G. Schmidt, 994-1002. Nonadiabatic motion of a particle in axisymmetric fields.

H. Lorber, 1003-1009. Theory of high-impedance plasma devices using the pressure of an RF field.

B. Berotti, 1010-14. Theory of the electrostatic probe in a strong magnetic field. II.

P. Chung, 1015-16. Langmuir potential associated with Couette flow of a viscous plasma.

D. Wells, 1016-18. Observation of eddy rings in a plasma.

Phys. Fluids, 5, No. 9 (1962).

J. Melcher, 1037-43. Electrohydrodynamic and magnetohydrodynamic nonlinear surface waves.

J. Rosciszewski, 1044-47. Analogy between the Rayleigh problem and the flow behind a shock wave in magnetohydrodynamics.

H. Dickinson et al., 1048-56. Experimental study of Rayleigh-Taylor instability in a plasma.

E. Harris, 1057-62. The Rayleigh-Taylor instabilities of a collapsing cylindrical sheath in a magnetic field.

J. Greene et al., 1063-69. Equilibrium and stability of magnetohydrodynamic systems possessing helical symmetry.

L. Combes et al., 1070-75. Behavior of a plasma in magnetic fields with acute-angled geometry.

O. Eldridge and M. Feix, 1076-80. One-dimensional model of a plasma in thermodynamical equilibrium.

R. Rosa, 1081-90. Hall effects and ion slip in a nonuniform gas.

P. Auer, 1091-94. Adiabatic electron fluid in the presence of strong space-charge forces.

H. Kuehl, 1095-1103. Electromagnetic radiation of an electric dipole in a cold anisotropic plasma.

D. Tidman, 1104-1112. Radio-frequency emission from electrons in small-scale electric fields of shock waves.

D. Beard and J. Baker, 1113-20. Synchrotron radiation losses in a hot plasma.

A. Krauz, 1128. Production of a barium plasma.

A. Carswell, 1128-30. Observation of flow in a gas by means of low-density plasma flows.

R. Kilb et al., 1131-33. Stabilization effects due to chamber walls in theta-pinch configurations.

W. Drummond, 1133-34. Scattering of microwaves by unstable plasma waves.

II. Nuclear Power Engineering

Nuclear reactor theory and calculations. Reactor design. Performance of nuclear reactors and reactor power stations.

Trudy inst. fiz. akad. nauk Gruz. SSR, 8 (1962).

V. V. Goncharov, 3-14. Research reactors.

S. A. Skvortsov, 15-23. Nuclear electric power generating station.

V. I. Gomelauri and G. V. Ratiani, 25-40. Determination of local and average heat transfer coefficients for fuel elements of the IRT research reactor.

T. V. Golashvili, 41-50. Resonance absorption of neutrons in heterogeneous reactors.

A. Kh. Breger, 51-58. Indium-gallium radiation loop of the IRT nuclear reactor.

Atomkernenergie, 7, No. 11 (1962).

R. Haberli et al, 385-91. Study of radiation stability of diphenyl under dynamical conditions.

P. Baertschi, 392-96. On cost factors for organic coolants containing deuterium.

K. Singer et al., 397-402. Study of pyrolysis of polyphenyls.

H. Abel-Larsen, 403-404. Organic coolant loops for studying heat transfer and accumulation of operating experience.

E. Fischer et al., 405-10. Experimental loop of the Gestacht reactor for studying organic coolants.

G. Melkonian et al., 411-18. Irradiation capsules for organic materials.

Atomkernenergie, 7, No. 12 (1962).

W. Junkermann and E. Böhm, 450-56. Improved low-power gas reactor.

G. Ortner, 471-76. The Wiener Hochschule atomic institute.

N. Christodulu, 477-80. Natural coolant circulation with pumping in a maritime boiling ractor.

Atompraxis, 8, No. 11 (1962).

E. Knoglinger, 414-19. Thermal stresses in graphite spherical fuel elements.

P. Koss and H. Bildstein, 420-23. Study of nuclear fuel particles with antifragmentation cladding.

P. Gilli, 431-38. Features of the design and construction of nuclear power facilities.

P. Günter, 438-40. Possibilities for improving the heat transfer characteristics of pressurized-water reactors.

K. Kadlez, 440-44. Development of nuclear engineering.

Energia Nucleare, 9, No. 11 (1962).

A. Kind and G. Rossi, 628-34. Simplified model for determining thermal neutron spectra in a fuel element.

G. Zorzoli, 635-39. Theoretical analysis of flux variation in annular fuel elements.

Kernenergie, 5, No. 10/11 (1962).

D. Falkenberg, 701-34. Status of development of fast breeder power reactors.

Kertechnik, 4, No. 10 (1962).

G. Riesch, 433-37. Start-up of the AEG research reactor.

W. Köhler, 438-40. Neutron flux in irradiation channels of the FRM reactor.

H. Dresia, 441-43. Simple method for measuring thermal flux.

H. Säufferer, 453-58. Sensitivity in monitoring fuel elements for leaks in a water-cooled reactor.

I. Everson and K. Jay, 459-61. The DIDO research reactor and its place in the British nuclear power development program.

K. Diebner, 465. West Germany's first critical assembly.

Kerntechnik, 4, No. 11 (1962).

K. Diebner, 519-20. Problems related to the formation of surface deposits in using organic fluids in nuclear reactors.

Nucl. Engng., 8, No. 80 (1963).

R. Allardice, 8-11. Chemical processing of spent fuel from a fast reactor.

W. Lunning, 12-14. Irradiation of fissile samples in the core of a heavy-water moderated and cooled reactor.

R. Saunders, 15-19. Irradiation experiments program at the DRAGON reactor.

- - - , 30-33. First reactor of the University of London.

M. Donne and F. Bowditch, 20-29. Heat transfer at elevated temperatures.

Nucl. Power, 8, No. 81 (1963).

G. Coast, 38-43. Engineering problems encountered in building the DRAGON reactor.

- - - , 44. Design of a reactor for the Union of South Africa.

R. Coombe, 47-50. Neutron energy spectrum. I. Measurements in the 0.5-15 MeV region.

W. Lunning, 51-54. Performance and utilization of the Dounreay materials testing reactor.

W. Proctor, B. Wilson, 56-59. Analog simulation of a one-dimensional model of a nuclear reactor.

Nucleonics, 20, No. 12 (1962)

D. John and J. Wade, 52-55. Heavy-water reactor costs.

T. Moteff, 56-60. Radioactivants measure neutron spectrum and flux.

Reactor Sci. and Technology, 16, No. 9 (1962).

W. Megaw and F. May, 427-36. Iodine behavior in reactor vessels.

H. Depuydt and Neve de Mevergnies, 447-53. Average cross section of $S^{32}(n, p)P^{32}$ and $Al^{27}(n, \alpha)Na^{24}$ reactions for neutron fission.

T. Ryves and M. Scott, 455-63. Source method in measurement of subcritical reactivity.

III. Nuclear Fuels and Materials

Nuclear geology and primary ore technology. Nuclear metallurgy and secondary ore technology. Chemistry of nuclear materials.

Geol. rud. mestorozhd., No. 6 (1962).

E. N. Baranov et al., 33-45. Changes in host rock near ore veins in a uranium deposit.

R. P. Rafal'skii and K. F. Kudinova, 46-53. Experimental study of conditions governing deposition of uranium oxides from hydrothermal solutions.

Geokhimiya, No. 11 (1962).

V. A. Smirnov, 982-88. Uranium and thorium in igneous rocks of the Western Trans-Baikal region.

Doklady akad. nauk SSSR, 146, No. 5 (1962).

V. M. Vdovenko et al., 1078-80. On the structure of $UO_2(NO_3)_2 \cdot NO_2$.

Zhur. neorgan. khim., 7, No. 10 (1962).

K. N. Kovalenko et al., 2340-44. On thorium salicylates.

Zhur. priklad. khim., 35, No. 9 (1962).

V. G. Vlasov and V. M. Zhukovskii, 1888-93. Effect of addition of various oxides on the kinetics of the reduction of uranium trioxide by decomposed ammonia.

A. I. Zhukov et al., 1893-1900. Elution of uranium (VI) ions from columns containing sulfo cation exchange resins.

Radiokhimiya, 4, No. 6 (1962).

V. M. Vdovenko et al., 625-32. On the solvent extraction mechanism for U (VI) by solutions of tridecylamine fluoride.

A. G. Samartseva, 647-55. Adsorption of Pu (IV) on glass and on quartz.

V. I. Zemlyanukhin et al., 655-60. Study of complexing of americium with methylphosphinic di-isoamyl ester.

I. V. Andreeva et al., 660-67. Investigation of processes and products of the interaction between high-molecular-weight polymers and inorganic salts. I. Formation of polyacrolein-uranyl nitrate complexes.

V. I. Karpov, 667-71. Study of complex formation of the uranyl ion and orthophosphoric acid.

A. V. Lapitskii et al., 672-77. Study of complexing of thorium with several hydroxydicarbonic acids.

N. P. Ermolaev and N. N. Krot, 678-85. Some data on the behavior of uranium (IV) in nitrate solutions.

A. G. Samartseva, 696-700. Electrolytic precipitation of Am and Cm from aqueous solutions on a platinum cathode.

L. N. Lyubimova and V. G. Sochevanov, 701-706. Determination of uranium in ores and minerals by polarography.

A. N. Apollonova et al., 711-14. Partial yields of isobars, A = 138.

K. B. Zaborenko et al., 715-20. Note on the mechanism behind the penetration of a radioisotope in nuclear emulsion.

I. A. Kuzin et al., 732-37. Sorption of uranium on activated charcoal, from sodium thiocyanate solutions.

L. P. Firsova and M. F. Barakat, 740-42. Measurement of the activity of components of composite mixtures of organic materials containing carbon-14.

P. I. Chaikin and N. V. Golubev, 742-44. Effect of actinon and radon on the determination of thoron by the emanation method.

Econ. Geology, 57, No. 7 (1962).

F. Habshi, 1081-84. Relationship between uranium content in marine phosphates and other component elements of rock.

Energia Nucleare, 9, No. 12 (1962).

A. Facchini et al., 681-89. Solvent extraction of U, Ce, Zr, and Ru from nitrate solutions by tri-isooctylamine.

J. Inorg. and Nucl. Chem., 24, November (1962).

F. Baroncelli et al., 541-46. Solvent extraction of Pu (IV) nitrate by nitrates of tertiary long-chain amines.

F. Baroncelli et al., 547-59. Extraction of sexivalent uranium from nitrate solutions by tri-n-dodecylamine.

W. Keder, 561-70. Extraction of trivalent and sexivalent actinides from hydrochloric acid by tri-n-octylamine in xylol.

Nucl. Sci. and Engng., 14, No. 3 (1962).

M. Tetenbaum et al., 230-38. Study of ignition of uranium powder.

D. Olander, 287-94. Solvent extraction by tribytylphosphate-n-hexane. I.

Nukleonik, 4, No. 7 (1962).

C. Keller, 271-77. On the interaction between plutonium oxide and oxides of the alkali earths.

H. O. Denshlag and G. Herrman, 277-79. Electrolytic coating of homogeneous firm layers of uranium on aluminum.

IV. Nuclear Radiation Shielding

Radiation safety. Shielding against penetrating radiations.

Gigiena i sanitariya, No. 10 (1962).

N. N. Khvostov, 86-89. On public health rules in handling of radioactive materials and radiation sources.

Inzhener.-fiz. zhur., 5, No. 12 (1962).

D. L. Broder et al., 65-70. Application of the removal cross section technique to shielding calculations for shielding containing no hydrogen.

Radiokhimiya, 4, No. 4 (1962).

G. A. Mikhal'chenko and I. Kleinmann, 479-86. Chemical dosimetry measurements of beta sources.

V. I. Baranov and V. D. Vilenskii, 486-92. Determination of long-lived beta emitters in atmospheric fallout.

V. I. Baranov and V. D. Vilenskii, 493-96. Pb^{210} in fallout.

V. F. Oreshko et al., 499-502. Sorption of radiocobalt on peat.

Sbornik nauch. rabot. inst. okhrany truda VTsSPS, No. 4 (1962).

Radiation safety requirements for gamma facilities.

Trudy inst. okeanologii akad. nauk SSSR, 55 (1962).

I. E. Starik and Yu. V. Kuznetsov, 121-30. Note on procedures for determining radioelements in ocean sediments.

Atomkernenergie, 7, No. 12 (1962).

W. Herbst and G. Hübner, 481-86. Measuring terrestrial components of penetrating external radiation.

Atompraxis, 8, No. 11 (1962).

W. Push, 423-30. Direct measurement of radiation exposure dose suffered by personnel in reactor accidents.

- - - , 444-445. Facility for continuous monitoring of water activity.

Isotopentechnik, 2, No. 11 (1962).

J. Pazdernik, 341-43. Methods for measuring radioactivity of water in Czechoslovak water treatment laboratories, and comparison with measurement techniques in use elsewhere.

J. Inorg. and Nucl. Chem., 24, November (1962).

G. Johnson, 451-68. Nitric acid-filled radiation dosimeter.

Kernenergie, 5, No. 10/11 (1962).

J. Klumpar and M. Majerová, 774-81. Scintillation measurements of aqueous solutions of beta emitters.

W. Marquardt, 782-87. Measurements of atmosphere long-lived radioactivity.

F. Krüger and E. Atze, 787-90. Shielding from radiation in the direction of the axis of a cylindrical source with self-absorption.

Kernenergie, 5, Supplement (1962).

- - - B181-B218. Recommendations on radiation shielding by the International Commission on Radiological Shielding, Committee III. Shielding against x-rays of energies to 3 MeV and against beta and gamma emissions from sealed sources.

Kerntechnik, 4, No. 10 (1962).

H. Klessmann, 446. Miniaturized transistorized dosimeter.

Kerntechnik, 4, No. 11 (1962).

P. Sauermann, 481-84. Shielding against ionizing radiations.

J. Seetzen and K. Sayar, 485-84. On the feasibility of using prestressed concrete shielding as a reactor pressure vessel.

T. Jaeger, 492-98. Design of protective enclosures for power reactors.

A. Hönig, 499-503. Radiographic investigation of the structure of steel-reinforced concrete structures.

W. Futtermenger et al., 504-508. Determination of attenuation characteristics of shielding materials by measuring scattered radiation.

W. Hebel, 509-10. Shielding against gamma emissions of fission products.

S. Orecher and M Oberhofer, 516-17. Shielding against radiation from holes and beam ports in research reactors.

H. Witte, 517-18. Steel doors for shielding against ionizing radiations.

Nucleonics, 20, No. 12 (1962).

A. Glass, 66 ff. Optical-rotation dosimetry for Co^{60} gamma facilities.

S. Pawlicki, 74 ff. Shielding CVTR—a heavy-water pressure-tube reactor.

- - - , Tables of characteristics of neutron dosimeters, dose rate meters, and monitors.

Reactor Sci. and Technol., 16, No. 9 (1962).

J. Morris et al., 437-45. Removal of weak iodine concentrations from air on a plant-wide scale.

V. Radioactive and Stable Isotopes

Inzhener.-fiz. zhur., 5, No. 12 (1962).

N. V. Churaev, 41-47. Radiotracer investigation of the mechanism of moisture transport in drying processes.

Narod. khoz. Kazakhstana, No. 8 (1962).

S. Bukharbaev, 47-50. Radioactive isotopes in industry.

Trudy inst. fiz. akad. nauk Gruz. SSR, 8 (1962).

A. V. Bibergal' et al., 63-74. Experimental gamma pilot facility GUEP-20,000.

Trudy nauchno-issled. inst. teploenerg. pribor., symp 2 (1962).

M. G. Kozlov and L. A. Panteleeva, 59-71. Measurement of moisture of materials by nuclear magnetic resonance.

Isotopentechnik, 2, No. 11 (1962)

R. Altnau and E. Richter, 325-27. Radioisotope applications in power machinery building.

G. Milde, 328-35. Applications of radioisotopes in hydrogeological research.

G. Meier, 343-47. Spectroscopic analysis of stable isotopes.

Nucleonics, 20, No. 12 (1962).

R. Hammond, 45-49. Large reactors may distill sea water economically.

G. Murray, 50-51. Commercial sterilization with cobalt-60.

Jaderná Energie, No. 3 (1963).

V. Bartosek. On reactor transients during replacement of fuel elements at a constant speed.

M. Mozisek. Plastics in radiation dosimetry.

I. Petr. One way to measure small time intervals and short pulses with an oscilloscope.

David and Lubomir. Results of measurement of flux of thermal and resonance neutrons in the core of the VVR-S reactor.

Bartoníček. Use of a metal dosimeter in practice.

Kabát. Continuous measurement of level of fluids and free-flowing materials in tanks.

Soviet Journals Available in Cover-to-Cover Translation

ABBREVIATION	RUSSIAN TITLE		TITLE OF TRANSLATION	PUBLISHER	TRANSLATION Vol.	Issue	BEGAN Year
AÉ	Atomnaya énergiya		Soviet Journal of Atomic Energy	Consultants Bureau	1	1	1956
Akust. zh.	Akusticheskii zhurnal		Soviet Physics – Acoustics	American Institute of Physics	1	1	1955
	Astronomicheskii zhurnal		Soviet Astronomy – AJ	American Institute of Physics	34	1	1957
Astr(on). zh(urn).	Avtomaticheskaya svarka		Automatic Welding	Br. Welding Research Assn. (London)	12	1	1959
Avto(mat). svarka	Avtomatika i Telemekhanika		Automation and Remote Control	Instrument Society of America	27	1	1956
	Biofizika		Biophysics	National Institutes of Health**	6	1	1961
	Biokhimiya		Biochemistry	Consultants Bureau	21	1	1956
Byull. éksp(erim). biol. (i med.)	Byulleten' éksperimental'noi biologii i meditsiny		Bulletin of Experimental Biology and Medicine	Consultants Bureau	41	1	1959
DAN (SSSR) Dokl(ady) AN SSSR	Doklady Akademii Nauk SSSR	The translation of this journal is published in sections	Doklady Biological Sciences Sections (includes: Anatomy, biochemistry, biophysics, cytology, ecology, embryology, endocrinology, evolutionary morphology, genetics, histology, hydrobiology, microbiology, morphology, parasitology, physiology, zoology) — Life Sciences	National Science Foundation*	112	1	1957
			Doklady Botanical Sciences Sections (includes: Botany, phytopathology, plant anatomy, plant ecology, plant embryology, plant physiology, plant morphology) — Life Sciences	National Science Foundation*	112	1	1957
			Proceedings of the Academy of Sciences of the USSR, Section: Chemical Technology — Chemical Sciences	Consultants Bureau	106	1	1956
			Proceedings of the Academy of Sciences of the USSR, Section: Chemistry — Chemical Sciences	Consultants Bureau	106	1	1956
			Proceedings of the Academy of Sciences of the USSR, Section: Physical Chemistry — Chemical Sciences	Consultants Bureau	112	1	1957
			Doklady Earth Sciences Sections (includes: Geochemistry, geology, geophysics, hydrogeology, lithology, mineralogy, oceanology, paleontology, permafrost, petrography) — Earth Sciences	American Geological Institute	124	1	1959
			Proceedings of the Academy of Sciences of the USSR, Section: Geochemistry — Earth Sciences	Consultants Bureau	106-123	1-6	1956-1958
			Proceedings of the Academy of Sciences of the USSR, Section: Geology — Earth Sciences	Consultants Bureau	112-123	1-6	1957-1958
			Soviet Mathematics – Doklady — Mathematics	American Mathematical Society	130	1	1960
			Soviet Physics – Doklady (includes: Aerodynamics, astronomy, crystallography, cybernetics and control theory, electrical engineering, energetics, fluid mechanics, heat engineering, hydraulics, mathematical physics, mechanics, physics, technical physics, theory of elasticity sections) — Physics	American Institute of Physics	106	1	1956
	Elektrosvyaz'		Telecommunications	Am. Inst. of Electrical Engineers		1	1957
Entom(ol). oboz(r).	Entomologicheskoe obozrenie		Entomological Review	National Science Foundation**	37	1	1958
FMM	Fizika metallov i metallovedenie		Physics of Metals and Metallography	Acta Metallurgica	5	1	1957
FTT, Fiz. tv(erd). tela	Fizika tverdogo tela		Soviet Physics – Solid State	American Institute of Physics	1	1	1959
Fiziol. Zh(urn). SSSR	Fiziologicheskii zhurnal imeni I.M. Sechenov		Sechenov Physiological Journal USSR	National Institutes of Health**	47	1	1961
Fiziol(ogiya) rast.	Fiziologiya rastenii		Plant Physiology	National Science Foundation*	4	1	1957
	Geodeziya i aerofotosyemka		Geodesy and Aerophotography	American Geophysical Union			1962
	Geokhimiya		Geochemistry	The Geochemical Society	1	1	1956
Geol. nefti i gaza	Geologiya nefti i gaza		Petroleum Geology	Petroleum Geology	2	1	1958
	Geomagnetizm i aeronomiya		Geomagnetism and Aeronomy	American Geophysical Union	1	1	1961
	Iskusstvennye sputniki zemli		Artificial Earth Satellites	Consultants Bureau	1	1	1958
Izmerit. tekhn(ika)	Izmeritel'naya tekhnika		Measurement Techniques	Instrument Society of America	7	1	1958

Izv. AN SSSR O(td). Kh(im). N(auk)	Izvestiya Akademii Nauk SSSR: Otdelenie khimicheskikh nauk	Bulletin of the Academy of Sciences of the USSR: Division of Chemical Science	Consultants Bureau	16	1	1952
Izv. AN SSSR O(td). T(ekhn). N(auk): Metall. i top.	(see Met. i top)					
Izv. AN SSSR Ser. fiz(ich).	Izvestiya Akademii Nauk SSSR: Seriya fizicheskaya	Bulletin of the Academy of Sciences of the USSR: Physical Series	Columbia Technical Translations	18	3	1954
Izv. AN SSSR Ser. geofiz.	Izvestiya Akademii Nauk SSSR: Seriya geofizicheskaya	Bulletin of the Academy of Sciences of the USSR: Geophysics Series	American Geophysical Union	7	1	1957
Izv. AN SSSR Ser. geol.	Izvestiya Akademii Nauk SSSR: Seriya geologicheskaya	Bulletin of the Academy of Sciences of the USSR: Geologic Series	American Geological Institute	23	1	1958
Iz. Vyssh. Uch. Zav., Tekh. Teks. Prom.	Izvestiya Vysshikh Uchebnykh Zavedenii Tekhnologiya Tekstil'noi Promyshlennosti	Technology of the Textile Industry, USSR	The Textile Institute (Manchester)	4	1	1960
Kauch. i rez.	Kauchuk i rezina	Soviet Rubber Technology	Palmerton Publishing Company, Inc.	18	3	1959
	Kinetika i kataliz	Kinetics and Catalysis	Consultants Bureau	1	1	1960
	Koks i khimiya	Coke and Chemistry, USSR	Coal Tar Research Assn. (Leeds, England)		8	1959
Kolloidn. zh(urn).	Kolloidnyi zhurnal	Colloid Journal	Consultants Bureau	14	1	1952
	Kristallografiya	Soviet Physics – Crystallography	American Institute of Physics	2	1	1957
Metallov. i term.	Metallovedenie i termicheskaya obrabotka metallov	Metals Science and Heat Treatment of Metals	Acta Metallurgica	6	1	1958
	Metallurg	Metallurgist	Acta Metallurgica		1	1957
Met. i top.(gorn.)	Metallurgiya i toplivo (gornoye delo)	Russian Metallurgy and Fuels (mining)	Scientific Information Consultants, Ltd.		1	1960
Mikrobiol.	Mikrobiologiya	Microbiology	National Science Foundation*	26	1	1957
	Ogneupory	Refractories	Acta Metallurgica	25	1	1960
OS, Opt. i spektr.	Optika i spektroskopiya	Optics and Spectroscopy	American Institute of Physics	6	1	1959
Paleontol. Zh(urn)	Paleontologicheskii Zhurnal	Journal of Paleontology	American Geological Institute		1	1962
	Pochvovedenie	Soviet Soil Science	National Science Foundation**	53	1	1958
	Poroshkovaya Metallurgiya	Soviet Powder Metallury and Metal Ceramics	Consultants Bureau	2	1	1962
	Priborostroenie	Instrument Construction	Taylor and Francis, Ltd. (London)	4	1	1959
Pribory i tekhn. éks(perimenta)	Pribory i tekhnika éksperimenta	Instruments and Experimental Techniques	Instrument Society of America	3	1	1958
Prikl. matem. i mekh(an).	Prikladnaya matematika i mekhanika	Applied Mathematics and Mechanics	Am. Society of Mechanical Engineers	22	1	1958
PTE	(see Pribory i tekhn. éks.)					
	Problemy Severa	Problems of the North	National Research Council of Canada		1	1958
	Radiokhimiya	Radiochemistry	Consultants Bureau	4	1	1962
Radiotekh.	Radioteknika	Radio Engineering	Am. Institute of Electrical Engineers	16	1	1961
Radiotekhn. i élektron(ika)	Radiotekhnika i électronika	Radio Engineering and Electronic Physics	Am. Institute of Electrical Engineers	6	1	1961
	Stal'	Stal (in English)	Iron and Steel Institute	19	1	1959
	Stanki i instrument	Machines and Tooling	Production Engineering Research Assoc.	30	1	1959
Stek. i keram.	Steklo i keramika	Glass and Ceramics	Consultants Bureau	13	1	1956
Svaroch. proiz-vo	Svarochnoe proizvodstvo	Welding Production	Br. Welding Research Assn. (London)	5	4	1959
Teor. veroyat. i prim.	Teoriya veroyatnostei i ee primenenie	Theory of Probability and Its Application	Soc. for Industrial and Applied Math.	1	1	1956
Tsvet. metally	Tsvetnye metally	The Soviet Journal of Nonferrous Metals	Primary Sources	33	1	1960
UFN	Uspekhi fizicheskikh nauk	Soviet Physics – Uspekhi (partial translation)	American Institute of Physics	66	1	1958
UKh, Usp. khimi	Uspekhi khimii	Russian Chemical Reviews	Chemical Society (London)	29	1	1960
UMN	Uspekhi matematicheskaya nauk	Russian Mathematical Surveys	Cleaver-Hume Press, Ltd. (London)	15	1	1960
Vest. mashinostroeniya	Vestnik mashinostroeniya	Russian Engineering Journal	Production Engineering Research Assoc.	39	4	1959
Vop. onk(ol).	Voprosy onkologii	Problems of Oncology	National Institutes of Health**	7	1	1961
Zav(odsk). lab(oratoriya)	Zavodskaya laboratoriya	Industrial Laboratory	Instrument Society of America	24	1	1958
ZhAKh, Zh. anal(it). Khim(ii)	Zhurnal analiticheskoi khimii	Journal of Analytical Chemistry	Consultants Bureau	7	1	1952
ZhETF Zh. éksperim. i teor. fiz.	Zhurnal eksperimental'noi i teoreticheskoi fiziki	Soviet Physics – JETP	American Institute of Physics	28	1	1955
ZhFKh Zh. fiz. khimii	Zhurnal fizicheskoi khimii	Russian Journal of Physical Chemistry	Chemical Society (London)	33	7	1959
ZhNKh Zh. neorg(an). khim.	Zhurnal neorganicheskoi khimii	Journal of Inorganic Chemistry	Chemical Society (London)	4	1	1959
ZhOKh Zh. obshch. khim.	Zhurnal obshchei khimii	Journal of General Chemistry USSR	Consultants Bureau	19	1	1949
ZhPKh Zh. prikl. khim.	Zhurnal prikladnoi khimii	Journal of Applied Chemistry USSR	Consultants Bureau	23	1	1950
ZhSKh Zh. strukt(urnoi) khim.	Zhurnal strukturnoi khimii	Journal of Structural Chemistry	Consultants Bureau	1	1	1960
ZhTF	Zhurnal tekhnicheskoi fiziki	Soviet Physics – Technical Physics	American Institute of Physics	26	1	1956
Zh. tekhn. fiz.	Zhurnal vychislitel'noi matematika i matematicheskoi fiziki	U.S.S.R. Computational Mathematics and Mathematical Physics	Pergamon Press, Inc.	1	1	1962
Zh. vyssh. nervn. deyat. (im. Pavlova)	Zhurnal vysshei nervnoi deyatel'nosti (im I. P. Pavlova)	Pavlov Journal of Higher Nervous Activity	National Institutes of Health**	11	1	1961

*Sponsoring organization. Translation published by Consultants Bureau.
**Sponsoring organization. Translation published by Scripta Technica.

SOVIET RADIOCHEMISTRY

(RADIOKHIMIYA)

In cover-to-cover translation

A new Soviet journal (first issued in 1959) publishes research works emanating from the Khlopin Radium Institute, Academy of Sciences USSR, and is under the editorial supervision of Academician V. M. Vdovenko, director of the Institute. The other members of the editorial board include such top researchers as I.P. Alimarin, A. I. Brodskii, E. K. Gerling, A. A. Grinberg, V. R. Klokman, L. V. Komlev, B. V. Kurchatov, A. N. Nesmeyanov, A. V. Nikolaev, B. P. Nokol'skii, V. I. Spitsyn, I. E. Starik, and A. P. Vinogradov.

In present-day science and technology, where the radioactive properties of various substances are finding increased application in the study of chemical reactions and properties, it is of great importance that the Western scientific community be cognizant of Soviet progress in radiochemistry. The translations of SOVIET RADIOCHEMISTRY will provide a running account of Soviet progress in the chemistry of atomic elements, methods of research in radiochemistry, the study of radioactivity, the history of radiochemistry, and applied radiochemistry. The information and letters section contains concise accounts of interesting research in radioactivity.

Contributors to the journal include S. Z. Roginskii, I. V. Tananaev, P. I. Kondratov, A. D. Gel'man, Yu V. Egorov, V. P. Zaitseva, V. P. Shvedov, A. N. Ponomarev, V. S. Zlobin, and members of the editorial board.

The journal is issued bi-monthly, as will be the English edition. Translation began with the first issue of 1962.

Study of Coprecipitation of Microimpurities in Isothermal Relief of Supersaturation of a K_2SO_4 Solution. II. Coprecipitation of Lanthanum with K_2SO_4 • Crystallization Coefficents of Some Alkali-Metal Halides with Microconcentrations of One of the Components • Coprecipitation of Microgram Amounts of Molybdenum with Some Inorganic Precipitates • Temperature Dependence of Distribution Coefficents in the Extraction of Uranyl Nitrate from Aqueous Solutions with Diethyl Ether • Salting-Out Action of Group II Metal Nitrates in the Extraction of Uranyl Nitrate with Diethyl Ether • Physicochemical Characteristics of the Dynamics of Sorption of Radioactive Substances • State of Protactinium in Aqueous Solutions. VI. Adsorption Properties of Protactinium • Sorption of Some Radioactive Isotopes from Aqueous Solutions by Active Maganese Dioxide • Adsorption of Yttrium and Zirconium by Zirconium Phosphates • Structure of Uranyl Nitrate Dihydrate • Plutonium Fluorides • Hydrolytic Behavior of Plutonyl in Aqueous Solutions • Elution of Neptunium from the Anionite AM • Use of Ion Exchange to Study the State of a Substance in Solution. VIII. Study of Uranyl Carbonate Solutions by Ion Exchange • Chromatographic Separation of Protactinium from Zirconium, Titanium, and Niobium • Chromatographic Concentration of Astatine • Isolation of a Group of Carrier-Free Rare Earth Fission Products from Uranium and Thorium • Determination of Ms Thl by Ms Thll β-Particles in the Presence of Radium-226 • Determination of Radioactive Cesium by the Ferrocyanide Method • Determination of Low Levels of Radioactive Contaminants in Water • Reaction of Recoil Tritium Atoms with Benzene • Recoil Effect in Inner-Complex Compounds of Cobalt in the Reaction $Co^{59}(n, 2n)Co^{58}$ • Yields of Spallation and Fission Reactions Induced by High-Energy Particles • Mechanism of Zirconium Extraction by Organophosphorus Compounds • Effect of Structural Factors on the Thermodynamic Characteristics of the Extraction of Salts of Basic Dyes • Effect of the Amount of Absorbed Ions in a Chromatography Column on the Position of a Peak on the Elution Curve • Diffusion of Strontium-90 in Soil and Sand.

Annual subscription (6 issues): $95.00

(c/b) **CONSULTANTS BUREAU** 227 West 17 St., New York 11, N. Y.

Declassified and Approved For Release 2013/09/25 : CIA-RDP10-02196R000600100003-5